Topological States And Exotic Quantum Phases In Frustrated Low Dimensional Spin Systems

A Thesis submitted for the degree of

Doctor of Philosophy (Science)

in

Physics (Theoretical)

by

Monalisa Chatterjee

The Department of Physics

University of Calcutta

2024

List of publications/preprints included in the thesis

1. "Quantum Phase Diagram of a Frustrated Spin-1/2 Ferro-Antiferromagnetic Normal Laddder", **Monalisa Chatterjee**, Debasmita Maiti, and Manoranjan Kumar,
   ChemPhysChem 2022, e202200538

2. "Exotic phases and magnetization plateau in a frustated spin-1/2 ferro-antiferromagnetic zigzag ladder", **Monalisa Chatterjee** and Manoranjan Kumar,
   Manuscript under preparation.

3. "Quantum phases of ferromagnetically coupled dimers on Shastry-Sutherland lattice", **Monalisa Chatterjee *et al.***
   arXiv:2112.02975

4. "Singlet quantum phases of the frustrated spin-1/2 ladder with ferromagnetic (F) exchange in legs and alternating F-AF exchange in rungs",
   Monalisa Chatterjee, Manoranjan Kumar and Zontán G Soos,
   Phys. Scr. 99 025973 (2024)

5. "Spin-1/2 string correlations and singlet-triplet gaps of frustrated ladders with ferromagnetic legs and alternate ferromagnetic and antiferromagnetic rung",
   Monalisa Chatterjee, Manoranjan Kumar and Zontán G Soos,
   Phys. Rev. B 109, 094439 (2024).

6. "Magnon condensation in F-AF ladder in presence of magnetic field", **Monalisa Chatterjee** and Manoranjan Kumar,
   Manuscript under preparation.

DEDICATION

Dedicated to my parents,
Mr. Gurudas Chatterjee
and
Mrs. Ila Chatterjee
who planted the seed of knowledge in my mind
and nurtured it.

Acknowledgments

At first, I would like to express my deepest gratitude to my Ph.D. supervisor ***Prof. Manoranjan Kumar*** for his continuous support during the whole Ph.D. tenure. His proper guidance, motivation and encouragement help me a lot to complete my Ph.D. thesis successfully. He is one of the person in my life from whom I can learn how to work hard all day long, which is undoubtedly the the key to success in everyone's life. I also express my deepest appreciation to his meticulous effort during the pandemic period which also helped us to get a fruitful output even working from home.

I would also convey my gratitude to ***Prof. Zoltán G. Soos*** from Dept. of Chemistry at Princeton University, USA. Thanks to my supervisor once again for giving me the opportunity to work with Prof. Soos for almost 2.5 years continously. His immense knowledge, precious advice and invaluable guidance really a blessing to me in my journey. I'm extremely grateful to ***S.N.B.N.C.B.S.*** for allowing me to pursue my Ph.D. and I also thank my funding agency ***DST-INSPIRE*** for financial support.

I would also like to thank ***Prof. Ranjan Chowdhury*** at S.N. Bose Centre from whom I got guidance in the process of selection of supervisor and also many other fruitful suggestions whenever required. I am thankful of all the teachers and professors in my school, college and university from whom I got help and inspiration.

I would like to thank all of my senior group members: ***Aslam Da, Rakesh Da, Sudipta Da, Daya Da, Sudip Da, Debasmita Di, Singh Roy Di, Joy Da, Koushik Da, Sumit Da, Sambu Da*** and ***Sourav Da*** for their great support and helping hands. In particular, Rakesh Da, Sudip Da and De-

basmita Di's contribution to my doctoral journey is priceless. I am very much lucky having colleagues like ***Saniur*** and ***Jyotirmoy***. Both of them are very much friendly, enthusiastic and helpful, spending time with them also help me to get relief from my daily work pressure. I would be remiss in not mentioning my junior group members ***Manodip, Saurabh, Sayan*** and ***Anutosh*** who make my journey more enjoyable and smoother.

At last but not the least I would like to thank each member of my ***"Chatterjee family"*** for encouraging me in all of my pursuits and inspiring me to follow my dreams. I am grateful to those two special persons who have not only stood beside me in the battle of my life but also have led from the front. They are none other than my parents, ***Mr. Gurudas Chatterjee*** and ***Mrs. Ila Chattejee*** whose proper guidance, strong determination, perseverance and inspiration bring me at the door of my success. I won't be too wrong if I say that the creator of my destiny is my father. I am thankful of other two members of my extended family, my uncle ***Mr. Nilkanta Chatterjee*** and my grandmother ***late Shefalika Chatterjee*** who make my life full of joy and affection from the childhood. Though my grandmother is no longer with us but I can feel her presence at every breath. She was too much passinate about my study. I would also like to acknowledge my other grandparents, ***late Satya Chatterjee***, ***late Ratul Mukherjee***, and ***late Mangala Mukherjee***. This endeavor would not have been possible without the blessings of my other two uncles ***Mr. Probodh Kumar Chatterjee*** and ***Mr. Subodh Kumar Chatterjee***. I am thankful of all of my cousins, ***Mousumi Mukherjee***, ***Mouhua Banerjee***, ***Mita Mukherjee***, ***Krishnendu Chatterjee***, ***Santanu Chatterjee*** and ***Ronit Chatterjee***. My nieces, ***Popi***, ***Pomi***, ***Alo*** and ***Jonaki*** bring a lot of enjoyment in my life.

Contents

List of Figures

Chapter 1

Introduction

1.1 Introduction

In the era of the digital world, electronic devices play a pivotal role in making our ordinary lives efficient and comfortable. The importance of the electronic devices can easily be seen in terms of its market size, and the global market for electronics is USD 1,068.22 billion in 2022 and it is growing at a CAGR of 6.6 %. Consumer electronics are referred to as the devices and equipment that are used on a daily basis and this industry widely covers common people's application such as office gadgets like calculators, scanners, computers, fax machines, projectors, etc. These electronic devices are used in every walk of our lives, whether it's home appliances, office equipments, sports or any other area. In this chapter we will study the basic principle of electronic properties in solid state systems.

Electronic devices are made of materials that are generally solids in which the atoms are arranged in a periodic way and give rise to interesting electronic properties depending on the size, the distance between the nearest neighboring atoms, the Coulomb energy between the atoms, and so on. The overlapping orbitals of the atoms give rise to the path of the travelling electrons and the periodic pattern of the atoms gives rise to energy bands and these bands can be characterized by the valence band, which is filled by the electrons, and the

empty conduction band. If these two bands are separated by a gap, the system behaves as an insulator or semiconductor, and if the gap disappears, the system is a metal. To understand the formation of energy bands and their arrangements, we start from the scratch of atomic arrangement and their electronic interactions.

1.2 Many Body model Hamiltonian for a general system

Let us consider a general solid state with atoms consisting of nuclei and electrons with position vectors $\boldsymbol{R}_A$ and $\boldsymbol{r}_i$ respectively. Fig. 1.1 shows a schematic representation of nuclei and electronic coordinate in solid.

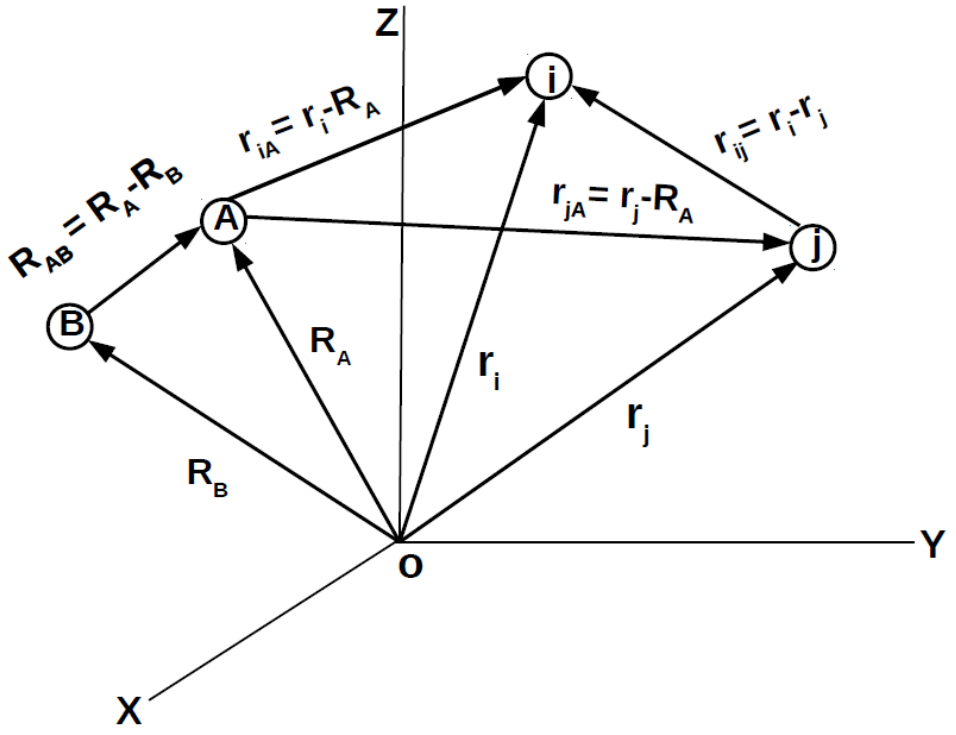

Figure 1.1: Schematic representation of molecular coordinate system. The electrons are represented by i, j and A, B represent the nuclei.

The non-relativistic time-independent Schrodinger equation can be written

as

$$H|\Phi\rangle = \epsilon|\Phi\rangle \tag{1.1}$$

where,

$$H = -\sum_{i=1}^{N}\frac{1}{2}\nabla_i^2 - \sum_{A=1}^{M}\frac{\nabla_A^2}{2M_A} - \sum_{i=1}^{N}\sum_{A=1}^{M}\frac{Z_A}{\boldsymbol{r}_{iA}} + \sum_{i=1}^{N}\sum_{j>i}^{N}\frac{1}{\boldsymbol{r}_{ij}} + \sum_{A=1}^{M}\sum_{B>A}^{M}\frac{Z_A Z_B}{\boldsymbol{R}_{AB}} \tag{1.2}$$

Here N and M represent the number of electrons and the number of nuclei respectively. The first term corresponds to the kinetic energy or hopping term of the electrons, and the second term represents the operator for the kinetic energy of the nuclei. The third term represents the Coulomb attraction between electrons and nuclei. On the other hand, the repulsion between electrons and nuclei is represented by the fourth and fifth terms respectively. $\boldsymbol{R}_{AB} = |\boldsymbol{R}_A - \boldsymbol{R}_B|$ is the distance between A^{th} and B^{th} nucleus, $\boldsymbol{r}_{ij} = |\boldsymbol{r}_i - \boldsymbol{r}_j|$ is the distance between i^{th} and j^{th} electron. The distance between i^{th} electron and A^{th} nucleus is $\boldsymbol{r}_{iA} = |\boldsymbol{r}_i - \boldsymbol{R}_A|$. According to the Born-Oppenheimer approximation [5], the electrons move in the field of the fixed nuclei since the nuclei move very slowly compared to electrons due to their heavier mass. So, the motion of the nucleus can be assumed to be frozen and it generates a potential energy surface which remains fixed. The nuclei degree of freedom is dropped and therefore the second term relating to the kinetic energy of the nuclei can be ignored and the last term relating to the repulsion between the nuclei can be considered constant. The remaining terms are the electronic Hamiltonian and can be rewritten as

$$H = -\sum_{i=1}^{N}\frac{1}{2}\nabla_i^2 - \sum_{i=1}^{N}\sum_{A=1}^{M}\frac{Z_A}{\boldsymbol{r}_{iA}} + \sum_{i=1}^{N}\sum_{j>i}^{N}\frac{1}{\boldsymbol{r}_{ij}} \tag{1.3}$$

In second quantization notation, a general many-body electronic Hamiltonian

for a solid can be written as

$$H = \sum_{<ij>,\sigma} t_{ij}(a^{\dagger}_{i,\sigma}a_{j,\sigma} + h.c) + \sum_{<ijkl>}\sum_{\sigma,\sigma'} V_{ijkl}a^{\dagger}_{i,\sigma}a^{\dagger}_{j,\sigma'}a_{l,\sigma'}a_{k,\sigma} \tag{1.4}$$

where, t_{ij} is the hopping matrix element between two orbitals i and j of an electron. $a_{i,\sigma}$ and $a^{\dagger}_{i,\sigma}$ are the annihilation and creation operators respectively. V_{ijkl} is Coulomb repulsion of electrons and $ijkl$ are the indices of orbitals.

$$t_{ij} = \int d^3\boldsymbol{r}\phi^*_i(\boldsymbol{r})(-\hbar^2/2m\nabla^2)\phi_j(\boldsymbol{r}) \tag{1.5}$$

$$V_{ijkl} = 1/2\int d^3\boldsymbol{r}_1 \int d^3\boldsymbol{r}_2\phi^*_i(\boldsymbol{r}_1)\phi_j(\boldsymbol{r}_1)V(\boldsymbol{r}_1-\boldsymbol{r}_2)\phi^*_k(\boldsymbol{r}_2)\phi_l(\boldsymbol{r}_2) \tag{1.6}$$

Here, $V(\boldsymbol{r}_1-\boldsymbol{r}_2) = e^2/r_{12}$, indices 1 and 2 are electron coodinates.

In majority of solids the Coulomb interaction is short range due to screening of the potential. In fact the simplest model can have Coulomb interaction active only if two electrons occupy the same site. On the other hand if Coulomb interaction is very high in that case we can follow some approximation, such as (i) Only one orbital per site, (ii) hopping matrix element on onsite and next nearest neighbor site are non-zero only and V_{ijkl} is non-zero only when $i = j = k = l$ and then it is called as Hubbard U. In that case the Hamiltonian in Eq. 1.4 can be simplied as-

$$H = t\sum_{i=1}^{N}\sum_{\sigma}(a^{\dagger}_{i,\sigma}a_{i+1,\sigma} + h.c) + \sum_{i=1}^{N}\epsilon_i n_i + U\sum_{i=1}^{N} n_{i,\sigma}n_{i,\sigma'} \tag{1.7}$$

where, $n_{i,\sigma}$ and $n_{i,\sigma'}$ are number operators. First term is again corresponding to the kinetic energy of the system. Second term is the chemical potential of site i and last term represents Coulomb repulsion. It is non-zero only if two electrons

occupy the same site.

Limitation of Hubbard model

There are two limitations in Hubbard model: (i) There are only non-interacting band electrons at $U = 0$ and on the other hand (ii) at $t = 0$ when the system is broken down into a set of isolated atoms. This can be more relevant for large U limit.

The effective Hubbard U can be either attractive ($U < 0$) or repulsive ($U > 0$). In order to understand the transition between conducting and insulating systems, repulsive single-band Hubbard model was introduced simultaneously by Gutzwiller [6], Hubbard [7], and Kanamori [8]. On the other hand attractive Hubbard model ($U < 0$) is used to explain superconductivity in the system [9].

1.2.1 Heisenberg model

In the large U limit the double occupancy of the site is prohibited and at every site either there can have vacancy or single electron. Therefore, in this limit one can do the second order perturbation theory and map this model to $t - J$ model [10],

$$H = -t \sum_{\langle ij \rangle, \sigma} [(1 - n_{i,-\sigma}) c^{\dagger}_{i,\sigma} c_{j,\sigma} (1 - n_{j,-\sigma}) + h.c] + \frac{4t^2}{U} \sum_i [\boldsymbol{S}_i \cdot \boldsymbol{S}_j - \frac{n_i n_j}{4}] \quad (1.8)$$

Here, the first term represents the hopping of electrons without creating double occupancy and $(1 - n_{i,-\sigma})$ is responsible to prohibit double occupancy. The spin exchange between electrons at sites i and j with exchange strength $J = 4t^2/U$ is represented by the third term. In the limit of half-filling, this model reduces to isotropic Heisenberg model and this system is isolated in nature and each site has one electron. The charge degree of freedom is frozen but these electrons can still exchange the spins. The isotropic Heisenberg model can

be written as,

$$H = \sum_{\langle ij \rangle} J_{ij} \boldsymbol{S}_i \cdot \boldsymbol{S}_j \tag{1.9}$$

where, $\boldsymbol{S}_i$ and $\boldsymbol{S}_j$ are the spin operators at sites i and j respectively. Second order perturbation theory gives $J = 4t^2/U$. If J is positive the spins are antiferromagnetically alligned and on the other hand the spins in the system gets a ferromagnetic alignment when J is negative. The spin $\boldsymbol{S}_i$ is a vector quantity and it is $3D$ in nature. Therefore, the system is isotropic when the interaction strength is same in all three spatial directions and it is anisotropic when the interaction strength is different in different directions. So, the general Hamiltonian can be written as,

$$H = \sum_{\langle ij \rangle} J_{ij}^{\alpha,\beta} \boldsymbol{S}_i^{\alpha} \cdot \boldsymbol{S}_j^{\beta} \tag{1.10}$$

where, $J_{ij}^{\alpha,\beta}$ is anisotropic exchange interaction and α/β= x, y or z.

When $J_{ij}^{x,x}$=$J_{ij}^{y,y} = 0$ and $J_{ij}^{z,z} \neq 0$, the system reduces to simple Ising model. On the other hand when $J_{ij}^{x,x}$=$J_{ij}^{y,y}$ and $J_{ij}^{z,z} = 0$, Eq. 1.10 reduces to,

$$H_{XY} = \sum_{\langle ij \rangle} J_{ij} (S_i^x S_j^x + S_i^y S_j^y) \tag{1.11}$$

where, S_i^x, S_i^y and S_i^z are the components of spins along x, y and z directions respectively and this model is called as XY model. The model is converted to isotropic Heisenberg model when $J_{ij}^{x,x} = J_{ij}^{y,y} = J_{ij}^{z,z} = J$ and Eq. 1.10 can be written as,

$$H = J \sum_{\langle ij \rangle} \boldsymbol{S}_i \cdot \boldsymbol{S}_j \tag{1.12}$$

Again, the model is called the Heisenberg XYZ model when $J_x \neq J_y \neq J_z$ and $\alpha = \beta$, the Hamiltonian reduces to,

$$H = \sum_{i}^{N} [J_x S_i^x S_j^x + J_y S_i^y S_j^y + J_z S_i^z S_j^z] \tag{1.13}$$

Finally, in 1972, Rodney Baxter gave a solution of the XYZ model [11]. He came across the XYZ spin chain by studying a $2D$ classical lattice model called the eight-vertex model, which is equivalent to the $1D$ XYZ spin chain.

On the other hand, when J_x, $J_y \neq J_z$ in Eq. 1.10, the model is Heisenberg XXZ model. It was solved in 1966 by C. N. Yang and C. P. Yang in a series of papers [12–14]. The model is called as Heisenberg XXX model when $J_x = J_y = J_z$. In 1931, Hans Bethe proposed an analytic method to construct the eigenstates for the XXX spin chain [15].

The physics of the Heisenberg XXX model strongly depends on the sign of the coupling constant J and the dimension of the space. The ground state is always ferromagnetic if J is positive. On the other hand at negative J, the ground state (gs) is generally antiferromagnetic. Based on Bethe ansatz, the antiferromagnetic ground state in the thermodynamic limit $N \to \infty$ was first studied by Hulthén in 1938 [16].

The study of excitations on the antiferromagnetic vacuum was performed by J. des Cloiseaux and J. J. Pearson [17]. In $1D$, the nature of correlations in the antiferromagnetic Heisenberg model depends on the spin of the magnetic dipoles. Only short range order exists when the spin is integer. There is quasi-long range order in a system with half-integer spins.

These different types of Heisenberg model with different exchange interactions are crucial in understanding magnetic properties of materials and stabilization of magnetic phases and their phase boundaries. These phase transitions are driven by quantum fluctuations at temperature $T = 0$ [18]. These systems become even

more interesting to study when frustration is introduced and depending on the corresponding exchange strength, exotic phases set in the system. In this thesis we are mostly interested in the gs properties of the quantum models. Before going to specific model system, let us discuss about some of the quantum phases in the system.

1.3 Exotic phases and their properties

The gs of the frustrated system can be the zoo of various types of quantum phases and these phases have specific behavior. We discuss some of these phases like antiferromagnetic phase, Néel phase, spin liquid phase, dimer phase, spiral phase, ferromagnetic and ferrimagnetic phases, stripe phase, Haldane phase etc., which are commonly stabilized in the low dimensional systems.

1.3.1 Antiferromagtic and Néel phase

Antiferromagnetic (AFM) phase in a spin system is characterized by the neighboring spins aligning in opposite directions as shown in Fig. 1.2 resulting in a cancellation of net magnetic moments and leads to a net zero magnetization, i.e. antiferromagnetic materials are non-magnetic. The phenomenon was first introduced by Lev Landau in 1933. This type of AFM phase can be short range or quasi-long range order generally found in low dimensional frustrated magnets and long range order in $2D$ or higher dimensions.

Sublattice magnetization operator [19] is defined as

$$\boldsymbol{m}_s = \frac{1}{N}\sum_{i=1}^{N} \phi_i \boldsymbol{S}_i \tag{1.14}$$

$\boldsymbol{m}_s$ is the magnetic order parameter of a system with Heisenberg interactions (e.g, the magnetization of a ferromagnet or the sublattice magnetization of an antiferromagnetic system) and $\phi_i = \pm 1$ is the staggered phase factor.

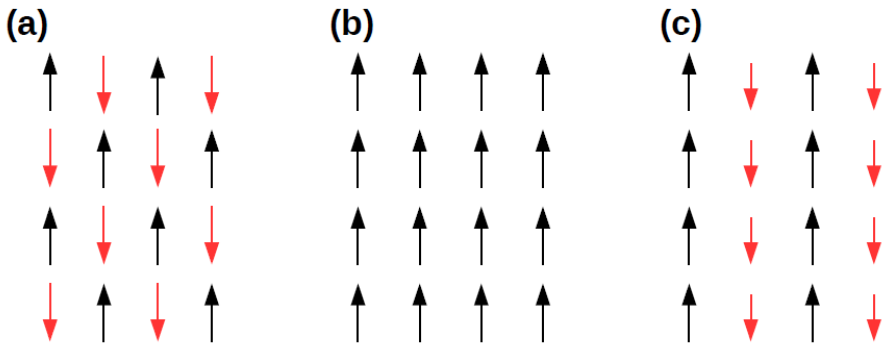

Figure 1.2: Schematic representation of different phases: (a)AFM, (b)FM and (c) Ferrimagnetic phase.

Néel order phase is a special case of antiferromagnetic arrangements of spins in lattice which has a long range order (LRO). In a Néel state $\langle \boldsymbol{m}_s \rangle \neq 0$ in the thermodynamic limit. In case of finite system, one can get a non-zero value of m_s although the direction of the vector remains fluctuating over all angles. So, in order to detect the presence of this phase in finite system, a quantity which is independent of direction, e.g., $|m_s^2|$ or $\langle |m_s| \rangle$ should be used [19].

1.3.2 Ferromagnetic and Ferrimagnetic phase

Ferromagnetism is a phase in which all the spins are aligned in a particular direction, resulting in a net magnetization in the system. The arrangement of spins in this phase is shown in Fig. 1.2 (b).

In a ferrimagnetic system where magnitude of the spins are not equal, i.e. let the system consists of two sublattices A and B. Sublattice A consists of spins with magnitude S_1 and sublattice B is consists of spins with magnitude S_2. Then the net magnetization per unit cell will not be zero rather it is $(S_1 - S_2)$ if $(S_1 > S_2)$. The spin alignment is shown in Fig. 1.2 (c).

In case of conventional ferrimagneism, spontaneous magnetization has quantized value [20] which follows the Lieb–Mattis theorem [21] but there is another type of ferrimagnetism which is induced in presence of frustration. This type of

magnetism does not have any fixed quantized value rather it continuously changes with the strength of frustration and it is called partial ferrimagnetism [22–24]. There are many studies existed in the literature which shows that this type of magnetism generally have incommensurate quasi-long range order [24, 25]. Recently it is also predicted that this phase can be characterized as a spontaneously magnetized Tomonaga–Luttinger liquid (SMTLL) [26].

1.3.3 Stripe $(\pi, 0)$ and $(0, \pi)$ phases

These types of phases generally occur in $2D$ systems. In case of stripe $(\pi, 0)$ phase, the spin configuration has a propagation vector $(k_x, k_y) = (\pi, 0)$. Here, all the spins along y-direction are arranged ferromagnetically and they form stripe like pattern along x-direction. On the other hand spin modulations has been occured with wave vector π along x-direction. The reverse situation has been happened for stripe $(0, \pi)$ phase [27]. The spin alignments are shown in Fig. 1.3 (a) and (b) respectively.

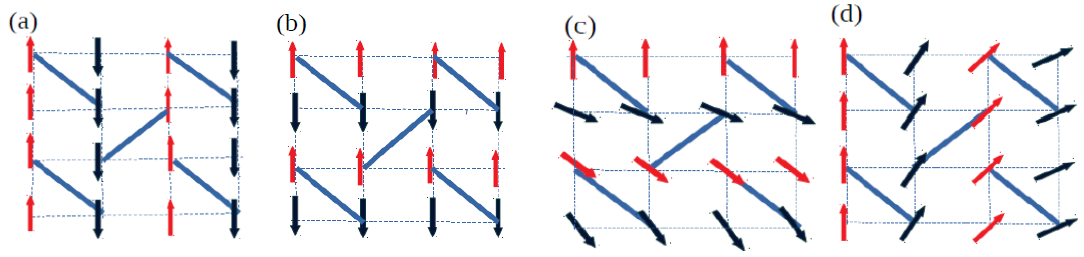

Figure 1.3: Schematic representation of different types of stripe and spiral phases: (a) stripe (π,0), (b) stripe (0, π), (c) Y-spiral and (d) X-spiral.

1.3.4 Non-collinear or spiral phase

This type of phase is generally identified by finite angle between two nearest spins known as pitch angle (ϕ). If $\phi = 0$, the phase is FM and if $\phi = \pi$, the phase is AFM. In spiral phase ϕ lies between 0 and π. For spin-1/2 normal

and zigzag ladder model spiral phase shows quasi-long range order behavior and ground state is gappless [28]. For $2D$ model the system can show spiral order along x- or y-direction and in that case the spins on other direction are alligned ferromagnetically as shown in Fig. 1.3. (c) and (d). Depending on these types spin alignments, the phases are named as X-spiral or Y-spiral phase [27].

1.3.5 Different types of dimer phases

Dimer phase in spin system refers to that phase where the entanglement between two spins are very strong which makes the pair of spins almost isolated from other part of the system. Dimer can be singlet or triplet type. Singlet means total spin (S) is zero whereas triplet is $S = 1$ state. In the perfect dimer phase the gs wave function can be represented as a product of dimer singlets: $|\psi\rangle \equiv \prod_d \frac{1}{\sqrt{2}}(|\uparrow\downarrow\rangle - |\downarrow\uparrow\rangle)_d$, where d labels a dimer.

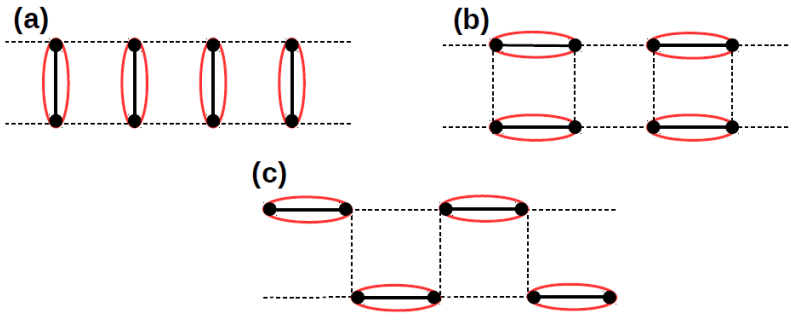

Figure 1.4: Schematic representation of different types of dimer phases: (a) rung singlet, (b) columnar dimer and (c) staggered dimer.

There is a lot of literature dealing with different types of dimer phases like columnar dimer, rung singlet, staggered dimer etc. in thefrustrated spin-1/2 ladder model [29–31] as shown in Fig. 1.4. For rung singlet phase, the dimer bond is formed along the rung of the ladder for very strong rung interaction of AFM type. On the other hand dimer are formed along the legs in case of columnar dimer model on spin-1/2 ladder AFM ladder system. Dimer order

parameter can be calculated to make a boundary between these two phases.

$$D(i,n) = \langle \boldsymbol{S_i} \cdot \boldsymbol{S}_{i+1,n} \rangle - \langle \boldsymbol{S}_{i-1,n} \cdot \boldsymbol{S}_i \rangle \tag{1.15}$$

where i is the site number and n is leg. Dimers on one leg are shifted by one bond with respect to other leg in staggered dimer phase [31].

1.3.6 Haldane phase

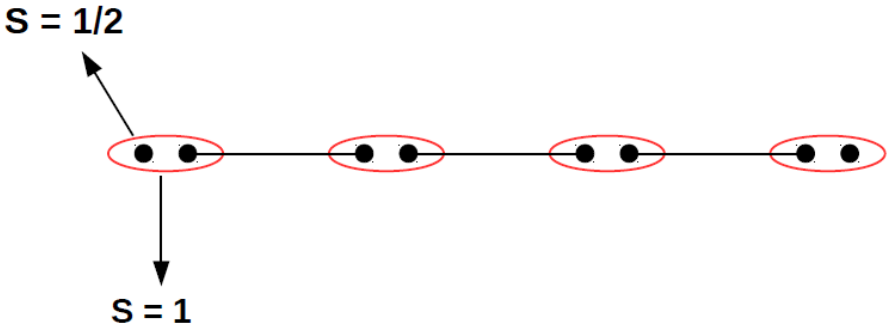

Figure 1.5: Every $S = 1$ spin consists of two $S = 1/2$ spins and each spin-1/2 forms singlet bond with another spin-1/2 on neighboring $S = 1$ site.

In a spin system, the Haldane phase refers to a unique quantum phase of matter found in a $1D$ magnetic system. It is characterized by a finite energy gap in spin excitation spectrum despite the absence of conventional magnetic order. This phase arises due to the interplay of quantum fluctuations and spins interactions, exotic properties such as topological order which will be discussed in detail in the next section. In a spin-1 chain, the spin-1 can be treated as two spin halves and one spin-1/2 at site i form a singlet bond with spin-1/2 at site $i-1$ or $i+1$ and there is a free spin-1/2 at the edge. The correlation function decays exponentially and has a large spin gap. The gs is fourfold degenerate.

1.3.7 Quantum spin liquid phase

Quantum spin liquid is another interesting phase which does not have any magnetic order. It is generally detected by long range quantum entanglement and fractionalized excitations. In 1973, Phil Anderson first proposed this phase. This phase can be both gap or gapless type.

1.4 Spin models

Let us now consider some low dimensional model systems like $J_1 - J_2$ spin-1/2 model, some spin ladder systems like normal and zigzag ladder and Shastry-Sutherland lattice model in $2D$ and discuss the quantum phases and their phase boundaries.

1.4.1 One dimensional spin systems

In this section we will consider the one-dimensional $J_1 - J_2$ spin-1/2 chain model.

The normal Heisenberg antiferromagnetic spin-1/2 model on a spin chain is an interesting system with gapless spectrum and quasi-long range order gs. However, when spin exchange to the nearest neighbor is induced, the system becomes frustrated. In this system we can consider the nearest and next nearest neighbor interactions J_1 and J_2 respectively as shown in Fig. 1.6.

The Hamiltonian can be written as,

$$H(J_1, J_2) = J_1 \sum_i \boldsymbol{S_i} \cdot \boldsymbol{S_{i+1}} + J_2 \sum_i \boldsymbol{S_i} \cdot \boldsymbol{S_{i+2}} \tag{1.16}$$

The system shows a variety of interesting behaviors at different limits of interaction. When $J_2 = 0$ the system is behaving like linear Heisenberg antiferromagnet (HAF) with nondegenerate ground state and quasi-long-range order (QLRO) at wave vector $q = \pi$ for $J_1 > 0$ limit. On the other hand when $J_1 = 0$ and

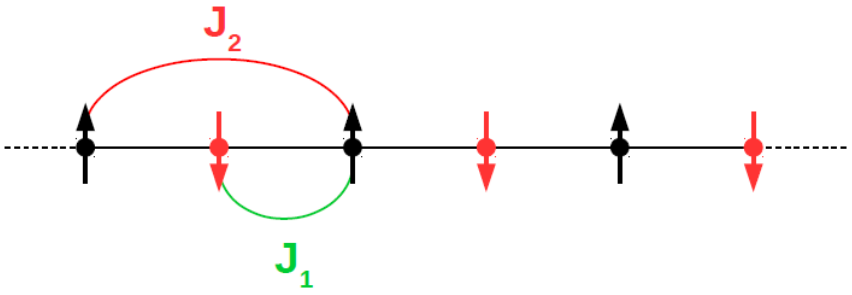

Figure 1.6: Schematic representation of $J_1 - J_2$ model with J_1 as nearest neighbor and J_2 as next nearest neighbor interactions respectively.

$J_2 > 0$ the system converts to HAFs on sublattices of odd and even numbered sites. QLRO order is observed at $q = \pi/2$. The gapless QLRO(q) phases have divergent S(q) peaks while gapped phases have finite peaks.

The exact ground state (gs) at $g_{MG} = J_1/J_2 = 1/2$ is known as the Majumdar–Ghosh point [32], and Hamada *et al.* [33]. discussed the quantum critical point (P_1) at $g = -4$ as shown in Fig. 1.7. On the other hand the critical point P_4 at $1/g = 4.148$ is obtained by Okamoto and Nomura [34] using exact diagonalization (ED) of finite systems, level crossing and extrapolation. Z G Soos *et al.* [1] has given the numerical evidence for the quantum critical points P_2 and P_3 in Fig. 1.7 between gapped IC phases and a gapless decoupled phase with QLRO($\pi/2$).

The details of quantum phase diagram of the $J_1 - J_2$ model as shown in Fig. 1.7 has been discussed in Z G Soos *et al.* [1]. The gapless FM phase with LRO (0) is valid in the sector with $J_1 < 0$ and $J_2/J_1 \leq -1/4$, including $J_2 < 0$. In the sector $J_1 > 0$ and $J_2/J_1 \leq 0.2411$, the gapless AFM phase with QLRO (π) holds.

The decoupled phase with QLRO ($\pi/2$) which is gapless is in the sector with $J_2 > 0$ and $-1.24 \leq J_1/J_2 \leq 0.44$. Gapped IC and dimer phases with doubly degenerate gs and finite order spin-spin correlations are lying between gapless phases with nondegenerate gs. Dimer phase has wave vector ($q = \pi$) and it is

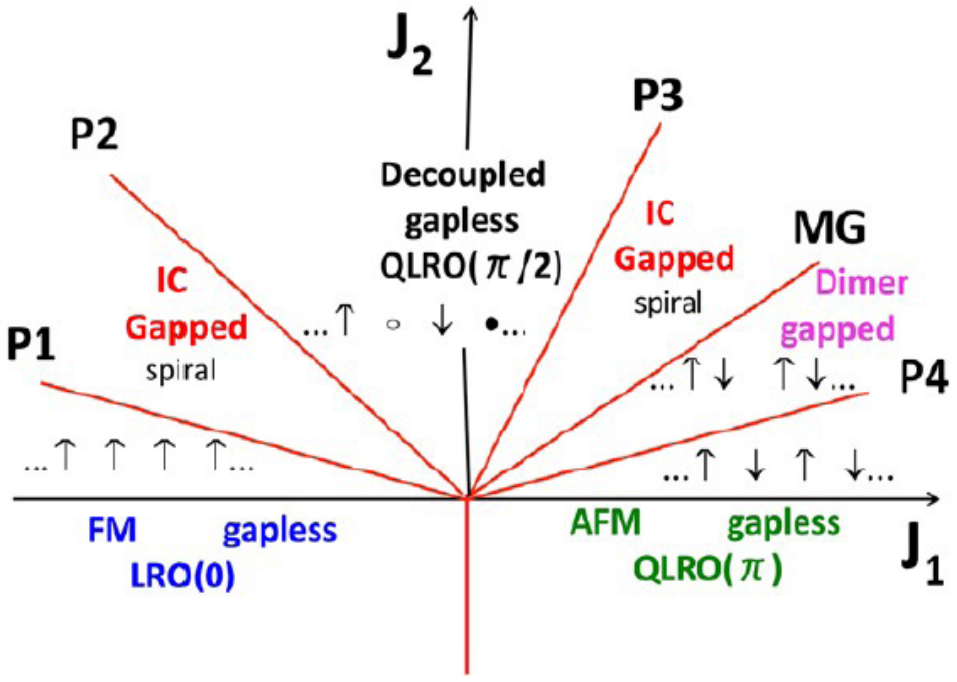

Figure 1.7: The quantum phase diagram for the $J_1 - J_2$ model ($J_1 < 0$ and $J_2 > 0$) has been constructed [1]. $P_1 = -4$ is the transition point between gapless FM and gapped incommensurate (IC) phase. $P_2 = -1.24$ is at the boundary between IC gapped and decoupled gapless phase. The decoupled phase extends between P_2 and P_3 ($P_3 = 0.44$). The IC gapped phase extends to the MG point where $J_1 = 2J_2$. Then the dimer phase is introduced and it ends at $P_4 = 4.148$. Finally a gapless FM phase is created.

lying in the sector $2 \leq J_1/J_2 \leq 4.148$. On the other hand the IC phase has variable wave vectors ranging from 0 to $\pm\pi/2$ in the sector $-4 \leq J_1/J_2 \leq -1.24$ and $\pm\pi/2$ to $\pi(= -\pi)$ in the sector $0.44 \leq J_1/J_2 \leq 2$.

In the next section, we will give a brief review on quasi-one dimensional systems.

1.4.2 spin ladders

Spin-1/2 ladder system is one of the active area of research because of the existence of interesting phases like dimer [35], spiral phase [36], spin liquid [37] etc.

Generally, there are two types of ladder geometries: Heisenberg AFM normal ladder (NL) configuration where the spins on different legs are directly interacting with each other by rung interaction and on the other hand the spins in one leg is shifted by half of the lattice unit in case of zigzag ladder (ZL) configuration as shown in Fig. 1.8 (a) and (b) respectively.

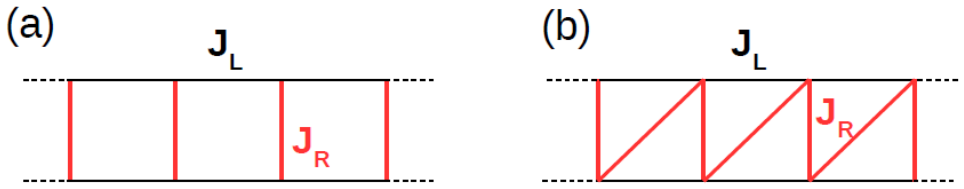

Figure 1.8: Schematic representation of NL and ZL where J_L and J_R are interaction strength along leg and rung respectively.

Many real materials can be mapped by these ladder models. The Heisenberg antiferromagnetic (HAF) spin-1/2 NL have been realized in $SrCu_2O_3$ [38], $(VO)_2P_2O_7$ [39] etc., whereas ZL geometry is realized in $(N_2H_5)CuCl_3$ [40], $LiCuSbO_4$ [41], $LiSbVO_4$ [42], Li_2CuZrO_4 [43] etc. The behavior of HAF NL is completely different from HAF ZL. The AFM NL system is a spin liquid with a spin gap and a spin correlation in the short range. It has been suggested that the spin gap decreases smoothly with the decrease of the rung exchange interaction and decreases to zero only when the rung interaction strength approaches zero [28]. The rung interaction induces the formation of a singlet dimer between the two closest spin-1/2s on different legs.

The ZL in the weak rung coupling limit $J_R/J_L < 0.44$ behaves like two independent HAF spin-1/2 chains [1], and shows gapped spiral phase for $0.44 < J_R < 2$. It is showing gapped dimer configuration for $2 < J_R/J_L < 4$ [1].

Ladders with AFM J_L and FM J_R is also very much interesting to study. For very small value of J_R limit, the system behaves like two independent Heisenberg

chains which is forming decoupled phase. On the other hand, for very large J_R limit the two spins on two different legs form triplet along the rung and the system behaves like Heisenberg spin-1 chain. The critical transition point is proposed to be around $|J_R|/J_L = 0.6$ above which Haldane gap appears [44].

Roji and Miyashita have studied the $S = 1/2$ ladder model consisting of two legs with FM interaction J_R along legs and AFM interaction J_R along rungs. FM LRO is existed along each chain when $J_R = 0$. On the other hand rung dimers are formed for large J_R limit. Gap is opened for any finite value of J_R which is shown both analytically [45, 46] and numerically [47].

The ground-state properties of $S = 1/2$ Heisenberg ladders with a FM leg, AFM leg, and AFM rungs have been studied using exact diagonalization method in Sekiguchi *et al.* [48]. Partial ferrimagnetic state is the most dominating phase in phase diagram which extends over a wide region. It is also supported by non-linear sigma model and perturbation calculations. Partial ferrimagnetic state is a spontaneously magnetized Tomonaga–Luttinger liquid with incommensurate magnetic correlation. Similar type of model has been also studied by Debasmita Maiti *et al.* [28].

There are many other ladder models which have been studied extensively, such as ladder with diagonal and off-diagonal interactions [49–52], skewed ladder [53–55] etc.

1.4.3 Two dimensional lattice model

Frustrated $2D$ magnets are realized in layered materials, and these $2D$ geometries: square, triangular, kagome and Shastry-Sutherland lattice (SSL) are particularly interesting because 2D is supposed to be a critical dimension in the domain of the Mermin-Wagner theorem [56]. $2D$ system is very difficult to solve, although various analytical techniques like spin wave theory [57], renormalization group method [58, 59], Schwinger boson mean field theory [60], some semi-anlytical techniques like series expansions [61], variational theory, and nu-

merical techniques like exact diagonalization [62,63], quantum Monte Carlo etc. give some ideas about the gs and the excited state properties of these systems. In this section we will focus only on Shastry-Sutherland lattice model.

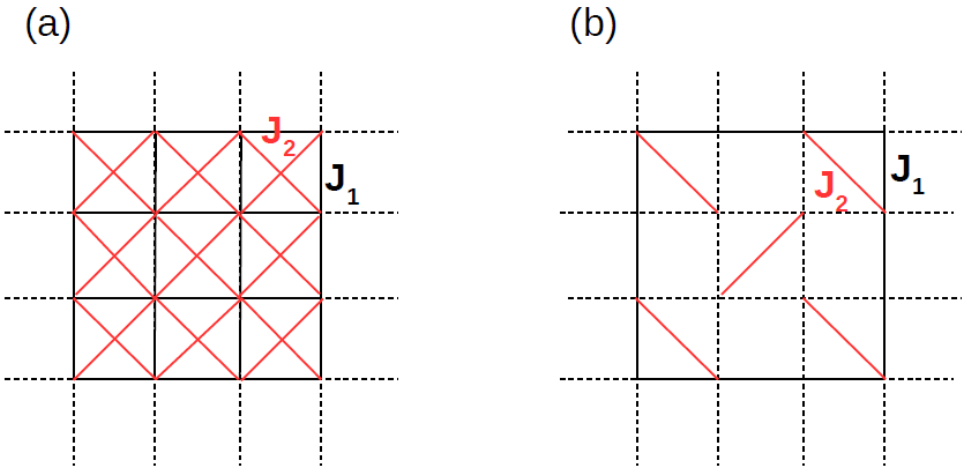

Figure 1.9: Schematic representation of square and Shastry-Sutherland lattice in (a) and (b) respectively where J_1 is nearest neighbor and J_2 is next nearest neighbor interaction.

The HAF spin-1/2 model on Shastry-Sutherland lattice (SSL) is one of the interesting model to investigate due to its exotic magnetic behavior. The structure of SSL is very similar to square lattice, only the difference is that in case of SSL, alternate square has diagonal bond as shown in Fig. 1.9 (a) and (b). SSL model was first proposed by Shastry and Sutherland in 1981 [64]. Most of the works done on SSL till today are mainly focussed on Heisenberg model [65,66], Ising model [67,68], $t-J$ model [69], $t-J-V$ model [70]. We are interested in J_1-J_2 Heisenberg model on SSL lattice.

The Hamiltonian can be written as,

$$H(J_1,J_2) = J_1 \sum_i \boldsymbol{S_i}\cdot\boldsymbol{S_{i+1}} + J_2 \sum_i \boldsymbol{S_i}\cdot\boldsymbol{S_{i+2}} \tag{1.17}$$

where J_1 and J_2 are NN and NNN interactions respectively. J_1-J_2 Heisenberg model on SSL is exactly solvable when diagonal bond interaction (J_2) is exactly

equal to the twice of leg or rung interactions i.e. $J_2 = 2J_1$. Antiferromagnetic SSL model is a very well studied model. SSL model can be realized in many real materials like $SrCU_2(BO_3)_2$ [71], Yb_2Pt_2Pb [72], $RB_4(R = La - Lu)$ [67] The ground state of this system has Néel and dimer order for the small and large J_2/J_1 limit respectively.

Corboz *et al.* [73] predicted the existence of a long range plaquette phase between the Néel and dimer regions using the PEPS technique. They also found the phase boundaries with very high accuracy. The phase transition between the dimer and the plaquette phase occurs at $J = 0.675$. On the other hand, the phase transition between plaquette and Néel phase occurs at $J = 0.765$. Both types of phase transitions are of the first order type.

Based on finite-size scaling of excited level crossings and order parameters, Yang *et al.* [74] predicted a spin liquid phase in this model which lies in a very narrow region between plaquette-singlet and antiferromagnetic states using DMRG. They also mentioned the heat capacity measurements in $SrCu_2(BO_3)_2)$ as a evidence of the proposed spin liquid at pressures between 2.6 and 3 GPa. Ronquillo and Peterson *et al.* [75] predicted the topological gs by using entanglement entropy calculations.

The model with NN interaction as FM type and NNN as AFM type remains to be investigated. $(CuCl)LaNb_2O_7$ was originally predicted to be a $S = 1/2$ frustrated square lattice [76]. In 2010 Tassel *et al.* [77] showed by band structure calculations that this material is a distorted ferromagnetically coupled SSL. In 2011 Furukuwa *et al.* [27] studied this model theoretically using mean-field calculations and exact diagonization. To the best of our knowledge, this is the only study of this model with some discrepancies. Mean-field calculations have predicted the existence of FM, dimer, spiral and stripe order phases and their phase diagrams have been constructed. On the other hand, the spiral order phase has not been detected in the exact diagonalization method. This may be due to the lack of larger system size calculations. The phase boundaries obtained in

the ED calculation are also inconsistent with those obtained in the mean field calculations, suggesting that further studies on this model need to be carried out.

1.5 Correlated spins in external magnetic field

We now switch the gear and discuss the most easily solvable problems. Let us start with simple $1D$ J_1-J_2 model in an external magnetic field which can be easily implemented experimentally. The zigzag chains are realized in $SrCuO_2$ [78], $(N_2H_5)CuCl_3$ [40], F_2PIMNH [79] etc. It is noted that in an external magnetic field, many exotic quantum phases such as magnetization plateau, vector chiral phase, quardupolar phase etc can exist. If J_1 and J_2 both are of AFM types, a 1/3 magnetization plateau has been arisen in $M-h$ curve [80–82]. For large field limit, two magnon-bound state is formed. The phase diagram of this model has been discussed in Kouichi Okunishi *et al.* [80, 81]. The system shows a gapped dimer phase, 1/3-plateau phase, FM phase at saturation field, TLL_1 and TLL_2 phase.

The magnetization-1/3 plateau accompanying the spontaneous breaking of the translational symmetry with the period 3 appears for $0.56 < \alpha < 1.25$, $\alpha = J_2/J_1$. the cusp singularities in the magnetization curve show quite interesting behavior [80, 81]. The high field cusp merges into the 1/3 plateau at $\alpha = 0.82$. The low field cusp also merges into the 1/3 plateau at $\alpha = 0.75$. However, it reappears at $\alpha > 0.7$. Two types of cusp mechanisms are discussed. One type of cusp is based on the shape change of the dispersion curve and other one attributed to the formation of the bound state related to the even-odd behavior of the magnetization curve. In the 1/3 plateau region the system shows "up-up-down" type long-range order and the gs has large excitation gap.

Since the boundary effect decays rapidly. In presence of anisotropy in the model, both gapless and gapped chiral phases, where the chirality has a finite LRO while the spin correlation falls either algebraically or exponentially have

been observed [83–85].

In case of FM J_1 and AFM J_2, the $J_1 - J_2$ model has been realized in many real materials, such as $LiCuSbO_4$ [41], $LiCu_2O_2$, [86], $Rb_2Cu_2Mo_3O_{12}$ [87], Li_2CuZrO_4 [43], $Ba_3Cu_3In_4O_{12}$ [88], $Ba_3Cu_3Sc_4O_{12}$ [89] etc. Literatures suggest [90], [91], [92] the existence of metamagnetic or spin multipolar phase in presence of the high axial magnetic field for by field theoretical and numerical studies. The phase is called multipolar because different number of magnon-bound pair is formed depending on the ratio of J_2 and J_1. The nomenclature of each phase is also set depending on the number of magnon bound state. It is called dipolar, quadrupolar, octupolar, and hexadecapolar phases depending on the numbers of bound pairs 1,2,3 and 4 respectively. The quadrupolar phase is a Tomonaga-Luttinger liquid of hard core bosons [91] and Each boson is composed of two magnons. Chubukov predicts that this phase has dimerized ground state (gs) [93], but it is shown that there is no dimerization in Hikihara *et al.* [91]. Pitch angle (θ), the binding energy (E_b), the order parameter (ρ_q) and the steps in the magnetization cuve are used to characterize the spin-nematic phase. The pitch angle (θ) can be calculated from spin density and spin-spin correlation function in Aslam *et al.* [90].

Binding energy is another interesting parameter to detect the spin-nematic phase. Binding energy is defined as

$$E_b(n) = \frac{1}{2}[E(n+2) + E(n) - 2E(n+1)] \tag{1.18}$$

Finite value of binding energy signifies formation of 2-magnon bound states i.e. flipping two spins is more favorable than flipping one spin if even number of spins are flipped. Multi-magnon bound state means many magnon bound states are favorable. The jumps in the M -h curve are a smoking gun-evidence for the condensation of magnons. For spin-nematic phase the jump in magnetization

curve is 2. In this phase the local parameter is defined as [90],

$$\rho_q = \langle \Psi_{n+2} | S_i^+ S_{i+1}^+ | \Psi_n \rangle \tag{1.19}$$

where $\langle \Psi_n |$ and $\langle \Psi_{n+2} |$ are gs of $S^z = n$ and $n+2$ spin sector. Both of these two sectors are degenerate in the presence of magnetic field. The order parameter gives a non-zero value in this phase. Dynamical structure factor $S(q, \omega)$ [94] can be also analyzed in order to detect the quadrupolar phase. It is also seen that the momentum of most intense peak of the structure factor varies linearly with M for a given magnetization.

Hikihara *et al.* [91] gave a detailed explanation of different types of multi-magnon bound states. Spin-nematic phase is analogous to Tomonaga-Luttinger liquid (TLL) of hard-core boson. It is described as the bound-state of two magnons with total momentum $k = \pi$. In this case transverse spin correlations, $\langle s_0^+ s_1^- \rangle$ is of short range order. Nematic correlations, $\langle s_0^+ s_1^+ s_l^- s_{l+1}^- \rangle$ as well as longitudinal spin correlatins $\langle s_0^z s_1^z \rangle - \langle s_0^z \rangle \langle s_l^z \rangle$ exhibit power law decay. In this phase, nematic correlations decay slowly than longitudinal spin correlations. Triatic phase is nothing but three magnon bound state with total momentum $k = \pi$. Correlation function $\langle s_0^+ s_1^+ s_2^+ s_l^- s_{l+1}^- s_{l+2}^- \rangle$ shows quasi-long range order. On the other hand both transverse correlations, $\langle s_0^+ s_l^- \rangle$ and nematic correlations, $\langle s_0^+ s_1^+ s_l^- s_{l+1}^- \rangle$ decay exponentially showing short range order. The longitudinal spin correlations $\langle s_0^z s_l^z \rangle - \langle s_0^z \rangle \langle s_1^z \rangle$ follows algebraic decay. In quartic phase, four magnons are condensed and can be detected using a similar approach. Characterization of spin-nematic and other multi-magnon states is still an open problem.

Sudan *et al.* [92] also predicted the existence of the VC and multipolar phases using the ED. The VC phase is another interesting phase. It is the kind of phase in which both the spin parity symmetry and the inversion symmetry should be spontaneously broken. The order parameter of this phase is calculated by means of the broken symmetry state in a finite magnetic field. The VC phase is

only present in a narrow region of the parameter space J_2/J_1 and its existence is demonstrated by means of ED and DMRG. The VC phase has tremendous potential applications in improper multiferroic systems [95].

Apart from this $1D$ model, many $2D$ systems such square lattice, Shastry-Sutherland lattice etc show different interesting phases in presence of magnetic field. Tsutomu *et al.* [96] has studied the Shastry-Sutherland lattice model in presence of magnetic field using strong coupling expansion method. In absence of field, the correlated hopping process forms bound states of triplet excitations. Above the critical field, the bound states of the quintuplets become elementary particles in the ground state and they condense, while at large magnetization the bound states in the ground state are destroyed and the triplet excitations become elementary particles. Triplet excitations are essential for the plateau transitions at $m_{sat} = 1/3$ and $1/2$. Magnetic excitations show insulator-supersolid transitions at magnetization $m/m_{sat} = 1/3$ and $1/2$ which create magnetization plateaus. K. Siemensmeyer *et al.* [97] predicted another $2D$ material TmB_4 which has an excellent realization of a frustrated magnet on the SSL by magnetization and neutron diffraction experiments. At low temperature and low field, the system is showing Neél order spin arrangement. On the other hand ferrimagnetic order is formed at high field limit and interestingly the intermediate phase with magnetization plateaus at fractional values $M = M_{sat} = 1/7$, $1/8$ and $1/9$. It is speculated that by mapping this model to the FQHE in a $2D$ electron gas with strong Coulomb interactions on a high-field lattice, a consistent description of plateaus and spatial structures can be obtained.

Recently ref. [98] studies the ground state and stability of the fractional plateau phase (FPP) with $M/M_{sat} = 1/8$ of this material. It has been demonstrated that in the same place of the phase diagram, both the stable and metastable (dynamic) fractional plateau states can be observed as it depends on the way in which they are reached. The FPP states are thermodynamically stable when the sample is cooled in a constant magnetic field. On the other hand, these

states appear to be of dynamic origin after zero-field cooling and subsequent magnetization.

The $J_1 - J_2$ Heisenberg model on a square lattice is another suitable candidate for investigation. A spin-1/2 Heisenberg antiferromagnet on a simple square lattice has been studied by Syromyatnikov *et al.* [99] using the bond-operator technique. It is observed that at high field, close to the saturation value, quantum fluctuations drastically change the dynamical properties of the model. Quantum fluctuations generate several short-wavelength magnon modes, which do not qualitatively change the long-wavelength spin dynamics.

The model becomes more interesting when nearest-neighbor interaction is of ferromagnetic type. The phase diagram consisted of canted AFM, nematic and FM phase [100]. In absence of magnetic field, the system does not show any nematic phase. On the other hand at larger J_2 limit, the nematic phase stabilizes in a narrow region near the pair-condensation field. The sequence of the multi-pair BEC transitions is suggested to bridge the d-wave pair BEC and the first-order FM-AFM transition lines [101].

1.6 Bose-Einstein condensation (BEC)

In general, BEC has been observed with bosonic atoms in liquid helium and cold gases [102]. Matsubara and Matsuda [103] pointed out an exact correspondence between a quantum antiferromagnet and a Bose lattice gas. A quasiparticle can be created in a spin system by exciting a spin wave. This quasiparticle is called magnon and like phonons, magnons also obey Bose statics with integer spin. However, the analogy between spins and bosons has turned out very fruitful in the antiferromagnetic systems where spin pairs $S = 1/2$ form dimers with a spin singlet ground state ($S = 0$) and a triplet ground state ($S = 1$). This type of triplet bosonic excitations are called triplons. The triplons are similar to magnons. There are many real materials such as $ACuCl_3(A = Tl, K, NH_4)$, $BaCuSi_2O_6$,

$Cu(NO_3)_2 \cdot 5D_2O$, $Cs_3Cr_2Br_9$, $(CH_3)_2CHNH_3CuCl_3$ and $(C_4H_{12}N_2)Cu_2Cl_6$ where BEC has been observed [104–109].

An isolated dimer has a ground state with a total spin of $S = 0$ and a triply degenerate excited state with total spin $S = 1$. If the interdimer interactions are weak, the ground state is composed of non-magnetic singlets, and it remains disordered down to absolute zero temperature with no long range magnetic order. When interdimer interactions are introduced into the system, the triplon excitations become mobile. External field (H) controls the triplon density. Phase diagram shows two critical points: H_{c1} and H_{c2}. The ground state is only consisted of singlets when $H < H_{c1}$. Here, ground state can be approximated by the direct product of singlet states on each dimer. Bose condensation occurs when spin gap vanishes. The critical properties of the magnet in the vicinity of this phase transition are determined by the quantum critical point (QCP) of the BEC universality class, which lies at $T = 0$ and $H = H_{c1}$. Close to the QCP, the phase boundary $T_c(H)$ has a power law behavior: $T_c \propto (H - H_c)^{\phi}$ where $\phi = z/d$, d is dimensionality and z is dynamical critical exponent.

When $H_{c1} < H < H_{c2}$ magnetization increases and more triplons are appearing in the ground state. Above H_{c2} magnetization attains its saturation value. Ref. [102] discussed some correspondence between Bose gas and quantum antiferromagnet which are listed below. (1) Triplons ($S = 1$ quasiparticles) can be compared with particles in Bose gas. (2) Total magnetization (S^z) is equivalent to boson number. (3) The field (H) in quantum antiferromagnet plays a similar role to the chemical potential in Bose gas. (4) On the other hand, transverse spin stiffness can be compared to superfluity density in Bose gas.

Inspite of all these types of similarities, there are lots of differences between Bose gas and triplons in quantum antiferromagnet. Here, Bose gas is treated under microcanonical ensemble whereas canonical ensemble is applicable in case of triplons as triplon density is controlled by external magnetic field [102]. In practicle case, there are a lots of differences between them. Triplons are much

lighter in weight and higher in density than atomic gases. Therefore condensates survive upto much higher temperatures in magnets. On the otherhand we that $U(1)$ symmetry in bose gas can be compared with $O(2)$ symmetry in quantum antiferromagnet. Cold atomic systems have the important advantages that the phase is exactly $U(1)$ symmetric. In case of magnets even very weak anisotropic interactions can break the corresponding $O(2)$ symmetry in the plane perpendicular to the magnetic field. Therefore experimentally, It is really challenging to apply the magnetic field exactly along a symmetry direction.

Experimentally, BEC materials are divided into three categories: (1) At First $T-H$ must be constructed and then various parameters must be estimated. (2) The uniaxial symmetry has to be verified by means of electron spin resonance and inelastic neutron scattering, and (3) various thermodynamic properties such as magnetization, specific heat etc. have to be calculated to observe how they depend on temperature. Nikuni *et al.* [104] has shown how the longitudinal magnetization $M_z(T)$ at constant magnetic field $H_{c1} < H < H_{c2}$ depends on temperature. Near phase boundary, Nikuni's results are

$$\frac{n(T)}{n(T_c)} = (\frac{T}{T_c})^{3/2}, T \geq T_c \tag{1.20}$$

$$\frac{n(T)}{n(T_c)} = 2 - (\frac{T}{T_c})^{3/2}, T < T_c \tag{1.21}$$

It indicates that at $T = T_c$, there is a minima in the magnetization curve and it explains the magnetization results of many real materials like $TICuCl_3$, $Pb_2V_3O_9$ etc. On the other hand the specific heat curve shows λ-like anomaly. Measurements on $TICuCl_3$ shows that this anamoly grows and shifts in temperature as the magnetic field is increased above H_{c1}.

Finally, It can be concluded that most of BEC has focused on $S = 1/2$

dimer systems. However, higher spins and dimers with higher spins like DTN, $Ba_3Mn_2O_8$, F_2PNNNO have shown BEC-related phenomennon [110].

1.7 String order parameter and topological phases

One of the most attractive areas in condensed matter physics is the study of topological phases in spin systems. Haldane phase is the most simplest example to understand the toplogical behavior. There are different topological classes of Haldane phases in odd and even integer spin (S). Even-S Haldane phase is not protected, it can be adiabatically transformed into the trivial phase [111]. On the other hand, the odd-S Haldane phase is non-trivial. Here the symmetries are protected.

Generally topology is identified by the presence of edge spin and exponential decay of singlet-triplet gaps as discussed by Haldane [112]. On the other hand, the hidden topological order can be fully identified and characterized by a set of nonlocal string order parameters. In 1989, Girvin and Arovas [113] has investigated a direct analogy between the topological order in integer quantum antiferromagnets and the topological order in the fractional quantum Hall effect (FQHE) by using the idea of Rommelse and den Nijs [114]. In 1992, Hida *et al.* [115] has investigated spin-1/2 alternating Heisenberg chain with alternating exchange couplings J and J'. Here, ground state changes continuously from Haldane to dimer phase. Here, the main intention is to reveal that these two phases are two extreme cases of a single phase. For that reason Hida introduced string correlation function $O^z{}_{str}(i-j)$ and string order parameter O^z_{str} which are defined below,

$$O^z_{str}(i-j) = -\langle S^z_i exp[i\pi(S^z_{i+1} + S^z_{i+2} + ... + S^z_{j-1}]S^z_j\rangle \tag{1.22}$$

$$O^z_{str} = \lim_{|i-j|\to\infty} O^z_{str}(i-j) \tag{1.23}$$

Here, S^z_i is the z-component of S. The order parameter remains finite in Haldane phase and it vanishes in trivial phase. Sometimes the system does not show the edge spin and also the singlet-triplet gap does not follow the exponential decay, in this case the entanglement entropy, in particular the entanglement spectra is used to characterize the topological nature of the system. The entanglement entropy (EE) of a state is a measure of the correlation or entanglement between two parts of a composite system, and it can show a significant change when the gs undergoes a qualitative change in a quantum phase transition (QPT). On the other hand, double degeneracy in entanglement spectra can identify the non-trivial phases [116].

1.8 Outline of the thesis

In the PhD thesis, I mainly studied low-dimensional frustrated spin-1/2 Heisenberg models on two-legged F-AF ladders and ferromagnetically coupled Shastry-Sutherland lattices (SSL). My thesis is organized in the following way:

Chapter 2: We used two numerical methods: exact diagonalization (ED) and the density matrix renormalization group (DMRG) technique to solve all the problems in my thesis. The details of these two numerical methods have been discussed in this chapter.

Chapter 3: This chapter considers a two-legged ladder model on both normal and zigzag ladder configurations with ferromagnetic (F) and antiferromagnetic (AF) legs and F/AF rungs. In the first part we discussed about normal ladder (NL) configuration. The quantum phase diagram is composed of five different quantum phases, such as the ferromagnetic, non-collinear ferrimagnetic (NCF),

$m - 1/4$, antiferromagnetic and dimer phase, which arise due to the competing exchange interactions in the system. Different phases are characterized using the correlation functions which are calculated by the density matrix renormalization group method. Most of the region in the phase diagram is dominated by NCF phase which shows quasi long range order behavior.

The second part of this chapter basically deals with F-AF bilayer model with zigzag ladder (ZL) configuration where spins on one leg is shifted by half of the lattice unit. In both of the cases it is observed that NCF is the most dominating phase which is showing quasi-long range order behavior. For larger AFM rung interaction limit NL forms dimer whereas ZL forms spin-fluid phase. For larger FM rung interaction, the spins of the two legs are ferromagnetically aligned for both of the ladders. Furthermore, a large magnetization plateau is observed in ZL in presence of magnetic field. This chapter is based on two works, one of them is published in chemphyschem (doi.org/10.1002/cphc.202200538) and other one will be submitted soon.

Chapter 4: We discuss ferromagnetically coupled distorted Shastry-Sutherland lattice (SSL) model, which gives a very rich phase diagram consisting of spiral, stripe, dimer and FM phases. The spiral phase was predicted by a previous study using mean-field calculations, but the ED could not confirm it. Our DMRG calculations confirm the spiral phase. We also calculated the phase boundaries using larger system size which is more accurate than the previous study. This manuscript is communicated (arXiv:2112.02975).

Chapter 5: We discussed the quantum phase diagram of AFAF model which consists of two ferromagnetic legs and alternating ferro- and antiferromagnetic rungs. The curvature $E''(s)$ of the states with lowest energy $E(s)$ per dimer and spin $0 \leq s = S/N \leq 1$ indicates that this model has three singlet quantum phases. The Dimer phase has $E''(s) < 0$ for one or more states. All states have $E''(s) > 0$ in the Haldane-DAF and AF phases. Increasing J_F leads to a $S = 1$ chain whereas for large J_L limit this system behaves like $J_1 - J_2$ model. This

work has been published in Phys. Scr. 99 025973 (2024).

Chapter 6: We examined the topological properties of this model in this chapter. We have developed spin-1/2 string correlation functions in general. String correlation functions directly probe spin correlations and their range in singlet ground states. They provide more information than the binary choice of finite range in gapped systems, infinite range in gapless systems, especially in systems with two spins-1/2 per unit cell. The minimum N^* of $g_2(N)$ is the estimated range of spin correlations at J_L, J_F and $J_A = 1$. This chapter is based on the published paper in Phys. Rev. B 109, 094439 (2024).

Chapter 7: Here, we have discussed how the ground state properties of this AFAF model is changed when magnetic field is applied. The jumps in the $M - h$ curve are a smoking gun-evidence for the condensation of magnons. These jumps in magnetization, $\Delta S^z = 2, 3, 4, ...$ represent quadrupolar, octupolar etc. phases. To understand the condensation process we also map the spin model Hamiltonian with hard-core boson model. In the dimer limit, each singlet dimer breaks up into triplons at the critical field, and these triplons form a Bose gas with zero chemical potential. In this work, we are analysing different types of this magnon condensation in detail, and this work is ongoing.

We have made a summary based on all the project works included in my thesis in **Chapter 8**.

Chapter 2

Numerical Method

2.1 Numerical method

We have already discussed in the first chapter of my thesis the importance of solving the model system in different dimensions due to its immense application in understanding different properties of real materials. We have also discussed how quantum fluctuations can affect the system. In general, it is very difficult to solve these models analytically. Only a few systems can be solved in the non-interacting or mean-field limit. The analytical methods include perturbation theory, spin-wave analysis [57], non-linear sigma model [112], field theoretical methods like bosonization [117] etc. The simplest model is the Ising model in the $1D$ case, and Onsager has solved this model in the $2D$ case. On the other hand, the Bethe approach has solved a few low energy states of isotropic spin-1/2 systems. However, most of the model Hamiltonians can be solved in different approximation methods which can be either analytic or numeric.

Any static or dynamic quantity of a system can be obtained only if the eigen-states of the model Hamiltonian of the system are available and for that the Hamiltonian of the system should be exactly diagonalized. In such scenario, the model Hamiltonian can be solved numerically in order to get the exact solu-

tions. Exact numerical method includes exact diagonalization (ED) where the total Hamiltonian is solved exactly means without any approximation and it is only applicable for finite system sizes due to exponential increase in basis size. If we consider fermionic system in that case each site has four possible electronic configurations which includes empty site $|0\rangle$, singly occupied site $\langle\uparrow\rangle$ or $\langle\downarrow\rangle$ and doubly occupied site $\langle\uparrow\downarrow\rangle$, in such systems both charge and spin degees of freedoms have been considered. So, total degrees of freedom is 4^N. On the otherhand for spin systems, total charge of freedom is completely frozen, here each site can have only two types of spin configuration either spin up $\langle\uparrow\rangle$ or spin down $\langle\downarrow\rangle$. In this case spin degrees of freedom is 2^N.

In my thesis, I have mainly used two numerical techniques: exact diagonalization for solving small systems as it is unable to solve large system size Hamiltonian due to the exponentially increasing dimension of Hamiltonian matrix with system size and DMRG for larger system size calculations. Exact numerical method includes exact diagonalization (ED) where the total Hamiltonian is solved exactly means without any approximation and it is only applicable for finite system sizes. On the other hand density matrix renormalization group (DMRG) method is an approximate numerical tool to solve larger system sizes which can be also useful to understand the systems in thermodynamic limit with some proper scaling or extrapolation. We are going to present a detailed discussion on these methods in this section.

2.1.1 Exact Diagonalization

Eigenvalues and eigenstates of the Hamiltonian are needed to understand various properties of the model Hamiltonian, and therefore the Hamiltonian matrix needs to be diagonalized. The model Hamiltonian can be diagonalized exactly by using exact diagonalization method which has basically three different steps: (a) Basis state should be first constructed. (b) After that many body Hamiltonian matrix

should be formed in that basis state. (c) Finally, the Hamiltonian should be diagonalized. For spin system z- axis is taken as the axis of quantization and the spins have only two types of spin configurations, either spin up (1) or spin down (0). The spin components along x- and y-axis are S^x and S^y repectively which can be expressed in terms of raising and lowering operators S^+ and S^- respectively.

$$S^x = \frac{1}{2}(S^+ + S^-) \tag{2.1}$$

$$S^y = \frac{1}{2i}(S^+ - S^-) \tag{2.2}$$

The Hamiltonian matrix becomes symmtric in this basis. For a $S = 1/2$ spin system the number of basis states goes as $NC_{N/2}$, $NC_{N/2-1}$, $NC_{N/2-2}$ .... where m_s is $0, 1, 2, ...$ respectively.

The entire Hilbert space is considered in this method and the dimension is increased exponentially with system size but the main advantage is that most of the matrix elements of a Hamiltonian with short range interaction are zero. So only the non-zero elements need to be stored in sparse matrix form.

On the other hand, according to quantum mechanics we know that if two operators commute with each other, then they must have a common set of eigenfunctions. In our discussion $[H, S^2] = 0$ as well as $[H, S^z] = 0$ i.e. Hamiltonian matrix commutes with both of the operators S^2 and S^z. The Hamiltonian matrix in a S^z basis is a block diagonal matrix for each of the conserved quantities of a system. This property of block diagonalization makes the system more efficient and also reduces the computational cost.

The situation becomes more complicated when frustration is coming into the picture due to the presence of huge degeneracy in gs and low-lying excited states. This makes it very slow to run, and also makes convergence very poor. To overcome this problem, different types of symmetry are used. The symmetry

operations such as translation, spin parity, inversion, etc., are used to separate the degenerate states in the different symmetry subspaces. Sometimes only one symmetry is used at a time and sometimes two symmetries are used together. We discuss briefly different types of symmetries briefly in the following:

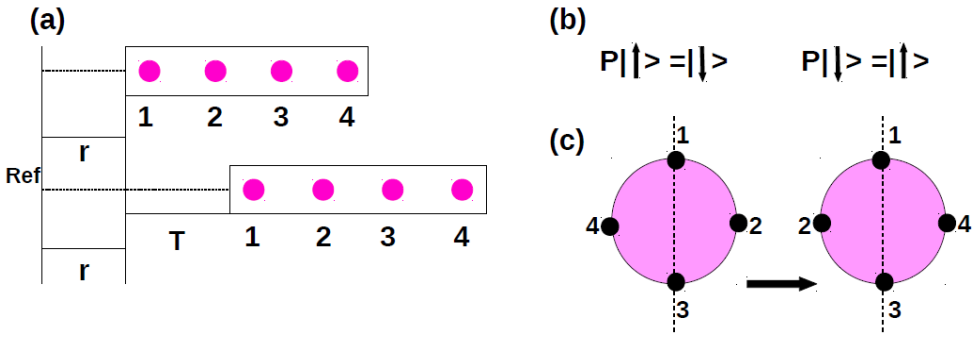

Figure 2.1: (a) Due to translational symmetry, the system shifts its location along a particular direction without any rotation or reflection. (b) Spin-parity symmetry flips spins at each site. (c) The system is rotated through an axis due to inversion symmetry.

(a) Translational symmetry: Translational symmetry is the invariance of a system of equations under any translation. For spin system if each spin is shifted to its next location, then the entire system will be invariant in periodic boundary condition (PBC) as shown in Fig 2.1 (a).

(b) Spin-parity: This symmetry is only valid for $S^z = 0$. Here, all spins are rotated by an angle π around x- and y-axis and total Hamiltonian remains invariant after this operation as shown in Fig 2.1 (b).

(c) Inversion: In this case all spins have a rotaion about an axis passing through site 1 and $N/2+1$ by an angle π and the Hamiltonian remains invariant in PBC as shown in Fig 2.1 (c).

Let U is a unitary symmetry operator of size $N_1 \times m$, after applying rotation operation the Hamiltonian in different symmetry subspaces becomes, $\tilde{H} = U^\dagger H U$

with dimension $m \times m$ where $N_1 > m$ i.e after applying the symmtry operations in the Hamiltonian, the dimension of the Hamiltonian in the new symmetry space is reduced. It makes the whole program more efficient and also removes the convergence issue created due to huge degeneracy in the gs and low lying excited state.

There are many algorithms like the Lanczos [62], modified Lanczos and Davidson methods [63] which can be used to find some low-lying energy states. In my thesis work, we have used Retrup's algorithm [118] which is a modification of the Davidson algorithm to a non-symmetric matrix. The brief outline of the Retrup's algorithm is given below.

(1) Let us consider H is a large sparse Hamiltonian matrix with dimension $N \times N$.

(2) Now, we also consider a set of n orthonormal guess vectors, $(\boldsymbol{v}_i : i = 1, 2, ..., n)$.

(3) Next, a small matrix $h^{(n)}$ has to be constructed with these initial guess vectors so that $h_{ij}^{(n)} = \langle \boldsymbol{v}_i | H | \boldsymbol{v}_j \rangle$.

(4) Now, $h_{ij}^{(n)}$ is diagonalized by exact diagonalization routines,

$$h^n \boldsymbol{a}_k^{(n)} = \lambda_k \boldsymbol{c}_k^{(n)}, \qquad k = 1, 2, ..., m \tag{2.3}$$

(5) Here, $\boldsymbol{a}_k^{(n)}$ are the eigenvectors of the corresponding eigenvalues λ_k of the small matrix.

(6)Approximate eigenvectors of the large matrix can be written as,

$$\boldsymbol{C_k}^{(n)} = \sum_{i=1}^{n} c_k^{(n)}(i)\boldsymbol{v}_i \tag{2.4}$$

Where, ${c_k}^{(n)}$ is the i^{th} component of k^{th} eigenvecor of the small matrix.

(7) The i^{th} component of correction vector, $\boldsymbol{P}_k^{(n)}(i)$ is,

$$\boldsymbol{P}_k^{(n)}(i) = \frac{\boldsymbol{R}_k^{(n)}(i)}{\lambda_k^{(n)} - H_{ii}} \tag{2.5}$$

(8) The residual vector $\boldsymbol{R}_k^{(n)}$ is given by,

$$\boldsymbol{R}_k^{(n)} = (H - \lambda_k^{(n)} I)C_k^{(n)} \tag{2.6}$$

Here, I is the unit matrix.

(8) The initial space $(\boldsymbol{v}_i : i = 1, 2, ..., n)$ is now expanded with a normalized vector obtaining from Gram-Schmidt orthogonalization of $\boldsymbol{P}_k^{(n)}$ to the set of vectors $(\boldsymbol{v}_i : i = 1, 2, ..., n)$ i.e.,

$$\boldsymbol{v}'_{n+1} = \boldsymbol{P}_k^{(n)} - \sum_{i=1}^{n}(\boldsymbol{P}_k^{(n)} \cdot \boldsymbol{v}_i)\boldsymbol{v}_i, \qquad \boldsymbol{v}_{n+1} = \frac{\boldsymbol{v}'_{n+1}}{||\boldsymbol{v}'_{n+1}||} \tag{2.7}$$

(9) The whole procedure is then repeated until the threshold is exceeded by the dimensionality of the small matrix.

(10) The iteration is finished when the eigenvalue converges within a chosen accuracy.

Drawback:- The computational cost in the above method varies as N^2 , therefore, larger system size can not be solved by using this method. However the gs and few low-lying excited state calculations can be done using different types of symmteries upto system size of 36. For, larger system size calculations, one can use other reliable approximate numerical techniues like Quantum Monte Carlo (QMC), renomalization group (RG) [119], matrix product state (MPS) [120] etc.

2.1.2 Density Matrix Renormalization Group Method:-

We have already discussed that it is very difficult to solve the quantum many-body problem for larger system sizes as the dimension of Hilbert space increases exponentially with system sizes. Let the dimension of Hilbert space is d. If the system size is L, then the dimension of Hilbert space will be d^L. For spin system it will be 2^L as $d = 2$ for such systems. On the other hand for fermionic system $d = 4$, in that case the dimension of total Hilbert space is 4^L. The DMRG is an iterative, variational method that reduces the effective degrees of freedom to the ones that are most important for a given target state. The most interested state to be studied is the ground state. Steve White first introduced this method in 1992 [121]. It is mainly based on mainly exact diagonalization (ED) and numerical renormalization group (NRG) tecnique. In 1975, Wilson applied the renormalization group (RG) method to the Kondo lattice [58, 59] and achieved great success. Later, this method was extended to solve the gs of quantum many-body systems in real space. However, the results of real space

RG in quantum systems turned out to be quite inaccurate. White explained the main reason for the failure of this method and proposed a new technique called the DMRG method, which retains only the states with the largest eigenvalues of the density matrix of the system block and performs a truncation of irrelevant degrees of freedom.

DMRG technique has an immense application in studying different types of systems ranging from Ising model in transverse field, Heisenberg model, fermionic systems, bosonic systems even up to Kondo effects, quantum dot problems. My thesis is based on the study of spin systems with different models in various dimensions. This method is very helpful to handle such spin-1/2 systems in $1D$ and quasi $1D$ cases. Additionally, it is also capable of producing satisfactory and accurate results for $2D$ cases. Different quantities like spin-gaps, spin-spin correlations, string correlations, spin-density can be calculated for larger system sizes by using this method with very high accuracy. It is not only capable of dealing with spin-1/2 systems, but many systems such as spin-3/2 [122], spin-2 [123] Heisenberg chains can also be solved numerically using this method. Different types of quasi-$1D$ systems like two-leg ladder with normal ladder configuration, zigzag ladder configuration, 3/5, 5/7 skewed ladders can be also studied very successfully. $2D$ systems like square lattice [124,125], triangular lattice [101,126], Kitaev model [127,128], Shastry-Sutherland lattice [66,129], kagome structure [130,131] can be also investigated by using this method. This method can not only helpful to deal the static properties but it can also help to observe the dynamic properties. Thermodynamic properties like specific heat, magnetic susceptibility in low-dimension for both spin and fermionic systems can be also studied by this method. DMRG method is consisted of two algorithms:

(a) **Infinite algorithm:** Here, new sites are added at each iteration until the desired system size is achieved (b) **Finite algorithm:** After the infinite algorithm, finite algorithm is applied in order to get more accuracy in the result.

Now, in the fillowing we have given an elaborate discussion on this tecnique:

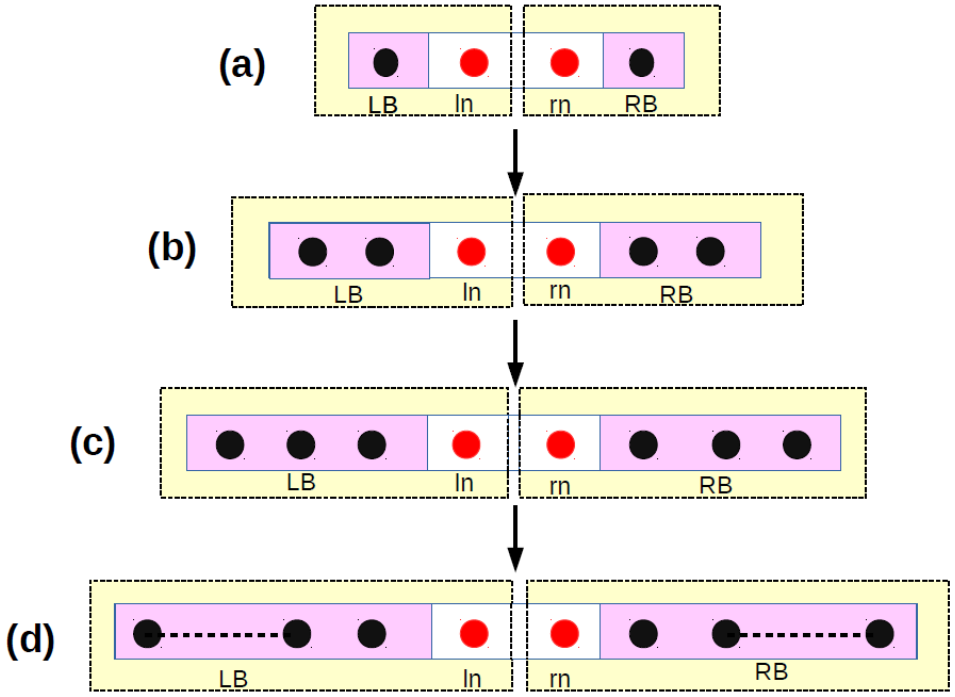

Figure 2.2: A schematic diagram of infinite DMRG is shown. Black and red circles denote the old and new sites respectively. Black dashed boxes represent the system and environment blocks respectively.

Let us consider four sites consisting of a superblock which is containing left block (LB), right block (RB), left new site (ln) and right new site (rn) as shown in Fig. 2.2. The Hamiltonian of the superblock is $H = H_{LB} \otimes H_{ln} \otimes H_{rn} \otimes H_{RB}$. Now, the whole superblock is devided into system block (i) and environment block (j). System block contains left block and left new site. On the other hand environment block is composed of right block and right new site. Now, we have to calculate the gs eigenvalues and eigenvectors and we have to construct the eigen function ψ in terms of new basis of system and environment block:

$$|\psi\rangle = \sum_{ij} C_{ij}|i\rangle|j\rangle \tag{2.8}$$

Here, $|i\rangle$ and $|j\rangle$ are the basis states of system and environment blocks. The matrix element of the density matrix of system block is

$$\rho_{ij} = \sum_{k} C^{*}_{ik} C_{kj} \tag{2.9}$$

The major contribution comes from the most probable eigenstates of the density matix. So, we only retain the eigenstates with largest eigenvalues of density matrix. Let us consider the dimension of density matrix (ρ) is $M * M$. Now a reduced density matrix (ρ') has to be constructed which will keep only the largest eigenvectors corresponding to the largest eigenvalues. Now, the dimension of the new reduced density matrix will be $M \times m$ where ($M > m$). The next step is to renormalize all operators involved in the system block with new density matrix basis. The renormalized Hamiltonian and operators can be now written in the form.

$$\tilde{H} = (\rho')^{\dagger} H \rho' \tag{2.10}$$

$$\tilde{O} = (\rho')^{\dagger} O \rho' \tag{2.11}$$

Here, $\tilde{H}$ and $\tilde{O}$ represent the effective Hamiltonian and operators in the new system block. $(\rho')^{\dagger}$ is the transpose of (ρ'). Now we add two new sites with system and environment blocks and the whole composite system form the new superblock. Now the new superblock has to be diagonalized and all the steps described in the above should be repeated again unless until the desired system size is achieved. Now, the above elaborate process is summarized below:

(1) The process has been started with four sites which forms superblock.
(2) The eigenvalues and corresponding eigenvectors are now calculated by diagonalizing the superblock.
(3)The density matrix (ρ) of the system block is constructed from the obtained eigenvectors.
(4) Now ρ is diagonalized and only the eigenvectors corresponding to the largest eigenvalues are kept which reduce the dimension the density matrix.
(5) The operators and the Hamiltonian are now renormalized in the new reduce density matrix space.
(6) Now again two new sites are added with system and environment blocks which construct the new superblock.
(7) After that the above steps from (2) to (5) have to be repeated unless until the desired system size is achieved.

After performing the infinite algorithm, we might not be able to achieve sufficient accuracy when calculating different ground state properties such as spin-spin correlations, spin density, string correlations, etc. This is happening due to a lack of adequate wavefunctions. Finite algorithm in the DMRG process should be performed in order to get an accurate result. Now, this algorithm is discussed below along with a schematic diagram as shown in Fig 2.3.

(1) At the end of the infinite algorithm, the desired system size has been achieved, and the superblock contains an equal number of sites for both the left and right blocks. The finite algorithm starts with the diagonalization of this superblock obtained at the end of the infinite algorithmic procedure.

(2) The gs eigenvectors are now found out.

(3) A new site will now be added to the system block and a site will be re-

moved from the environment block so that the total size of the system remains the same. Now the system block is consisted of old left block and one new site. Now, the reduced density matrix is formed.

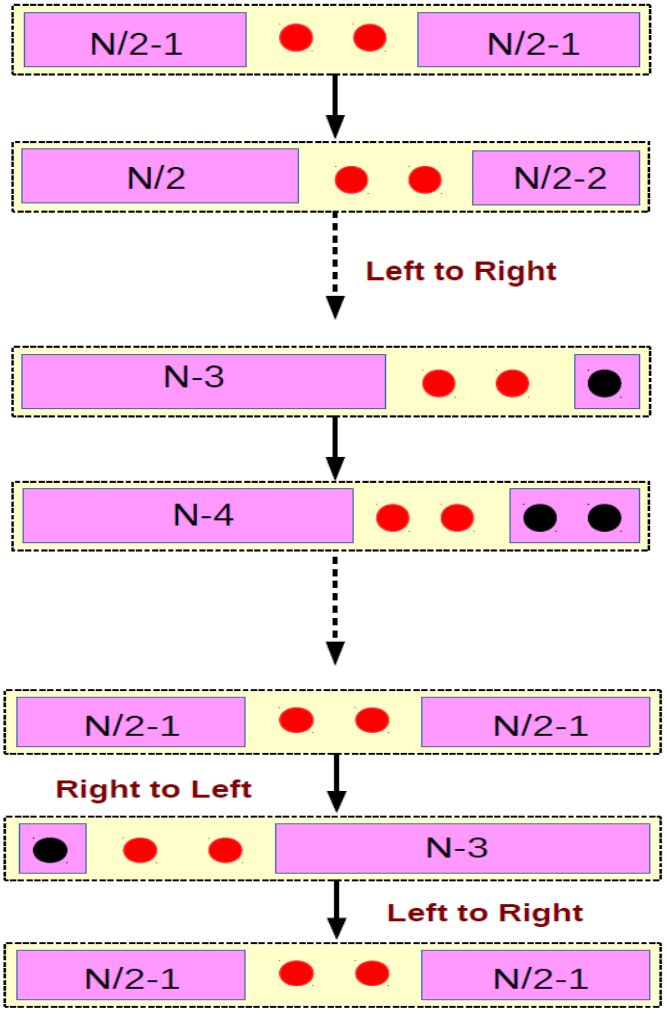

Figure 2.3: The finite DMRG for a $1D$ chain is shown schematically. The black circles represent the new sites. Black dashed box is the final system size reached at the end of the infinite algorithm. Pink boxes represent the left and right blocks of unequal lengths.

(4) Hamiltonian and operators of the system block are new renormalized in the new reduce density matrix space.

(5) Now one more new site is added to left block and the right block is shrunk. All the steps are repeated until the right block is reduced to a single site .

(6) Now right block is grown in size following the above steps unless until the left block is reduced to 1.

(7) In the final stage, new sites are added to the left block and sites are removed from the right block, and finally we reach a step where the left and the right block have the same size. This is called as one finite sweep. Generally, in order to get sufficient accuracy $7-8$ finite sweeps have to be taken.

DMRG algorithm works very well for $1D$ and even for quasi-$1D$ systems in open boundary condition (OBC) but in order to get rid of the edge effect in some cases we have to use the periodic boundary condition (PBC) but DMRG with PBC has also some drawbacks:

(1) The number of eigenvectors is greater in the case of PBC compared to the OBC algorithm. Let m be the number of eigenvectors in the density matrix in the OBC condition, in this case the number of eigenvectors required for PBC to achieve the same accuracy is m^2.

(2) The computational cost goes as m^6 for PBC, whereas for OBC it is m^3.

(3) In the conventional DMRG algorithm, the spin operators that form superblock are involved in a single renormalization for the OBC system, but in the case of PBC, at least two spin operators are renormalized repeatedly. The multiple time renomalization drastically reduces the accuracy.

In order to overcome all of the drawbacks of the DMRG algorithm in PBC, a modification has been done in the algorithm which is now discussed below.

Modified DMRG: It is observed that the multiple time renormalization of the of the creation and annihilation operators, i.e. S^+ and S^- for spin systems and a^+ and a^- respectively for fermionic systems, reduces the accuracy of the operators. It is also observed that the accuracy is significantly increased when the multiple renormalization has been avoided. In this new algorithmic process, new sites are added at both ends of the chain so that the superblock is formed by the second time renormalized operators.

In the conventional dmrg method, a large number of non-zero matrix elements are produced in the superblock Hamiltonian matrix due to the old-old sites interactions and the diago nalization of dense matrix goes as m^4 . But, here, the algorithm is formulated in this new process so that old-old sites interactions can be avoided and only old-new sites interaction are considered in the superblock which generates only a sparse Hamiltonian matrix, and its digonalization goes as m^3. Here, m is denoted as max.

The algorithms used in this modified process are discussed point by point below with a schematic representation as shown in Fig 2.4:

(a) At First, the superblock is made up of four sites. Each block contains only one site, among them two blocks are left block and right block respectively and on the other hand two other blocks are left new site block and right new site block. New blocks may contain more than one new site depending on the geometry of the model system.

(b) Now the superblock is diagonalized to obtain the eigenvalues and corre-

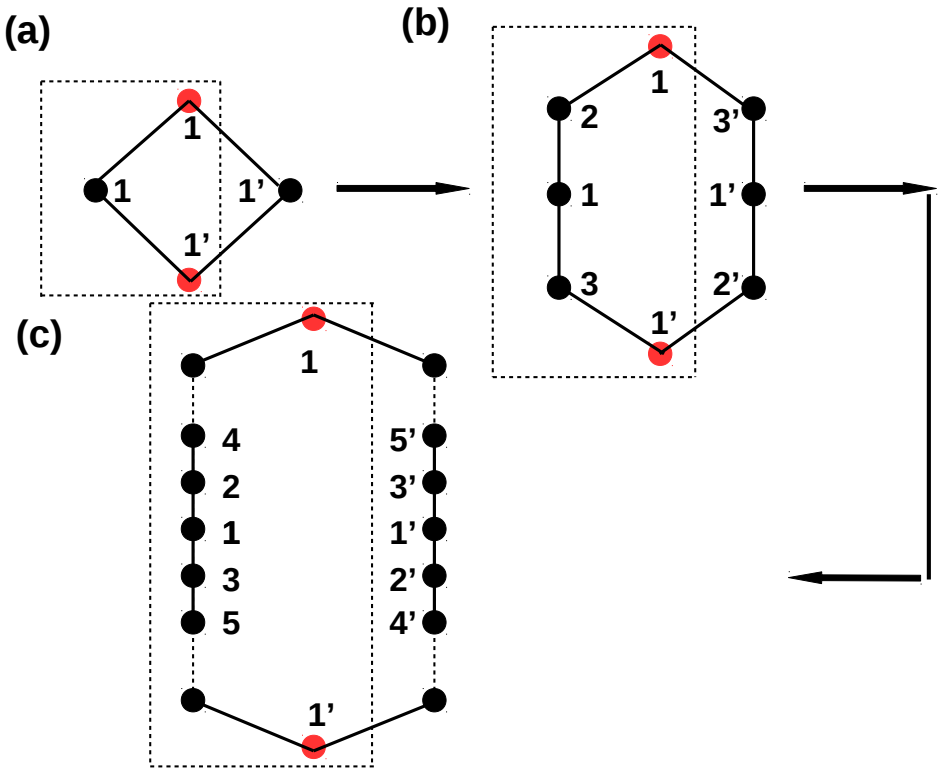

Figure 2.4: Schematic representation of the modified DMRG algorithm: (a) The algorithm can be started with one site at each block represented by black circles, and the two red circles are the new sites. The dashed box is the system block for the next step. (b) The superblock of the next DMRG step is shown. (c) Final step of the infinite DMRG consisting of the left and right blocks and two new sites.

sponding eigenvectors. Then the density matrix (ρ) is constructed, consisting of the left or right block and the two new site blocks.

(c) Now the reduced density matrix (ρ') is formed by taking only m number of largest eigenvectors corresponding to m number of largest eigenvalues.

(d) The operators and the Hamiltonian are now again renormalzed in the new reduce density matrix space following Eq. 2.10 and 2.11.

(e) Superblock is constructed using the effective Hamiltonian and operators

of the system block and two new sites.

(f) Now, steps from (b) to (e) are repeated till the desired system size is reached.

This method is very much helpful for $1D$ chain and as well as quasi-$1D$ ladder model. In my thesis work, I used this modified dmrg method for two-leg ladder model which gives us very fruitful and accurate results regarding to different quatities like string order correlations, singlet-triplet gap etc in PBC.

Chapter 3

Study of two-leg ladder system with ferro- and antiferromagnetic legs

3.1 Introduction

The competing interactions in frustrated magnetic systems may induce a zoo of exotic quantum phases and transition from one phase to the other can be tuned by changing the exchange parameters in the system [1, 19, 32, 34, 36, 132–134]. The confinement of electrons in these systems enhances the quantum fluctuations leading to strong quantum effect and the ground state (gs) behaves very differently from the corresponding classical system [135–137]. In principal, most of the solid materials are three dimensional. However, the magnetic exchange interactions can be confined only in some particular directions e.g. one dimensional ($1D$) systems like $LiCuVO_4$, $LiCuSbO_4$, Li_2ZrCuO_4, $(N_2H_5)CuCl_3$ are three dimensional solids but the localized spins are coupled effectively in one particular direction [40–43]. In order to model these solid state systems the simplest frustrated $1D$ model system is $J_1 - J_2$ model where J_1 and J_2 are ex-

change interactions between nearest and next nearest neighbor spins and this model exhibits interesting quantum gs phases such as gapless quasi-long range ordered phase [1, 34, 36, 133, 138], dimer phase [32, 35, 132, 133, 138], spiral order [36, 138, 139] etc.

In some cases spin exchange interactions are not restricted along one direction, but rather these chains can interact with their nearest neighbor chains and form spin ladder or quasi-one dimensional like structures [38, 39, 140] which may act as the bridge between one and two dimensional spin systems. Therefore, study of these systems may play a vital role in understanding crossover between one to two dimensional systems [88, 141, 142].

In last few decades, many quasi-one dimensional quantum spin materials such as $(VO)_2P_2O_7$ [39, 140], $SrCu_2O_3$ [38] etc have been synthesized where dominant spin exchange interactions act along weakly coupled ladders. The ladder with even number of legs effectively behaves like an integer spin chain with a large spin gap in the low energy spectrum and $(VO)_2P_2O_7$ [39, 140], $SrCu_2O_3$ [38] etc. are the examples of two-leg ladder materials exhibiting large spin gap. Odd leg ladder behaves as half odd integer spin chain and does not show presence of any gap to its lowest excitation. For example, the three chain ladder material $Sr_2Cu_3O_5$ shows gapless excited states [143].

Frustrated zigzag spin-1/2 ladder systems provide an opportunity to study various kinds of exotic phases like dimer phase [28, 138, 144], spiral phase [28, 138], ferromagnetic (FM) phase etc. at various rung interaction limit. The most important fact is that these kinds of spin-1/2 ladder structures are realized in many real materials. As for example, $SrCu_2O_3$ [38], $(VO)_2P_2O_7$ [39, 140] are the materials where Heisenberg antiferromagnetic (HAF) spin-1/2 normal ladder kind of structures are observed, whereas, $(N_2H_5)CuCl_3$ [40], $LiCuSbO_4$ [41], $LiCuVO_4$ [42], Li_2CuZrO_4 [43] etc. show the zigzag ladder kind of structures. The spin correlations in antiferromagnetic (AFM) normal ladder are short range in nature even though the system is non-frustrated. In fact, this system has finite

spin gap for any finite value of rung interaction due to formation of singlet dimer along the rung [35, 145, 146].

Two leg spin-1/2 ladder systems may have spins on one leg interacting by FM exchange interaction whereas on the other leg spins interact with AFM exchange interaction and nearest neighbor spins from two different legs can interact with either FM or AFM interaction as shown in Fig. 3.1. One can map this type of system as a interface of the two layered magnetic spin-1/2 system consisting of an AFM and a FM layer. In this case the two layers interact with direct AFM/FM exchange. Some preliminary information about the phases at the interface of bilayer FM-AFM magnetic thin films can also be obtained through the study of these spin-1/2 models. Suhl *et al.* [147] and Hong *et al.* [148] have shown similar interfaces by means of spin wave theory. This model is further simplified by considering only a inter-facial line of spins in the interface of both the layers. In this chapter, we will discuss the properties of this type of ladder model with two different spin configurations. We consider the arrangement of inter-facial spins in such a way that the the spins are directly facing each-other, generally called as normal ladder (NL) configuration. These NL are frustrated and the gs stabilizes the dimer singlet, non-collinear spin wave and ferri-magnetic phase [28,48]. Other type of spin configuration is called zigzag ladder (ZL) where spins on one leg is shifted by half of the lattice unit. In the first section, we will discuss about NL and ZL will be discussed in second section of this chapter.

3.2 Quantum Phase Diagram of a Frustrated Spin-1/2 Ferro-Antiferromagnetic Normal Ladder

The NL system exhibits ferrimagnetism and it can be explained in terms of Lieb–Mattis (LM) [21] theorem. The spin arrangements in NL is shown in the

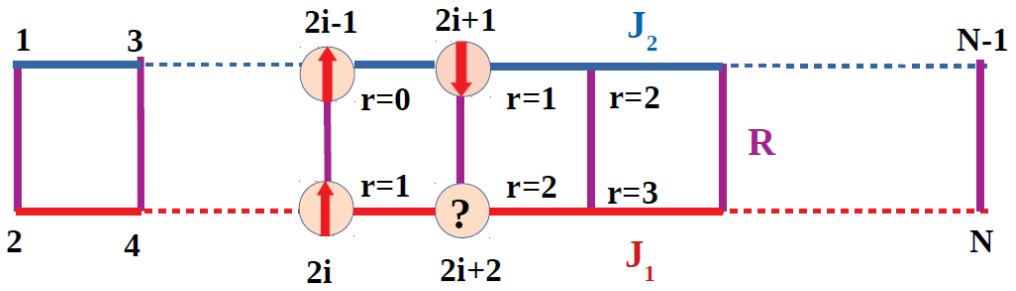

Figure 3.1: A schematic representation of FM-AFM model. The up and down spins on sites are shown by the arrows. The AFM exchange in one leg leads to frustration in spin orientation which is denoted by the question marked site. Rungs are indexed by i and sites on the upper and lower legs are indexed by $2i-1$ and $2i$, respectively, where i varies as $i = 1, 2, .., N/2$. The distance of spins from the reference spin at site $2i-1$ is denoted by r.

Fig. 3.1. This system is frustrated irrespective of the nature of rung exchange interactions. This ladder geometry with AFM inter-leg interaction has been studied in ref [28] keeping the interaction strength of both the leg same (J_1=J_2) and it was shown that the ground state magnetization is proportional to R^2 where R is AFM rung interaction. The results agree well with spin wave theory studies. The existence of decoupled, spiral and dimer phase have been shown for this model. In this chapter, we consider a more general model of two leg normal ladder which has different interaction strength along each of the legs and rung interaction can be either ferromagnetic or antiferromagnetic as shown in Fig. 3.1.

We study the gs properties and construct quantum phase diagram of this spin-1/2 ladder with Heisenberg FM exchange interaction J_1 in one leg, Heisenberg AFM exchange interaction J_2 in other leg and Heisenberg inter-leg exchange interaction (R). Here we plot the complete phase diagram in J_1-R plane. We have characterized the phases depending on magnetization and on the nature of the spin-spin correlations.

We have divided this section into few subsections. In Subsec. 1, we have discussed about the model Hamiltonian and the numerical methods which we have used here. Numerical results are given from Subsec. 2 to 6.

3.2.1 Model Hamiltonian and Numerical Method

In this work we consider a two leg ladder which has ferromagnetically coupled spins on one leg, whereas spins on the other leg are anti-ferromagnetically coupled, and spin on one leg interacts with its neighboring spin on the other leg through a rung interaction as shown in Fig. 3.1. The model Hamiltonian can be written as

$$H = H_{leg} + H_{rung}, \tag{3.1}$$

where

$$H_{leg} = \sum_{i=1}^{N/2-1} -J_1 \, \boldsymbol{S}_{2i} \cdot \boldsymbol{S}_{2i+2} + J_2 \, \boldsymbol{S}_{2i-1} \cdot \boldsymbol{S}_{2i+1}, \tag{3.2}$$

$$H_{rung} = R \sum_{i=1}^{N/2} \boldsymbol{S}_{2i-1} \cdot \boldsymbol{S}_{2i}. \tag{3.3}$$

The first term in Eq. 3.2 represents the FM exchange interaction J_1 between nearest neighbor spins along the lower leg and the second term represents the nearest neighbor AFM exchange interaction J_2 along the upper leg. Eq. 3.3 represents the exchange interaction between two neighboring spins on lower and upper legs or the rung interaction R. J_2 is set to 1 and defines energy scale in the system and J_1 and R are variable parameters.

We have used two numerical methods to solve the Hamiltonian in Eq. 3.1: exact diagonalization (ED) is used for small system sizes up to $N = 24$ spins and density matrix renormalization group (DMRG) technique is used for large system sizes. The DMRG method is based on systematic truncation of the irrelevant degrees of freedom at every steps of the growth of the system and it is a state-of-the-art numerical technique to solve one or quasi-one dimensional strongly correlated systems [121, 149]. In the conventional DMRG method the superblock

is formed using multiple times renormalized operators for a ladder system, and the multiple times renormalized operators reduce the accuracy of eigenvalues and vectors. Therefore, we use four sites DMRG algorithm where four sites are added at each step, and in this way the usage of twice renormalized operators to construct the superblock has been avoided [139, 150]. All the calculations are done for system with open boundary condition (OBC), and 300-400 eigenvectors of density matrix and 3-4 finite sweeps in our calculations are sufficient to keep the truncation error 10^{-10}.

3.2.2 Results

The main focus of this paper is to study the quantum phase diagram (QPD) in R-J_1 parameter space of the frustrated spin model in Eq. 3.1. In this parameter space of the model there are five quantum phases (QP): FM, non-collinear ferrimagnetic (NCF), $m - 1/4$, AFM and dimer phase. The phase boundaries are determined based on the nature of correlation functions and the nature of magnetization at the phase boundaries in different R limit is also analyzed. Stability of the ferrimagnetic state with R in presence of frustration is also studied. The NCF phase is sensitive to the R, therefore, magnetization as well as the pitch angle (θ) in this phase changes with R. All the results are presented into four subsections and in the first subsection we discuss the QPD of this model.

3.2.3 Quantum Phase Diagram

This model exhibits interesting quantum phases due to competing J_1 and R exchange interactions and there are five major quantum phases as shown in Fig. 3.2 in $R - J_1$ parameter space. In large FM R limit, the gs is in the FM state if $J_1 >> J_2$ and parallel spin arrangement is shown in Fig. 3.3 (a). For ferromagnetic R and moderate value of J_1, spins on the FM leg are arranged ferromagnetically, whereas these are arranged antiferromagnetically on the other

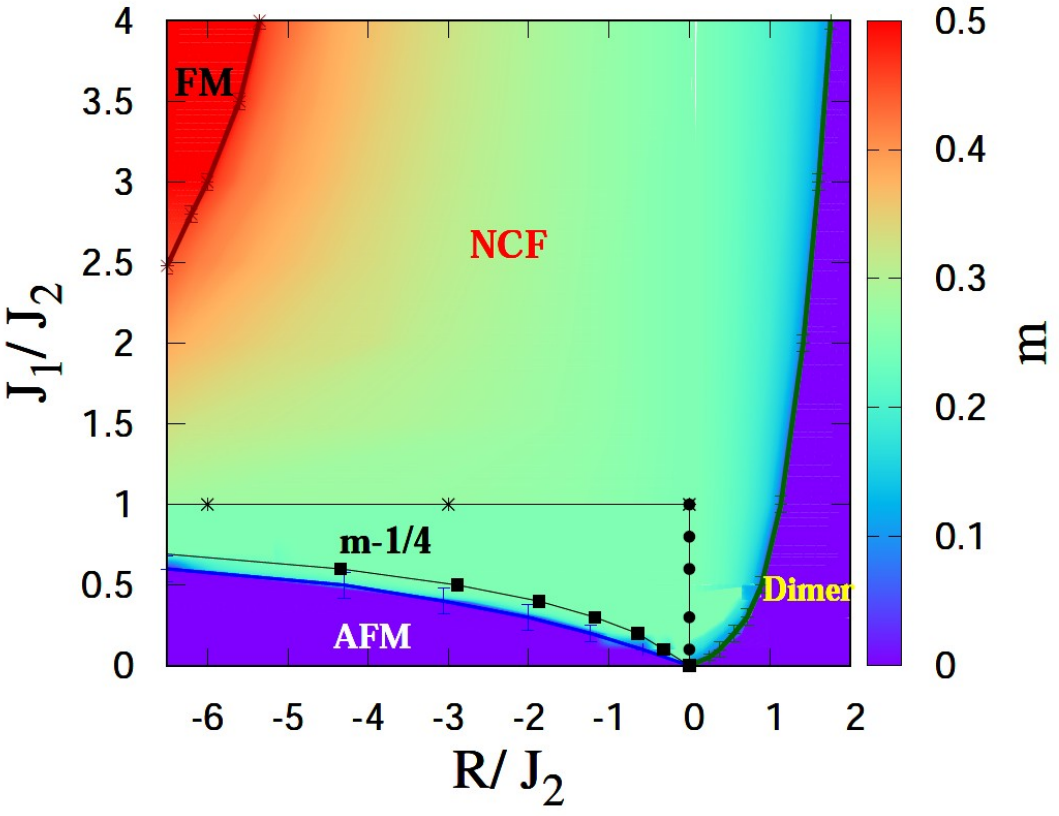

Figure 3.2: The quantum phase diagram of the Hamiltonian in Eq. 3.1 in J_1/J_2 vs. R/J_2 parameter space. Five different phases are observed for $-6 \leq R/J_2 \leq 2$ and $0 \leq J_1/J_2 \leq 4$. The phase diagram is mostly dominated by non-collinear ferrrimagnetic (NCF) phase. AFM and $m-1/4$ phase survive for small J_1/J_2 and $R/J_2 \leq 0$, whereas dimer phase is found at $R/J_2 > 0$. The FM alignments of spins can occur only at large J_1/J_2 and $R/J_2 < 0$. The color gradient represents the per site magnetization m.

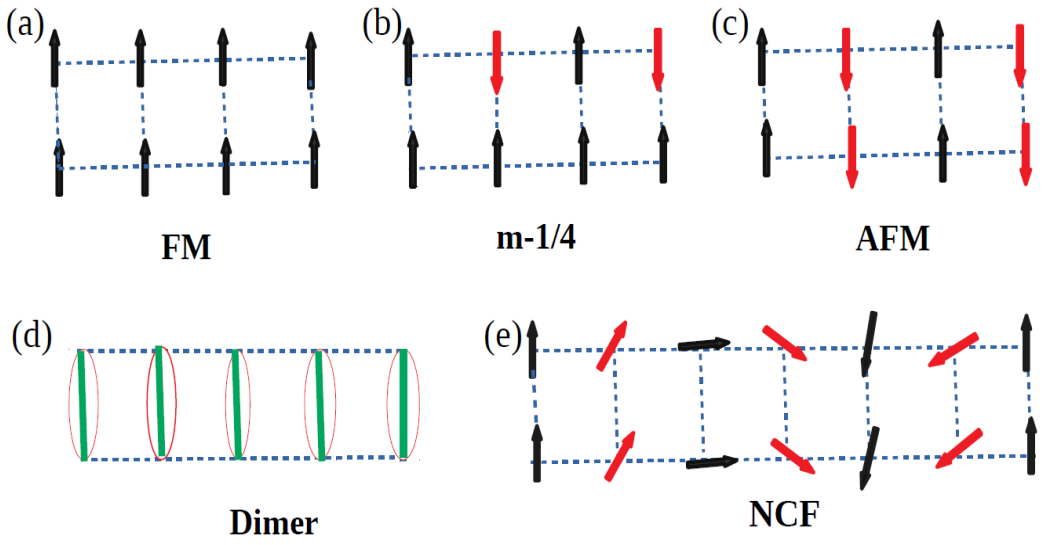

Figure 3.3: The schematic representation of different phases present in this model; (a) FM phase, (b) $m - 1/4$ phase, (c) AFM phase, (d) dimer phase and (e) NCF phase. The spin alignments are represented by the arrows, ellipses indicate dimers and green lines denote singlet bonds. See the text for details.

leg as the AFM exchanges still dominate. We call this phase as m-1/4 phase and this phase has moderate frustration as shown schematically in Fig. 3.3 (b). The gs has AFM spins arrangement in both of the legs for $J_2 >> J_1$ as shown in Fig. 3.3 (c). In this limit FM R leads to form the spin-1 along the rung, therefore, even on the FM leg AFM arrangement of spins develops.

In the moderate value of $J_1/|R|$ frustration in the system dominates and the non-collinear arrangement of the spin sets in the gs as shown in Fig. 3.3 (e). The magnetization in this phase can decrease or increase for AFM and FM R, as shown in color plot in Fig. 3.2. In the AFM R limit the rung bond forms singlet dimer in weak J_1 limit, but in strong J_1 limit the gs can have finite m and noncollinear arrangement of spins. Strong AFM rung exchange R limit the two spins from different legs can form perfect dimer and the gs wavefunction can be represented as product of the singlet dimers. The dimer phase in the gs induces

a short range order in the system and spin arrangement can be shown in Fig. 3.3 (d). In the FM, the NCF and the m-1/4 phases the magnetic moments are finite and have complex behavior, therefore in the next subsection we analyze the behavior of m as well as the stability of m-1/4 phase.

3.2.4 Magnetization and Stability of $m - 1/4$ Phase

The competing interactions $J_1 - J_2 - R$ in the system lead to frustration which may lead to non-trivial magnetic behavior. If both the legs are non-interacting ($R = 0$) then the per site magnetization m is 1/4, and mostly the non-zero magnetization contribution comes from the FM leg. In fact the ferrimagnetic phase is most dominant phase in the QPD in parameter space of $R - J_1$ as shown in Fig. 3.2. The variation of m as a function of $R(< 0)$ is shown for strong $J_1 = 2$ FM exchange limit for three system sizes in Fig. 3.4 (a). The inset shows $m - R$ curve in small R limit and m varies linearly with R. The gs is fully ferromagnetic in large R limit and in this case spins on FM leg dominates and align all the spins on AFM leg. The FM exchange R acts as an effective magnetic field on AFM leg and variation of m with R goes linearly upto $|R| = 6$.

In the weak $J_1 = 0.6$ limit, the interaction of AFM leg dominates and try to align the FM leg in AFM arrangement in large $|R| > 6.5$ limit. In the intermediate limit $(4.5 < |R| < 6.5)$, m decreases rapidly as shown in main Fig. 3.4 (b), and variation of m can be fitted with function

$$m = \alpha[1 - (R/R_c)^{\beta}]^{\gamma}, \tag{3.4}$$

where $\alpha = 0.25$, $\beta = 13.08$ and $\gamma = 0.742$. Here, R_c is ≈ -6.45. The fitting of the curve is shown in the inset of Fig. 3.4 (b). In small $|R| < 4.5$ limit $m - 1/4$ state is stable and shows long range order in AFM leg. In $4.5 < R < 6.5$ parameter regime, m weakly depends on system sizes. We note a ferrimagnetic regime of m with R and the finite size effect of width of this regime is weak.

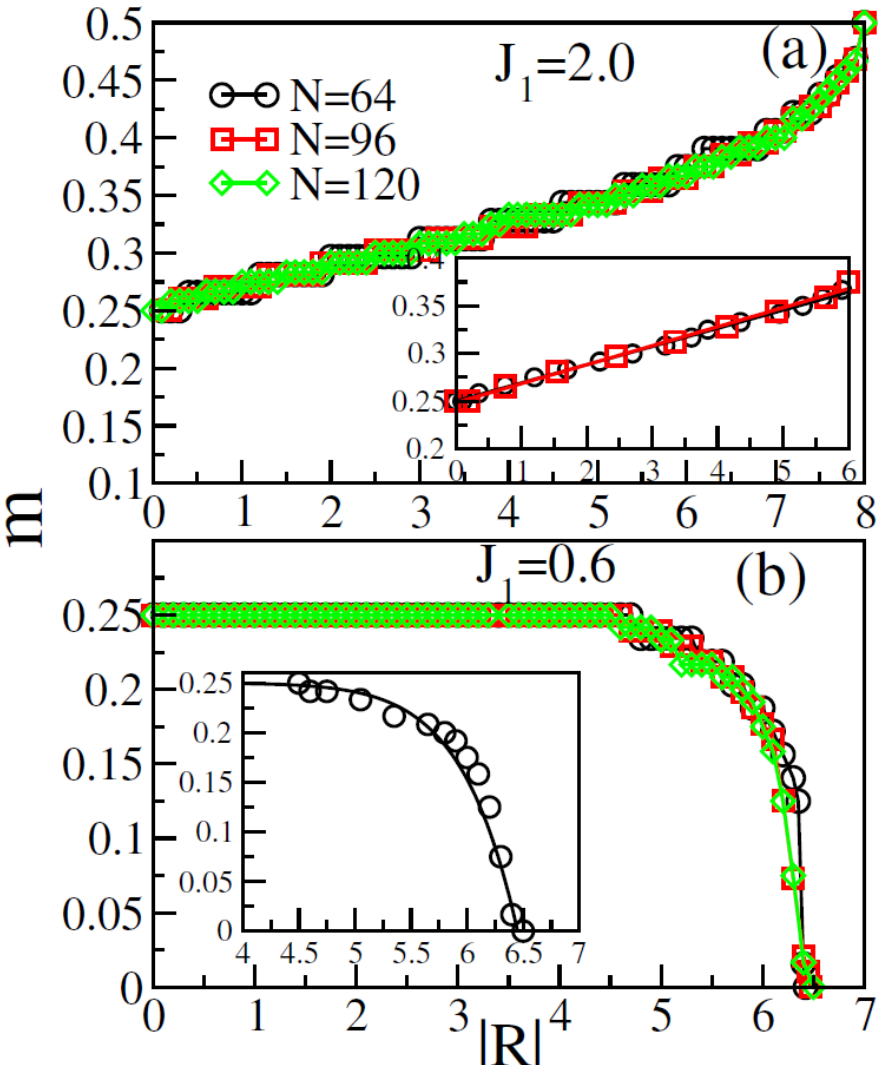

Figure 3.4: The magnetization m for FM rung interaction $R \leq 0$ as a function of $|R|$ for $J_1 > J_2$ in panel (a) and $J_1 < J_2$ in panel (b). The system sizes considered in both the panels are $N = 64$, 96 and 120. m varies from 0.25 to 0.5 for $J_1 > J_2$ whereas m varies from 0.25 to 0 when $J_1 < J_2$. Transition points from ferrimagnetic to FM and ferrimagnetic to non magnetic phase are very weakly dependent on system size. The linear variation of m as a function of R for $J_1 > J_2$ is shown in the inset of panel (a). Whereas m varies as $m = 0.25[1 - (R/R_c)^{13.08}]^{0.742}$ with $R_c = -6.45$ for $J_1 < J_2$ and shown in the inset of panel (b).

3.2.5 Spin-spin Correlations

In this subsection, spin-spin correlations in all five different phases are analyzed and the spin-spin correlation in longitudinal direction can be defined as $\langle S_i^z S_{i+r}^z \rangle - \langle S_i^z \rangle \langle S_{i+r}^z \rangle$ where $\langle S_i^z \rangle$ represents the z-component of the spin operator at site i, and the reference site is considered at the mid of AFM leg and the correlations are calculated along both of the legs with respect to the reference site. The product of average magnetization $\langle S_i^z S_{i+r}^z \rangle$ is substracted to get the correct correlation.

In the FM phase the correlation C(r) is a constant number, therefore, we do not show. The correlation in the dimer and AFM phases are shown in Fig. 3.5 (a) and (b) respectively. In the dimer phase the correlations in both of the legs decay exponentially, and the red curve represents $C(r)$ from AFM to FM leg. The large value of $C(r = 1) \approx -0.25$ shows the strong dimer formation along the rung, whereas the short range correlation is observed along both of the legs. In the AFM phase $C(r)$ shows an algebraic decay in both the legs. The AFM type of spin alignments on both of the legs are formed in small J_1 and FM R limit and AFM leg interaction is dominated in the both legs. As the exchange interaction is much smaller in the FM leg, the AFM arrangements are forced in FM leg through the FM rung interaction by forming effective spin-1 along the rung. The spin-spin correlation on both of the legs can be fitted with power-law equation

$$C(r) = Ar^{-0.05} cos(\pi r + B), \tag{3.5}$$

where B is a constant and exponent of the power law is very small i.e. it shows a quasi-long range order in the system.

In Fig. 3.6 (a), $C(r)$ is shown in the $m - 1/4$ phase for $J_1 = 0.6$ and $R = -1.0$ at $S^z = 30$. In this phase the spins on FM leg are aligned ferromagnetically, whereas in AFM leg spin arrangement is antiferromagnetic and it seems that

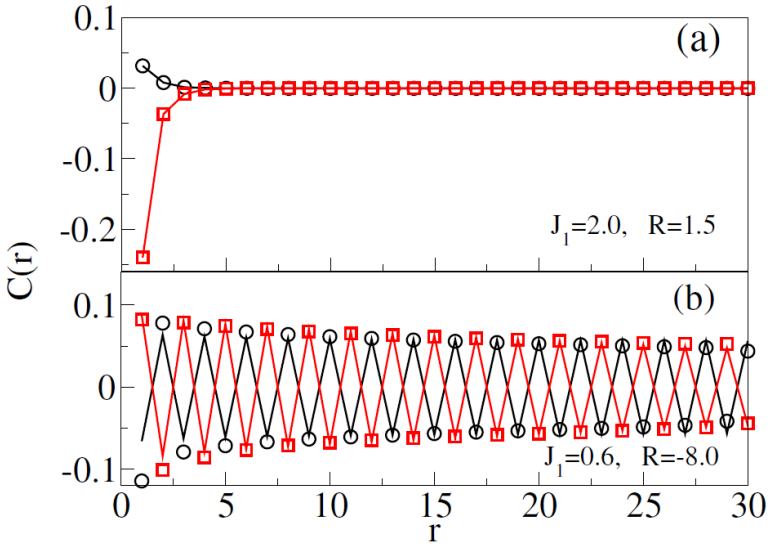

Figure 3.5: Panel (a) shows the correlation $C(r)$ in the dimer phase at leg ratio $J_1 = 2.0$ and R=1.5. The AFM alignment of the spins at $J_1 = 0.6$ and $R = -8.0$ is shown in panel (b). The correlation in both panels is shown for a system of $N = 120$ sites and the reference spin is considered at the middle of the AFM leg. Correlations are shown both along the AFM leg and FM leg and denoted by black circles and red squares, respectively.

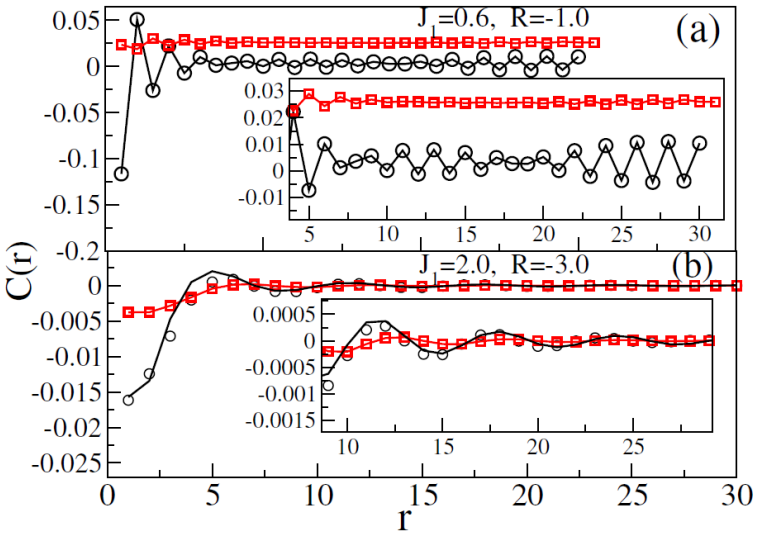

Figure 3.6: Panel (a) shows the correlation $C(r)$ in the $m - 1/4$ phase for $J_1 = 0.6$ and $R = -1.0$ at $S^z = 30$. The C(r) for NCF phase for $J_1 = 2.0$ and $R = -3.0$ is shown in panel (b). The correlation in both panels is shown for a system of $N = 120$ sites and the reference spin is considered at the middle of the AFM leg. Correlations are shown both along the AFM leg and FM leg and denoted by black circles and red squares, respectively.The insets are the zoomed C(r) plots.

there is soliton formation in the system as shown in the inset of Fig. 3.6 (a). The soliton in this system is very similar to $J_1 - J_2$ systems [132, 151]. The $C(r)$ in NCF phase are shown in Fig. 3.6 (b). The correlation function is a periodic function and have algebraic decay. It can be fitted with the function

$$C(r) = a_0 cos((r + a_1)/\lambda) r^{\alpha}, \tag{3.6}$$

where λ is proportional to the wavelength of spin density wave (SDW) and pitch angle (θ) can be defined as $\theta = 2\pi/\lambda$ where λ is a distance at which the $C(r)$ goes into the same phase. a_1/λ refers to the phase shift and α is algebraic exponent for this parameter regime. The variation of θ with parameter in NCF phase is important. However extracting θ from short range or fast decaying correlation is difficult. Therefore, we can calculate θ using the spin density.

3.2.6 Spin Density and Pitch Angle

In the NCF phase, the spin densities are calculated in AFM and FM legs separately as shown in Fig. 3.7 (a) and (b). Here, three S^z sectors (46, 48 and 54) for N=120 corresponding to three different values of rung interactions are shown and the spin density modulation decreases with increasing S^z sectors which means the SDW nature is more prominent with lower S^z values. Spin density and pitch angle for AFM rung interaction limit have been already well studied in ref. [28] for AFM R. The variation of spin density with distance at AFM and FM legs are shown in Fig. 3.7 (a) and (b) respectively. We notice that spin densities are high at the end of the chain and it decays exponentially as we go towards the mid of the chain.

The pitch angle (θ) can be easily extracted from the spin density variation $\langle S_i^z \rangle$ as it does not decay with distance which is the case for correlation function, and θ can be defined as $2\pi/L$ where L is distance at which spin changes its phases by 2π. Variation of θ vs R are shown in Fig. 3.7 (c), which are fitted by the

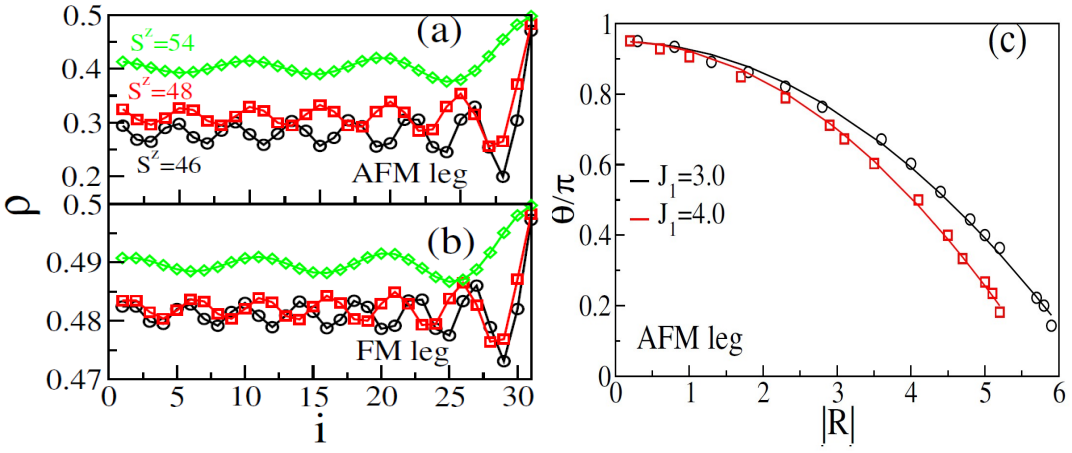

Figure 3.7: Panel (a) and (b) show the spin density for AFM and FM legs, respectively. The spin density is maximum at the boundary for both the legs. Both the panels show that the spin density modulation decreases with increasing $|R|$. Panel (c) shows the pitch angle θ for leg ratio $J_1 = 3.0$ and 4.0. Symbols are obtained from numerical calculations which are fitted by the equations, $\theta/\pi = 0.95 - 0.02233|R|^2$ and $\theta/\pi = 0.96 - 0.02824|R|^2$ respectively for two different leg ratios as shown by solid lines. θ is shown to vary from 0 to π with $|R|$ and indicates the existence of the incommensurate phase.

equations; $\theta/\pi = 0.95 - 0.02233|R|^2$ and $\theta/\pi = 0.96 - 0.02824|R|^2$ respectively for two different leg ratios.

3.3 Exotic phases and magnetization plateau in a frustrated spin-1/2 ferro-antiferromagnetic zigzag ladder

As an extension to the first part of this chapter, a zigzag ladder model as shown in Fig. 3.8 has been studied in this section. The main motive here is to observe the changes in the phase diagram of NL with the introduction of diagonal interaction.

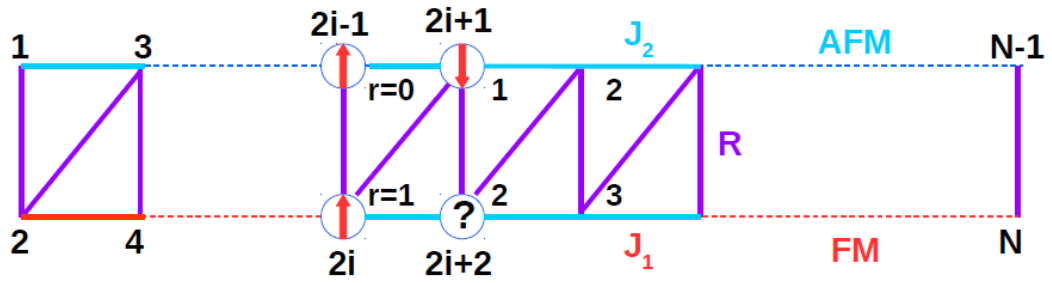

Figure 3.8: FM-AFM ladder model is represented schematically. The spins are represented by red arrows. Question mark represents the frustrated spin. The site index is denoted by i and r represents the distance from the reference point r.

3.3.1 Model Hamiltonian and Numerical method

A two-leg ladder model has been considered. Spins on one leg are interacting with each other by ferromagnetic interaction (J_1). On the other hand the exchange interactions (J_2) among the spins on other leg is of antiferromagnetic type. The spin Hamiltonian is

$$H = H_{leg} + H_{rung}, \tag{3.7}$$

where

$$H_{leg} = \sum_{i=1}^{N/2-1} J_1 \boldsymbol{S}_{2i} \cdot \boldsymbol{S}_{2i+1} - J_2 \boldsymbol{S}_{2i-1} \cdot \boldsymbol{S}_{2i} \tag{3.8}$$

$$H_{rung} = R \sum_{i=1}^{N-1} \boldsymbol{S}_i \cdot \boldsymbol{S}_{i+1}. \tag{3.9}$$

During our whole calculation $J_2 = 1$ and it defines the energy scale. On the other hand R and J_1 are variable parameters. Here, we also used the two numerical methods: ED and DMRG to solve the model Hamiltonian.

3.3.2 Results

In this section we focus on a comparative study with NL and ZL configurations. We have already studied the quantum phase diagram in the J_1-R parameter regime. For NL, the quantum phase diagram consists of five interesting phases: FM, non-collinear ferrimagnetic (NCF), $m-1/4$, AFM and dimer. On the other hand, when we introduce the diagonal interaction in the NL configuration in order to obtain the ZL configuration, the phase diagram shows a huge change, now it consisting of only three phases: FM, non-colliear ferrimagnetic (NCF) and spin-fluid phases. The phase boundaries are determined by the magnetization and the nature of the spin-spin correlations. All of these phases will be discussed in detail in the following sections.

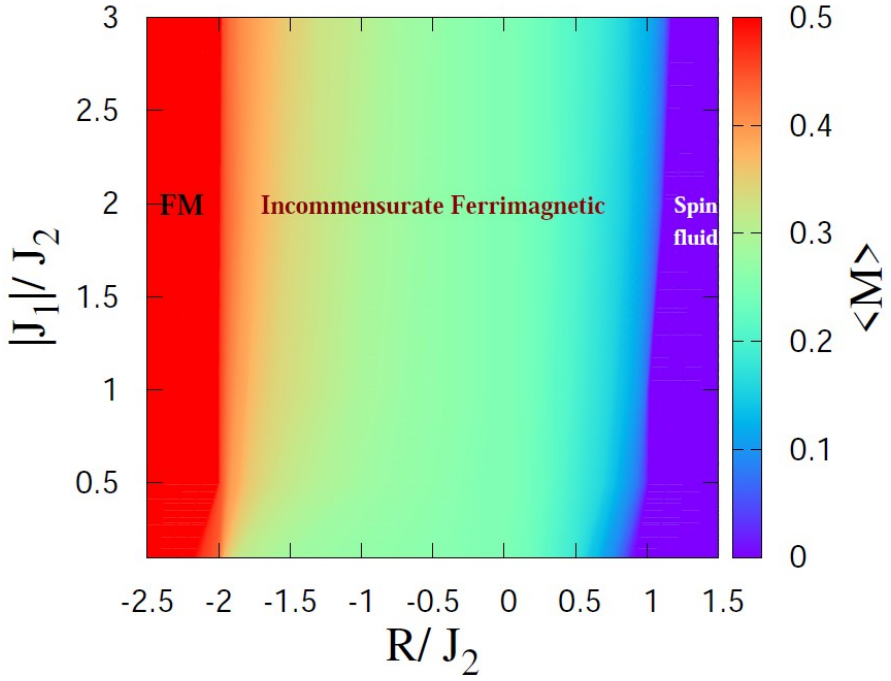

Figure 3.9: The quantum phase diagram of the Hamiltonian in Eq. 3.7 is shown in J_1 vs. R parameter space with three different phases: FM, NCF and spin-fluid for $-2.5 \leq R \leq 1.5$ and $0 \leq |J_1| \leq 3$. The change in magnetization ($\langle M \rangle$) is represented by the color gradient.

3.3.3 Quantum phase diagram

Due to the competition between J_1 and R, the model shows three different phases in $R-J_1$ parameter regime as shown in 3.9. The system always shows FM alignment of spins for large R values of FM type. In this case it is completely different from NL type of configuration where the system gets AFM or FM- type of spin alignments depending on the ratio of J_1 and J_2 and the difference between the behavior of NL and ZL is happening due to the presence of FM diagonal interaction.

For the intermediate values of rung interaction, the system exhibits non-collinear ferrimagnetic phase. The magnetization and the nature of spin-spin correlation are discussed in the next section. On the other hand the system is showing non-collinear ferrimagnetic and spin-fluid phase for intermediate and large R values of AFM type which is already explored.

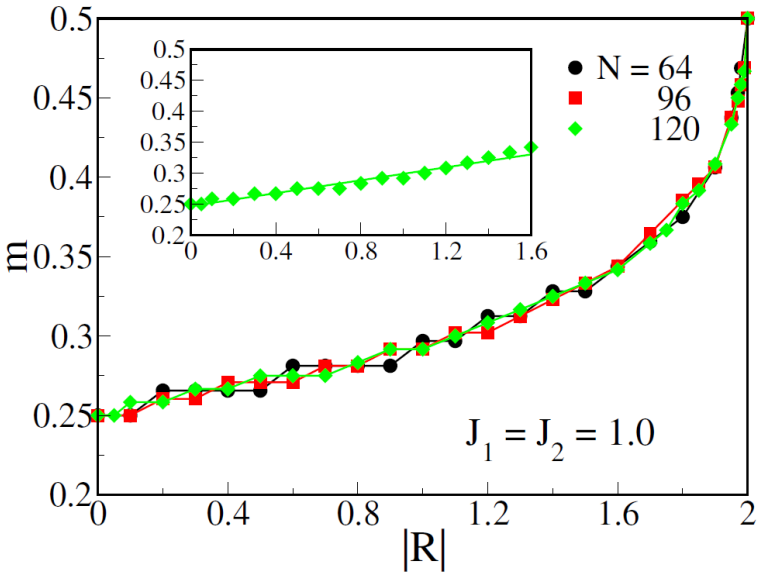

Figure 3.10: $m-R$ plot shows how magnetization is changing with FM R in ZL. The nature of this curve will be continuous in thermodynamic limit and m varies with R linearly upto $|R| = 1.6$ as shown in the inset.

3.3.4 Magnetization

Our previous study reveals that the magnetization ($\langle M \rangle$) varies from 0.25 to 0.5 and from 0.25 to 0 depending on the leg ratio in case of NL with FM R limit. On the other hand ($\langle M \rangle$) always varies from 0.25 to 0.5 when R is of FM types in ZL. It is also noticed that the magnetization plot has a step like behavior which is due to finite size effect, in the thermodynamic limit the plot will be continuous. The critical value between ferrimagnetic to FM phase is weakly dependent on system size. The nature of $m-R$ curve has been shown in Fig. 3.10 which shows a linear variation of m with R upto $R = 1.6$ as shown in inset of Fig. 3.10.

3.3.5 Spin-spin correlations

Spin-spin correlations in longitudinal direction is defined as

$$C(r) = \langle S_i^z S_{i+1}^z \rangle - \langle S_i^z \rangle \langle S_{i+1}^z \rangle \tag{3.10}$$

Here, reference site is considered at the mid of AF leg and with respect to this reference site the correlations are calculated along both of the legs. S_i^z represents the z-component of the spin operator at site i. In order to get the actual value of correlations the product of average magnetization has to be substracted from $\langle S_i^z S_{i+1}^z \rangle$. Here, r represents the distance of a particular site from the reference site.

Spin-fluid phase is already discussed in ref. [28]. For FM phase correlation is a constant number, so it is not shown. The most interesting phase to be discussed is the non-collinear ferrimagnetic (NCF) phase. Here the magnetization is changing with the rung interaction as shown by the color gradient in the phase diagram. This type of ferrimagnetism is of non-conventional type. The correlation in NCF phase has been calculated for a system of $N = 120$ sites and $J_1 = -2.0$ and $R = -0.3$ limit where reference spin is considered at the middle of the AFM leg. Correlations are shown both along the AFM leg and FM leg and denoted by black

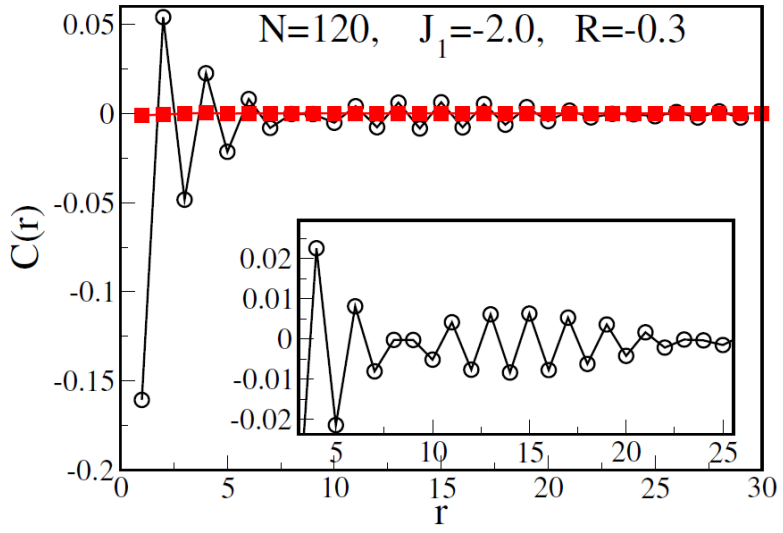

Figure 3.11: The correlation in NCF phase is shown for a system of $N = 120$ sites and the reference spin is considered at the middle of the AFM leg. Correlations are shown both along the AFM leg and FM leg and denoted by black circles and red squares, respectively.The insets are the zoomed C(r) plots.

circles and red squares, respectively in Fig. 3.11. The spin-spin correlations can be fitted by the power-law equation:

$$C(r) = a_0 cos((r + a_1)/\lambda) r^{\alpha} \tag{3.11}$$

where λ is proportional to the wavelength of the spin density wave. a_1/λ is phase shift and α is phase shift.

3.3.6 Spin-density and pitch angle

The spin-densities in the NCF phase for both of the legs are shown for $N = 120$ and $S^z = 40, 47$ and 54 in Fig. 3.12. Spin-density and pitch angle for AFM R limit are already discussed in ref. [28]. Here our main focus is to observe those

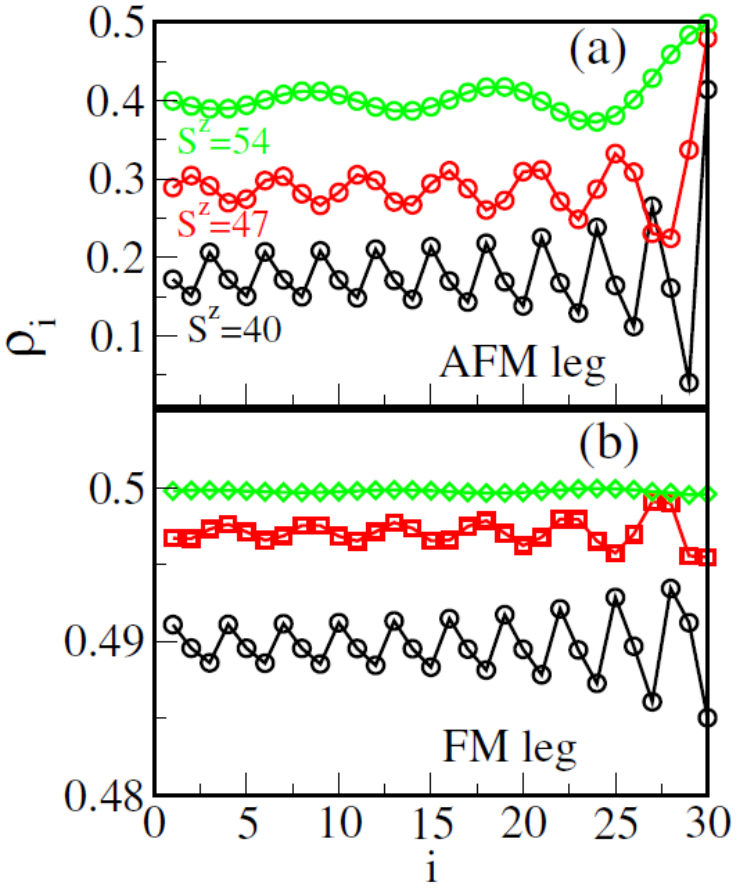

Figure 3.12: The spin density in the gs for AF and F legs is shown in panel (a) and (b) respectively. The gs spin density is represented by circles, squares and diamonds for three different S^z sectors (40, 47 and 54). The spin density is highest at the boundary. The spin density modulation decreases with increasing R.

quantities for FM R limit. Here, it is noticed that the spin-density modulation is decreases with increasing S^z. It means that the SDW phase is more prominent in lower S^z sectors.

Pitch angle (θ) can be also calculated from Eq. 3.11 where $\theta = 2\pi/\lambda$. Variation of θ is shown in Fig. 3.13.

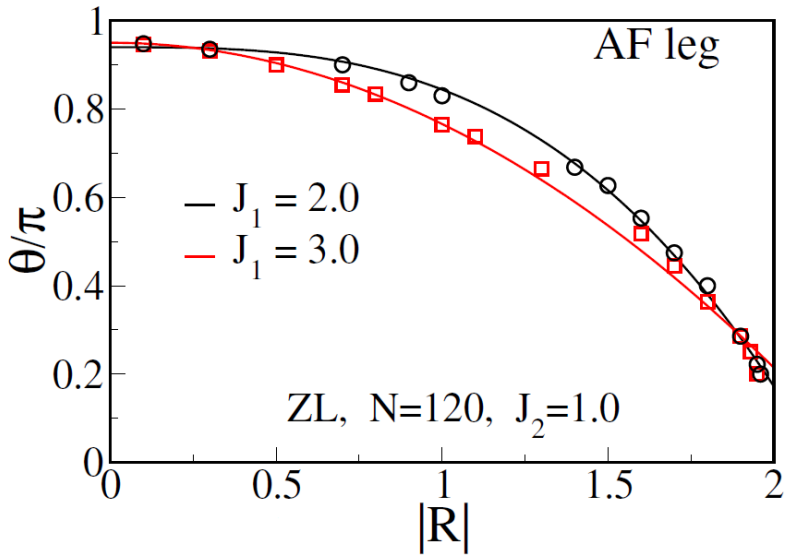

Figure 3.13: The black circles and red squares represent the calculated values of θ for $J_1 = 2$ and 3 respectively in the NCF phase. Both the curves can be fitted with the equation $\theta/\pi = a - b|R|^3$ where a=0.93 and 0.94, and b=0.094 and 0.098 for $J_1 = 2$ and 3 respectively.

3.3.7 In presence of magnetic field

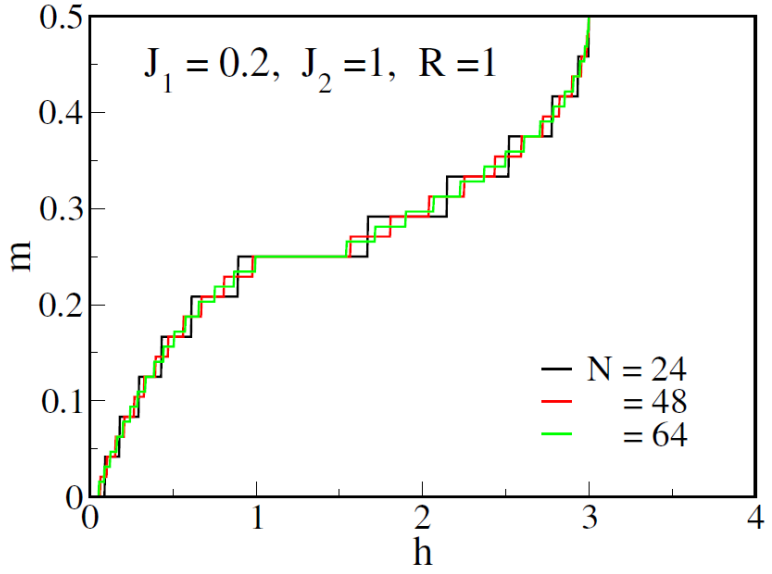

Figure 3.14: m-h curve shows step like nature which is coming due to finite size effect. The system shows a magnetization-$\frac{1}{2}$ plateau following OYA criteria.

When magnetic field is applied in the system, a magnetization-1/2 plateau is observed in case of ZL for AFM limit. Our previous study does not show any such magnetization plateau in presence of magnetic field in NL. Generalizing the Lieb-Schultz-Mattis (LSM)theorem [152], Oshikawa, Yamanaka, and Affleck (OYA) [153] established the necessary condition for the formation of plateaus in a $1D$ spin-S system. The OYA condition for observing a plateau at m is given by $Sp(1-m) \in Z$, where S is the spin of a site, p is the number of lattice sites per unit cell, and Z represents the set of positive integers. The condition is further generalized to n-leg ladder which is given by $nSp(1-m) \in Z$.

In our case $n = 2$, $S = 1/2$, $P = 4$, Z is integer for $m = 1/2$ and 1. So, OYA criteria is completely valid in our model. We have shown the $m - h$ curve for $N = 24$, 48 and 64 in Fig. 3.14. The steplike nature is due to finite size effect.

3.3.8 Conclusion

In this work, we study a spin-1/2 ladder composed of FM and AFM spin-1/2 chains and interacting through a normal rung interaction which can be ferromagnetic or antiferromagnetic. The main focus of this chapter is to construct the QPD of the ladder system for both of the spin configurations: normal ladder (NL) and zigzag ladder (ZL). Based on the arrangement of spins five different phases have been observed: AFM, ferrimagnetic phase, FM alignments of spins, $m - 1/4$ and dimer phase in J_1 and R parameter space in NL. We obtain AFM alignment of spins for FM rung interaction R for $J_1/J_2 \ll 1$. The $m - 1/4$ phase survives at $J_1 < J_2$. On the other hand, we have seen the FM arrangements of the spins at large FM R and J_1. For moderate R and J_1, NCF phase sets in the gs. The rung dimer appears at large AFM R caused by competition between FM J_1 and AFM J_2 as shown by perturbation theory [28].

The NCF phase in this system is particularly interesting and spins are non-

collinear in nature and shows algebraic decays in most of the parameter regime. For the FM R, m increases linearly with R when $J_1/J_2 \gg 1$, whereas the m decays algebraically for $J_1/J_2 \ll 1$ as shown in Fig. 3.4 (a) and (b). Interestingly, the pitch angle in this system goes as R^2 for $J_1 = 3$ and 4.

In case of ZL, the phase diagram is consisted of only FM, spin-fluid and NCF phases. Here, magnetization always varies from $N/4$ to $N/2$ depending on rung interaction of FM type. There is no non-magnetic region in presence of FM rung interaction. The more interesting thing is that this configuration shows magnetization-1/2 plateau in presence of external magnetic field which satisfy OYA criteria.

In summary, we have constructed the complete phase diagram of normal and zigzag spin-1/2 ladder system composed of a FM leg and an AFM leg and these two legs interact through FM or AFM rung interaction. This model is very much useful to get some preliminary informations at the interface of bilayer thin film. The competing interactions in the system induce frustration which give rise to various quantum phases, and the whole phase diagram is dominated by the NCF. The pitch angle (θ) in this phase can be highly sensitive to interaction parameters.

Chapter 4

Quantum phases of ferromagnetically coupled dimers on Shastry-Sutherland lattice

4.1 Introduction

Frustrated magnetic system is captivating because it delves into fundamental principles of quantum mechanics and statistical physics. These systems exhibit rich phase diagram with a variety of exotic phases like dimer [35], non-collinear spin wave [36], spin-liquid [37,154], non-trivial topological phase [155,156] in the ground state (gs). Understanding their behavior not only advances our knowledge of condensed matter physics but also holds potential for applications in quantum computing and materials sciences. Over the past few decades, these systems have been synthesized in different dimensions for example, in one dimensional geometry: $LiCuSbO_4$ [41], $LiCuVO_4$ [42] and $Rb_2Cu_2Mo_3O_{12}$ [87,157]; in ladder like geometry: $SrCu_2O_3$ [38] and $(VO)_2P_2O_7$ [39,140]; in two dimensional systems such as $ZnCu_3(OH)_6Cl_2$(Herbertsmithite) [158, 159] and α-$RuCl_3$ [160]. Their properties have been rigorously investigated theoretically as well [161].

In the presence of a magnetic field, these systems add another layer of complexity and richness to their behavior. The interplay between frustration, quantum fluctuations and the external magnetic field can lead to intriguing phenomena such as quantum phase transitions, spin-flop transitions and the emergence of novel magnetic phases such as multipolar [162], spin nematic [100], vector chiral [91], plateaus at different fractional magnetization [96, 155, 156, 163–165]. In order to understand their physical properties different models have been proposed like Heisenberg spin-1/2 J_1-J_2 model for one dimensional (1D) spin chain [1, 32, 35, 134], Heisenberg anti-ferromagnetic spin-1/2 model on Shastry-Sutherland lattice (SSL) [64] and square lattice [166] , J_1-J_2 model on square lattice [167, 168] etc.

Layered materials [169] often contain frustrated $2D$ structures where arrangements of atoms and molecules within the layers can lead to interesting properties and behaviors, but also challenges in terms of controlling and exploiting these materials effectively. These $2D$ geometries: square [170], triangular [171], kagome [159] and SSL [71, 129, 172] are interesting because $2D$ is said to be a critical dimension in the Mermin-Wagner domain [56]. Here, We are mainly interested in SSL which is shown in Fig. 4.1. SSL is a unique $2D$ lattice composed of two types of squares. The lattice is formed by arranging these squares in a periodic pattern, with dimers (pairs of spins) positioned along the diagonals of the squares. This distinctive arrangement gives rise to intriguing magnetic behaviors, making it a significant area of research. If we consider an isotropic Heisenberg spin-1/2 model on the SSL where the exchange interactions along the leg and rung of the square are $J_x = J_y$ and the interaction acting along the diagonal bond is $J = 2J_x = 2J_y$, then the model can be solved exactly by Shastry and Sutherland in 1981 [64]. In small and large J/J_y limit, the system is showing Néel and dimer order respectively when ($J_x = J_y$). Later, by using PEPS technique, the existence of a plaquette phase between Néel and dimer region has been predicted in Corboz *et al.* [73]. In 2021 Yang *et al.* [74] predicted a spin

liquid phase. On the other hand the topological properties of this model has been explored by Ronquillo and Peterson [75] through the calculation of entanglement entropy.

Among the layered magnetic materials, spin-1/2 layered copper oxyhalides $(CuX)A_{n-1}B_nO_{3n+1}$ are frustrated $2D$ magnets which have many interesting features just by tuning the composition [76, 173]. The CuX layers are sandwiched by non-magnetic layers, the anion orbitals are involved in exchange pathways but the cation orbitals replacement keeps the magnetic layer homogeneous. However, a small change in exchange interaction can be tuned by changing the lattice parameters, electrostatic fields, and crystal-field splittings [174]. The tuning of anion and cation composition can drive the system across the quantum critical points. Experimental results suggest that the gs can be tuned to have a collective singlet with a spin gap in $(CuCl)LaNb_2O_7$ [76, 175–177], a collinear stripe magnetic order in $(CuBr)LaNb_2O_7$ [173] and a magnetization plateau at 1/3 of the saturated moment in $(CuBr)Sr_2Nb_30_{10}$ [178].

$(CuCl)LaNb_2O_7$ was initially predicted as $S = 1/2$ frustrated square lattice [76], however, band structure calculations revealed that the simplest model for this material can be best described as strong antiferromagnetic (AFM) exchange interaction between fourth neighbors forming a strong singlet dimer and these dimers are coupled together by ferromagnetic (FM) interactions i.e this model looks like the Shastry-Sutherland model with ferromagnetic exchange J_x and J_y along square and antiferromagnetic diagonal exchange J [77]. This model was theoretically studied using mean-field and exact diagonalization (ED) methods on a small cluster and they predicated a plethora of phases in exchange parameter space [27]. In the intermediate FM coupling limit, they reported two types of stripe phases, $(0, \pi)$ and $(\pi, 0)$, separated by a non-collinear spiral phase. The dimer singlet stabilizes for $J_x, J_y < J/2$, whereas ferromagnetic gs is stable for large J_x and J_y [27]. We notice that the phase boundaries as well as the existence of different phases calculated from ED are not consistent with that

calculated from mean-field, for example, non-collinear phase does not appear in exact diagonalization results, but is present in the mean field calculations. Therefore, it is very intriguing to explore such an interesting model with a more sophisticated numerical tool like density matrix renormalization group (DMRG) method which can give accurate results for large lattice sizes.

In this work, we explore the ferromagnetically coupled $S = 1/2$ dimers on SSL with the DMRG method and re-investigate the quantum phase diagram of this model. The phase diagram is based on the nature of spin-spin correlations and ground state energy variation. The gs exhibits predominantly six types of phases: two types of stripe order with wave vector $(0, \pi)$ and $(\pi, 0)$ for large value J_y and J_x respectively. A perfect dimer phase exists for $J_x = J_y$ and this phase separates two types of spiral phases namely X-spiral with wave vector $(\theta, 0)$ and Y-spiral with wavevector $(0, \theta)$, where θ is the pitch angle. In the large limit of J_x and J_y the gs has ferromagnetic behavior. We also explore the effect of J_x and J_y on spiral behavior and pitch angle and we notice that spin ordering is very short range in most of the parameter regimes.

This chapter is organized as follows. In Sec. 4.2 , the model of the ferromagnetically coupled SSL and numerical methods are discussed. In Sec. 4.3, all the numerical results are presented and this section has four subsections. The quantum phase diagram is presented in Sec. 4.3.1., Sec. 4.3.2 and Sec. 4.3.3 discuss gs energy and spin-spin correlations in various phases of the phase diagram. Correlation length and bond orders are discussed in Sec. 4.3.4 and 4.3.5 respectively. The pitch angles are discussed in Sec. 4.3.6. Results are discussed and compared with literature in Sec. 4.4. In an appendix we presented results for the ground state energy per site and spin-spin correlation for various bond dimensions (m) and various system sizes.

4.2 Model Hamiltonian and numerical methods

We consider a Heisenberg spin $S = 1/2$ model on SSL where only diagonal interaction $J = 1$ is antiferromagnet and sets the energy scale of the system. The strength of ferromagnetic exchange interaction along the x-axis and y-axis on the square is represented by J_x and J_y respectively. The arrangement of the exchange interactions are shown in Fig. 4.1. Now onward we will call this model as Shastry-Sutherland model (SSM) and can be written as

$$H = -J_x \sum_{<ij>_x} \boldsymbol{S}_i \cdot \boldsymbol{S}_j - J_y \sum_{<ij>_y} \boldsymbol{S}_i \cdot \boldsymbol{S}_j + J \sum_{<ij>_d} \boldsymbol{S}_i \cdot \boldsymbol{S}_j \tag{4.1}$$

where the first sum runs for NN bonds along the x-direction, the second sum runs for NN bonds along the y-direction and the last sum runs for NN diagonal bonds in the square.

We use the exact diagonalization for system size up to 32 sites and the density matrix renormalization group (DMRG) method [119, 121, 149, 179] for large system size. The DMRG method is a state of art numerical method to handle the large degrees of freedom for a many-body Hamiltonian in low dimensions. This method is based on the systematic truncation of irrelevant degrees of freedom while growing the system sizes and optimising the wavefunction while doing the finite DMRG algorithm. In this work, we use a modified DMRG method [139] in which 4-new sites are added at each step to reduce the number of times of renormalization of operators used to build the super block [139]. We retain up to $m = 900$ block states which are the eigenvectors of the system block density matrix corresponding to the largest eigenvalues. The chosen value of 'm' keeps the truncation error to less than $\sim 10^{-8}$. We also carry out $10 - 12$ finite sweeps for improved convergence and to optimise the wave function. We use cylindrical geometry of the SSL and a periodic boundary is applied along the width of the

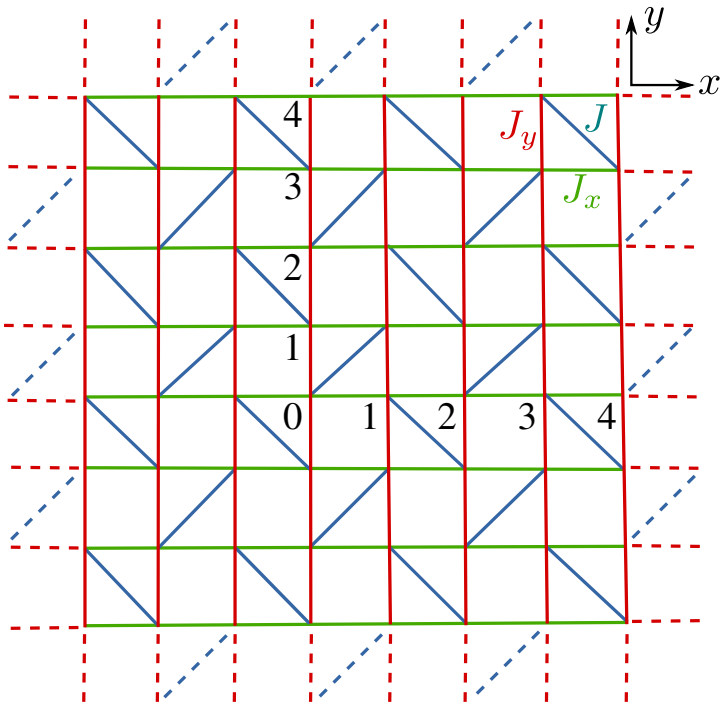

Figure 4.1: Figure shows a schematic diagram of SSL. The coupling constants along x-axis (J_x) and along y-axis (J_y) are FM and the diagonal bond couplings J are AFM in nature. The site index 0 is the reference site and the numbers along x-axis and y-axis represent the distance (r) from the reference site.

lattice and open boundary along the length. The largest system size studied is up to 12×8 (length $\times$ width) system size. We have analysed the convergence of energy with the various values of m in appendix. The per-site energies for 12×4 system are shown for $m = 256$, 512 and 900, whereas for 12×8 system, it is shown for $m = 256$, 512 and 700 in table 4.1. We notice that $m = 512$ is sufficient for accuracy up to 5^{th} decimal place for 12×4 and 4^{th} for 12×8 system. We also show the dependence of the spin-spin correlation function on m in table 4.2 and 4.3 of appendix. We notice that the spin-spin correlations are accurate up to 4^{th} decimal places. Interestingly this model gives amazing accuracy of energies as well as correlation function and these accuracy may be attributed to the short range correlation length.

4.3 Results

We calculated the spin-spin correlations $C(r)$ in order to identify different phases existed in the system. Six different types of spin-configurations have been identified depending on the nature of $C(r)$ which are described below.

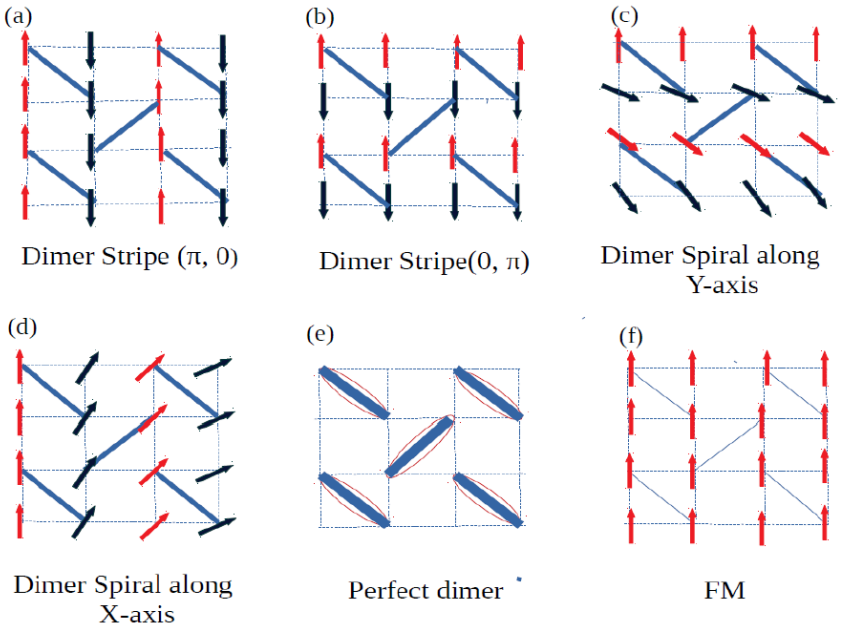

Figure 4.2: Figure shows a schematic diagram of different phases present in the ferromagnetically coupled dimers on the SSL, where arrows represent the spin alignments and the ellipses are the dimers (defined in the main text). (a) and (b) are two dimer-stripe phases with ordering wave vector $(0, \pi)$ and $(\pi, 0)$ respectively with a very strong both along diagonal direction. (c) and (d) are two non-collinear spiral phases, the dimer-spiral along x- and y- directions. (e) and (f) are the perfect dimer and FM phase respectively.

(a) Dimer stripe $(0, \pi)$ in which the spins are antiferromagnetically aligned along the y-direction and ferromagnetically aligned along the x-direction. (b) In the dimer stripe $(\pi, 0)$ phase, the system has a spin alignment that is exactly the opposite of (a). In this case the spins along the x-direction are antiferromagnetically aligned, while the spins along the y-direction have a ferromagnetic type of spin arrangement. (c) Dimer-spiral along x-direction phase, here the spins are arranged in a non-collinear pattern along x direction and ferromagnetic

arrangement is observed along y-direction. of spins along the x-direction and ferromagnetic ordering along the y-direction as shown in Fig. 4.2(c). (d) The spins arrangement is just opposite as mentioned in (c) in case of dimer-spiral along y-axis. (e) When $J_x = J_y$ the system forms perfect dimer. Here the gs can be written as a product of dimer singlets which is exactly solvable. (iv) In Y-spiral phase, spins have a non-collinear arrangements along the y-direction and ferromagnetic ordering sets in along x-direction as in Fig. 4.2(d). (f) The system has finally got the ferromagnetic type of spin configurations when J_x and J_y both are large.

4.3.1 Quantum Phase Diagram

In this section, we have constructed the quantum phase diagram in J_x-J_y parameter regime as shown in Fig 4.3. During the whole calculation we keep fixed $J = 1$, J_x and J_y are variables.

Our bond order calculation always predicts that the bond order along diagonal bond is very strong as compared to the bond order along leg and rung direction. Although stripe like spin alignment either along leg or rung is formed for large value of J_x or J_y which are dimer stripe $(0, \pi)$ and $(\pi, 0)$ phases respectively. In these phases correlation length > 1 which is used to separate out dimer phase from this stripe like spin aligned phases. The system gets long range FM type of spin ordering for larger values of J_x and J_y.

On the other hand perfect dimer phase is formed in the system when $J_x = J_y$. In this case $C(r) = -0.75$ along diagonal bond and it is exactly zero along leg and rung. This region is confined only along a line. We are also able to find out a small region near the FM phase where a non-collinear type of spin alignment is observed in the system along leg or rung direction. It is happening at the intermediate values of J_x and J_y due the competion between nearest neighbor of FM type and next nearest neighbor of AFM exchange interactions. It should be mentioned here that the system is always showing very short range order at

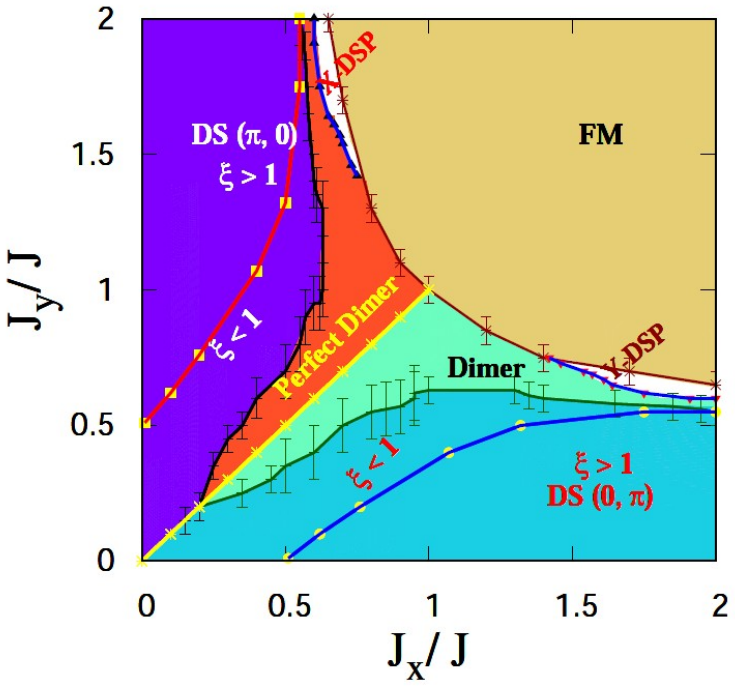

Figure 4.3: Figure shows the quantum phase diagram of the SSM. The phase diagram comprises six phases: Two stripe order phases with ordering wave vector $(0, \pi)$ and $(\pi, 0)$, two spiral orders along both the x- and y-directions, the X-spiral and Y-spiral phase respectively. The other two phases are a perfect dimer phase (the yellow line separating two spiral phases) and a phase with FM spin ordering along all directions of the lattice.

almost every regions in the phase diagram except the FM phase.

4.3.2 Ground state energy

Ground state energies are calculated for the model in Eq. 4.1 on a cylindrical geometry with periodic boundary condition (PBC) along the width (y-axis) and open boundary condition along the length (x-axis), and 12×4 system is used to calculate the accurate gs. In Fig. 4.4 the gs energy per site ε_{gs} is plotted as a function of J_y by keeping J_x fixed value of $J_x = 0.9$. Around $J_y \sim 1.1$ we saw a discontinuity in the gs energy, indicating a first-order phase transition from FM to X-spiral phase. The maxima of the energy curve is close to $J_x = J_y \sim 0.9$

which indicates the dimer line, and the small deviation of maxima from dimer line $J_x = J_y$ is due to the rectangular geometry of the lattice. The maxima shifts to $J_x = J_y$ line as we increase the width of the lattice. The smooth variation of ε_{gs} with J_y indicates the second-order dimer transition. No signature of spiral and stripe transitions is detected from the gs energy variation.

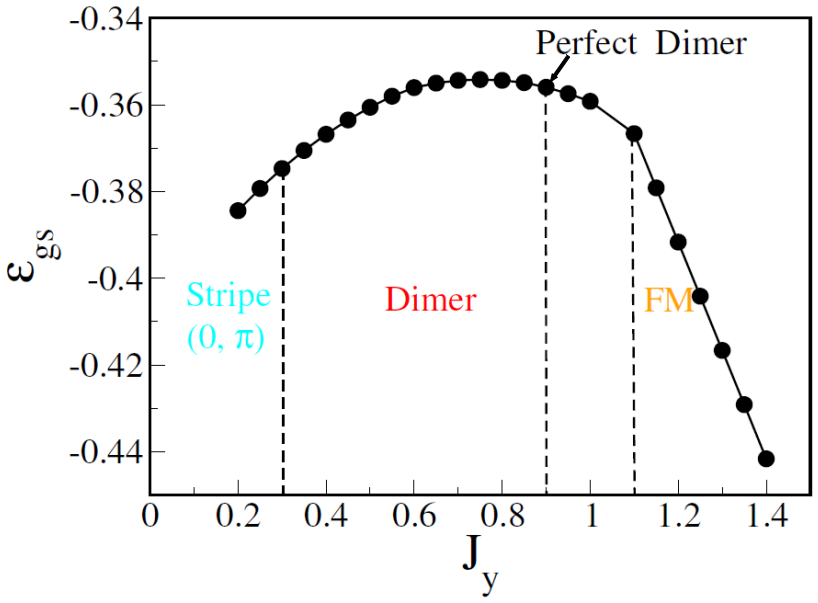

Figure 4.4: Figure shows gs energy per site (ε_{gs}) versus J_y plot at $J_x = 0.9$ for 12×4 lattice sites of the SSL. Around $J_y = 1.1$ we show a kink in the energy curve indicating a sharp phase transition from dimer to FM phase. Around $J_y = 0.3$ system transits from stripe $(0, \pi)$ to dimer phase. (Shaded lines are only for eye guide of the transition points).

4.3.3 Spin-spin correlation

In this subsection, we present spin-spin correlation $C(r)$ for various parameter regimes to validate the existence of different phases in the phase diagram in Fig. 4.3. We are dealing with isotropic system and total spin-spin correlations $C(r) = \langle \boldsymbol{S}_i \cdot \boldsymbol{S}_{i+r} \rangle = 3\langle S_i^z S_{i+r}^z \rangle$ where S_i^z represents the z-component of the spin operator at the reference site i. r is the distance between the spin site and

reference site along the x- and y-axis as shown in Fig. 4.1. The spin Hamiltonian in Eq. 4.1 has $SU(2)$ symmetry and one expects equal spin-spin correlation for all three spin components in the singlet sector. To understand the spin arrangements in different phases we have calculated $C(r)$ along different spatial directions. In Fig. 4.1, the site with 0 index represents the reference site, from which correlations are calculated in various directions, and distances r are shown in various directions with numerals as shown in Fig. 4.1.

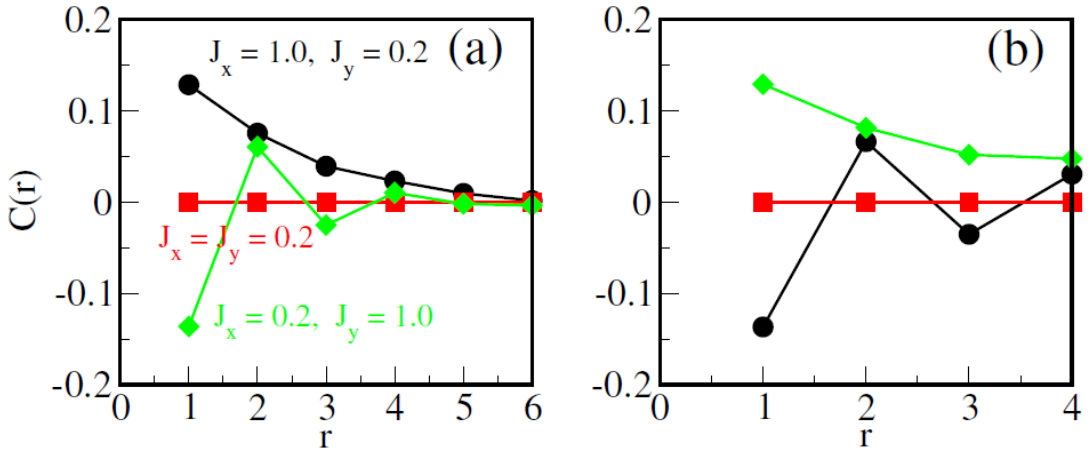

Figure 4.5: Figure shows the variation of spin-spin correlations $C(r)$ with distance (r) for 12×8 system size. Spin-spin correlations are calculated for different interaction limit. (a) $C(r)$ are calculated along x-direction. (b) $C(r)$ are calculated along y-direction.

In Fig. 4.5(a) we presented $C(r)$ along the x-direction, whereas Fig. 4.5 (b) represents the same for y-direction.

In Fig. 4.5(a) for $J_x = 1.0$ and $J_y = 0.2$, all the values of $C(r)$ are positive which correspond to an FM spin arrangement along x-direction. Whereas in Fig. 4.5(b) for same value of J_x and J_y, $C(r)$ shows an antiferromagnetic arrangement of spins along y-direction. This kind of spin arrangements correspond to a stripe spin ordering with a wave vector $(0, \pi)$ (see Fig.4.2(a)). For $J_x = 0.2$ and $J_y = 1.0$ the behavior of the spin correlation along the x-direction interchanges with the behavior along y-direction i.e antiferromagnetic arrangement along the x-

direction and ferromagnetic arrangement along the y-direction. This represents another kind of stripe phase with wave vector at $(\pi, 0)$ as shown in Fig. 4.2(b).

When $J_x = J_y (= 0.2)$, $C(r)$ along x-direction and y-direction are exactly zero, whereas, we found the correlation for diagonal bonds are -0.75. This shows a perfect dimer formation along the diagonal bonds and this phase is shown in Fig. 4.2(e). A perfect dimer phase is formed along $J_x = J_y \lesssim 1$ line. In low J_x and J_y limit $C(r > 1)$ have non zero value for $|J_x - J_y| > 0$, therefore the perfect dimer phase is only restricted to $J_x = J_y$. In the FM phase region $C(r)$ have all positive values in all directions. Spiral order phase will be discussed later.

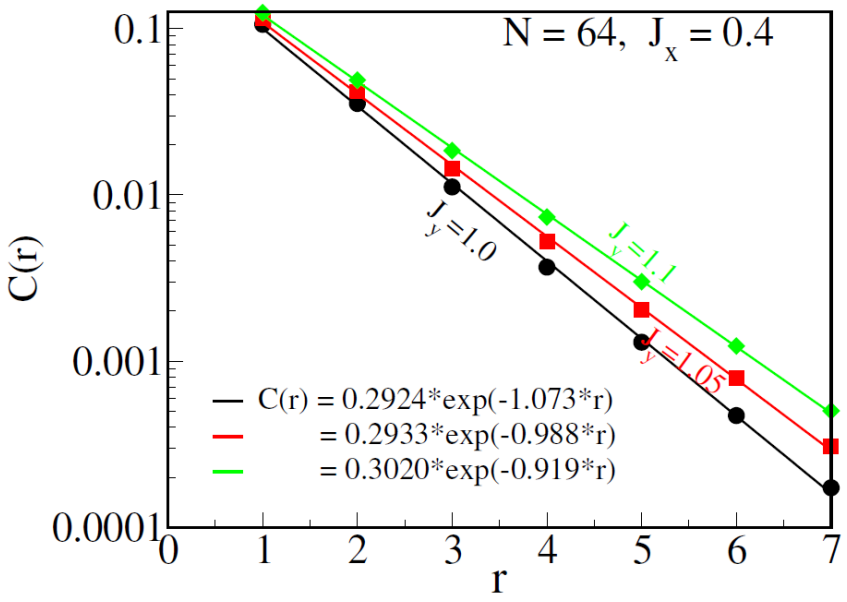

Figure 4.6: Figure shows the variation of correlation length ξ with J_y for a fixed value of J_x for N=64. We have drawn the phase boundary based on the variation of $\xi < 1$ and $\xi > 1$. During the whole region of phase diagram the spin-spin correlations decay exponentially which suggest very short range order existing in the system.

4.3.4 Correlation length

Fig. 4.6 shows the spin-spin correlation, $C(r)$ along the leg with 64 system sizes for a fixed value of $J_x = 0.4$. $C(r)$ is fitted by the follwing Eq.,

$$C(r) = a_0 exp(-r/\xi), \tag{4.2}$$

where a_0 is constant and ξ is the correlation length.

The system shows very short range order in most of the region of the phase diagram, although as we increase the value of J_y for a fixed J_x, ξ gradually increases from < 1 to > 1 but it completely dries out within 2-3 unit of length. We separated out the dimer phase from dimer-stripe phase by measuring this correlation length which suggests that for a particular value of J_y for a fixed J_x the system is showing some sort of stripe like spin configuration for either leg or rung direction when $\xi > 1$ but the system is always gapped.

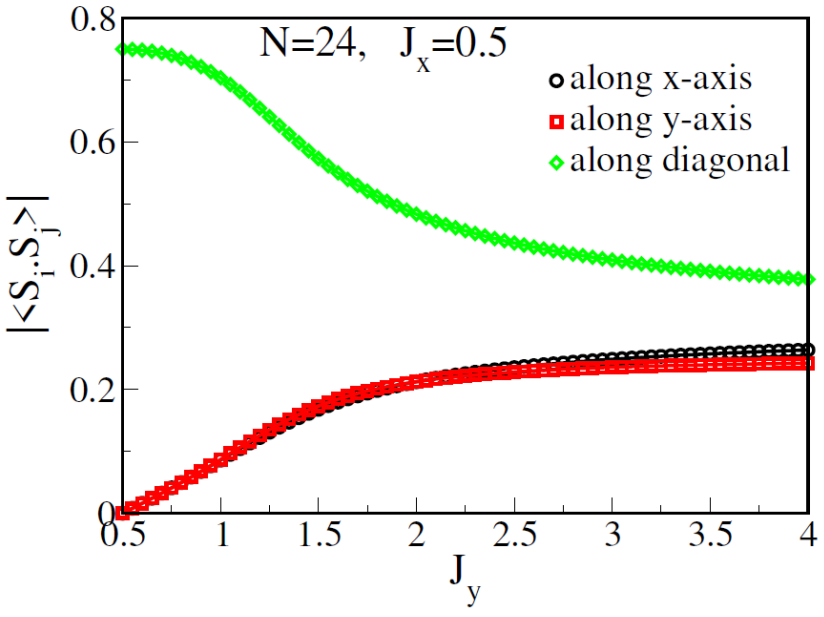

Figure 4.7: Figure shows the bond order along x-, y- and diagonal direction for 24 system sizes at $J_x = 0.5$. It is seen that the bond order along diagonal direction is always strong which says that dimer order is very strong in most of the region in the phase diagram.

4.3.5 Bond order

We have represented the bond order along x-, y- and diagonal direction for 24 system sizes at $J_x = 0.5$ for different values of J_y in Fig. 4.7. It is seen that the bond order along the diagonal bond is very strong in comparison to bond order along x- and y- directions. This calculation is also suggesting that the system does not have any gapless stripe order which was predicted in ref [27], rather we have found that above a particular value of interaction strength the system shows dimer order with stripe like spin-configuration with a finite gap.

4.3.6 Spiral phase and pitch angle

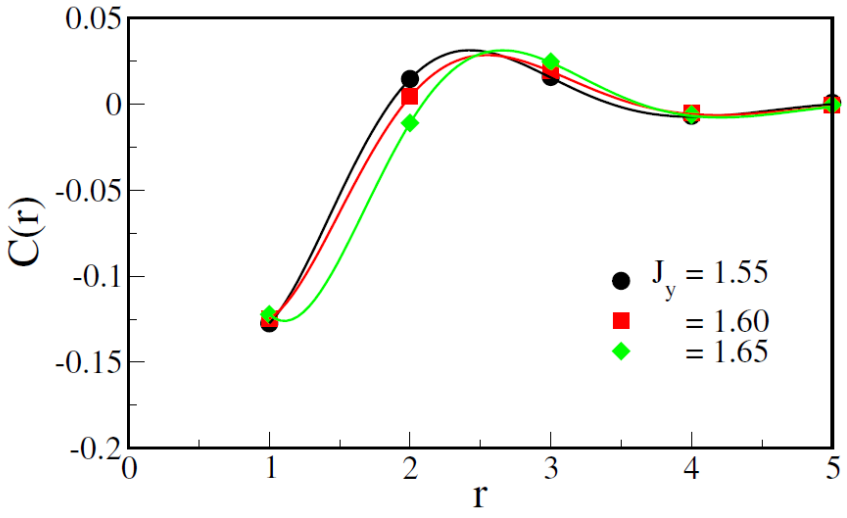

Figure 4.8: Figure shows the spin-spin correlation $C(r)$ along length (x-direction) for different J_y at $J_x = 0.7$. The solid curves represent respective fits with exponential decaying function. In both plots we have used 12×4 system size.

In a geometrically frustrated system wavevector or the pitch angle of a non-collinear spin ordering, in general, depends on the competing exchange interactions [28, 90, 180] and therefore, it is important to understand the behavior of pitch angle (θ) in various exchange interaction limits to quantify spin modulation in terms of the pitch angle Q_x and Q_y. Fig. 4.8 shows spin-spin correlation $C(r)$

for $J_x = 0.7$ for different J_y values inside the X-spiral region. $C(r)$ shows the exponentially decaying behavior with distance r. It indicates the non-collinear spin ordering along x-direction, representing the X-spiral phase. $C(r)$ in Fig. 4.8 shows an exponential decay, representing a very short-range correlation in the spiral region. Pitch angle (Q_x) can be calculated in the X-spiral phase, by fitting $C(r)$ with the following equation

$$C(r) = a_0 \cos(Q_x r + c)\ e^{-\frac{r}{\xi}}\ , \tag{4.3}$$

where ξ is the correlation length, a_0 and c are constants. To calculate the pitch angles in the Y-spiral phase, a similar correlation function can be applied as above, where Q_x will be replaced by Q_y. The pitch angle calculation confirms the existence of a very narrow spiral phase in the phase diagram. The spin alignment is non-colinear but still the bond order along diagonal bond is very strong, that's why we have called this phase as dimer spiral instead of spiral only.

4.4 Summary and conclusion

In this work, we construct a new quantum phase diagram of ferromagnetically coupled $S = 1/2$ on the SSL. Exchange couplings along length J_x and width J_y are ferromagnetic, whereas, the exchange couplings along diagonal bonds J are antiferromagnetic. The quantum phase diagram of the SSM in Eq. 4.1 consists of six phases and the phase boundaries are calculated based on spin-spin correlation and the gs energies obtained using the ED and the DMRG methods. Our numerical calculations are done upto 12×8 lattices and we have used PBC along the width and OBC along length. Almost everywhere in the phase space the order is short range, therefore, most of our calculations give reliable results for the two dimensional lattice of this model. The six phases in the phase diagrams are: (I) dimer stripe $(0, \pi)$, (II) dimer stripe $(\pi, 0)$, (III) perfect dimer, (IV) dimer spiral along X-axis, (V) dimer spiral along Y-axis and (VI) ferromagnetic

state. Our analysis also confirms the existence of spiral phases in this model for moderate FM couplings strength.

Our DMRG results are very different from the Schwinger-Boson mean-field theory in Ref. [27]. Although quantum phases predicted by mean-field theory are also found in the DMRG results but phases boundaries are quite different. DMRG calculations suggest that perfect dimer singlet phase is confined to only on $J_x = J_y$ line, whereas the mean-field calculation suggests a large area of this regime. Our result is consistent with the ED results [27]. Our results also suggest that second nearest neighbor correlation increases continuously with $|J_x - J_y|$ i.e. short range but finite correlation exists in the neighborhood of dimer line except the $J_x = J_y$ line where only diagonal correlations are non zero. The mean-field results suggest the non-collinear spin wave along the x- and y-direction but ED does not confirm the results [27]. DMRG results confirm both types of the non-collinear phases. The mean-field pitch angle variation is small compared to the DMRG value in most parts of the parameter regime.

Tassel *et al.* suggested that (CuCl)$LaNb_2O_7$ has ferromagnetic $J_y/J \sim 0.39$ and $J_x/J \sim 0.38$ [77] and therefore, we expect this system should behave like dimer as it is on $J_x = J_y$ dimer singlet line. Although, Tsirlin *et al.* shows different exchange interactions using the two types of DFT calculations [174]. However, the data of inelastic neutron scattering (INS) on powder samples shows that the dynamical structure factor has $S(Q, \omega)$ maxima around $Q \sim 0.5$Å, i.e. it is in a non-collinear regime. In our opinion this material is in the neighborhood of dimer phase but detailed theoretical investigation is required to understand the spin configuration in the system.

In conclusion, we numerically studied the SSM and constructed a new quantum phase diagram using the DMRG method. We have also calculated the correlation function and pitch angle which can be directly connected to INS data. The phase boundaries calculated from DMRG results are different from that of mean-field and ED calculations [27]. We hope that interesting quantum phases

in real material like (CuCl)$LaNb_2O_7$ and others [77, 181–183] can be revisited in light of this study. The short range spiral phase in the frustrated regime of the model can be manipulated by external probe like a magnetic field, doping, etc. and might lead to many interesting phases. The effect of field on phase diagram of the model in Eq. 4.1 is still an open problem.

4.5 Appendix

$L_x \times L_y$	J_x	J_y	m	ϵ_{gs}
12×4	0.6	0.21	256	-0.357791
			512	-0.357795
			900	-0.357798
12×8	0.6	1.0	256	-0.36989
			512	-0.36987
			700	-0.36984

Table 4.1: The table shows the gs energy per site (ϵ_{gs}) calculated for various bond dimensions (m). For the system size 12×4 gs energy calculated for $J_x = 0.6$ and $J_y = 0.21$, whereas for 12×8 system size, it is calculated for $J_x = 0.6$ and $J_y = 1.0$.

direction	r	$m = 256$	$m = 512$	$m = 900$
length	1	0.02154	0.02153	0.02152
	2	0.00652	0.00651	0.00650
	3	0.00182	0.00182	0.00178
	4	0.00056	0.00056	0.00053
	5	0.00015	0.00015	0.00014
width	1	-0.02269	-0.02269	-0.02267
	2	0.01006	0.01006	0.01008

Table 4.2: The table shows spin-spin correlation $\langle S_i^z S_{i+r}^z \rangle$ calculated for various bond dimensions (m) for 12×4 system size. The correlation calculated along length and width for $J_x = 0.6$ and $J_y = 0.21$, where the last three columns are the correlation values for the corresponding m.

direction	r	$m = 256$	$m = 512$	$m = 700$
length	1	-0.02095	-0.02097	-0.02088
	2	0.00354	0.00338	0.00328
	3	-0.00037	-0.00032	-0.00030
	4	0.000058	0.000050	0.000042
	5	-0.000006	-0.000019	-0.000004
	6	-0.000001	0.000033	0.000001
width	1	0.021093	0.021144	0.021042
	2	0.008490	0.008516	0.008512
	3	0.002574	0.002553	0.002526
	4	0.001771	0.001719	0.001769

Table 4.3: The table shows spin-spin correlation $\langle S_i^z S_{i+r}^z \rangle$ calculated for various bond dimensions (m) for 12×8 system size. The correlation calculated along length and width for $J_x = 0.6$ and $J_y = 1.0$, where the last three columns are the correlation values for the corresponding m.

Chapter 5

Singlet quantum phases of the frustrated spin-1/2 ladder with ferromagnetic (F) exchange in legs and alternating F-AF exchange in rungs

5.1 Introduction

The spin-1/2 Heisenberg antiferromagnet (HAF) with isotropic AF exchange $J_1 > 0$ between first neighbors has been central to theoretical studies of correlated many-spin systems, including the famous exact $1D$ solution based on the Bethe ansatz and the magnetism of inorganic [184, 185] and organic materials [186, 187] that contain $1D$ spin-1/2 chains. The addition of AF exchange $J_2 > 0$ between second neighbors introduces frustration and leads to interesting ground states such a bond order waves and spiral phases. The $J_1 - J_2$ model has been successfully applied to the magnetism of crystals with $1D$ chains of

$S = 1/2$ of Cu(II) ions [187]. In the AFAF model [2, 188] the exchange J_1 alternates between F and AF. The model has attracted recent attention its approximate realization in some materials, eg $Na_2Cu_2TeO_6$ [189, 190], $CuNb_2O_6$ [191], and $(CH_3)_2NH_2CuCl_3$ [192]. The $J_1 << 0$ limit of the AFAF model is the spin-1 HAF whose properties have been intensively studied since the Haldane's prediction that it is gapped. Quantum phases and phase diagrams have been a major thrust of $1D$ and $2D$ spin-1/2 models with strong correlations and exotic quantum phases both in zero and applied magnetic field.

In this chapter we obtain the quantum phase diagram of the frustrated F-AF ladder in Fig. 5.1 with isotropic AF exchange J_A in rungs $2r$, $2r+1$, F exchange $-J_F$ in rungs $2r$–1, $2r$ and F exchange $-J_L$ between neighbors r, $r+2$ in either leg. The ladder reduces to various spin-1/2 models. The AFAF model has $J_L = 0$ and alternate $J_1 = -J_F$ and J_A. The $J_1 - J_2$ model has $J_1 = J_A = -J_F$ and $J_2 = -J_L$.

The F-AF ladder has two noteworthy features. First, the ground state is either a singlet or ferromagnetic [193]; second, the ground state is a product of singlet-paired spins along a line where F exchanges cancel exactly. Both features are central in the following. A product of singlet-paired spins is the exact ground state [27, 32, 112, 121, 132, 134, 188] at special points of other $1D$ and $2D$ spin systems. We consider ladders with $2N$ spins-1/2, periodic boundary conditions and isotropic exchanges J_A, J_F and J_L in Fig. 5.1, and take $J_A = 1$ as the energy unit. The Hamiltonian is

$$H_{F-AF}(J_L, J_F) = \sum_{r=1}^{N} (\vec{S}_{2r} \cdot \vec{S}_{2r+1} - J_F \vec{S}_{2r-1} \cdot \vec{S}_{2r}) - J_L \sum_{r=1}^{2N} \vec{S}_r \cdot \vec{S}_{r+2}. \quad (5.1)$$

The ladder is equivalent to a $1D$ chain with two spins per unit cell, exchange $-J_L$ between second neighbors and alternating exchanges $-J_F$ and J_A between

first neighbors. The total spin $S \leq N$ and its z component S^z are conserved.

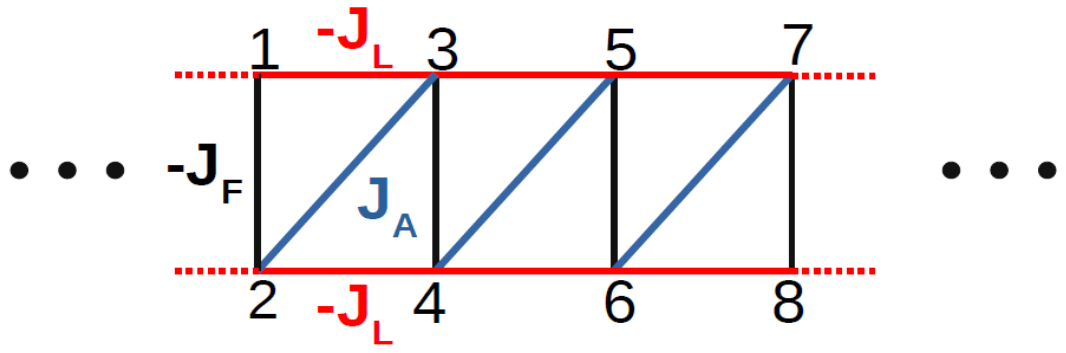

Figure 5.1: The F-AF spin-1/2 ladder with F exchange $-J_L < 0$ between spins r and $r+2$ in either leg, F exchange $-J_F$ in rungs $2r-1$, $2r$ and AF exchange J_A in rungs $2r$, $2r+1$.

The exchanges $J_A = 1$, J_L and J_F dominate in different regions of the positive quadrant of the J_L, J_F plane. Near the origin, the spins $2r$, $2r+1$ are singlet paired with ground state energy $\varepsilon_0(J_L, J_F)$ per dimer and singlet-triplet gap $\varepsilon_T(J_L, J_F)$. The exact energy is $\varepsilon_0(J_L, J_F) = \varepsilon_0(0,0) = -3/4$ along the line $J_L = J_F/2 \leq 1$ with cancelling F exchanges. Instead of competing, F exchanges cooperate in the F phase with fully aligned spins and energy per dimer

$$\varepsilon_F(J_L, J_F) = -(2J_L + J_F - 1)/4. \tag{5.2}$$

It follows that the F phase cannot be induced by large J_L if the net exchange $1 - J_F > 0$ between spins in different legs is AF; likewise, the F phase cannot be induced by large J_F if the net exchange $1 - 2J_L > 0$ between rungs is AF. The relation $\varepsilon_0(J_L, J_F) = \varepsilon_F(J_L, J_F)$ defines the boundary between the singlet and F quantum phases. Dmitriev *et al.* obtained the exact boundary and showed that intermediate S has higher energy [193]. In the present notation

$$J_F = 2J_L/(2J_L - 1), \qquad 2J_L, J_F \geq 1. \tag{5.3}$$

Eq. (5.3) is also the nonmagnetic/F boundary of classical spins [2].

We resolve the singlet phase of the F-AF ladder into three quantum phases. To do so, we consider the lowest energy per dimer, $E(S, 2N)$, with spin $S \leq N$ of a $2N$-spin ladder with J_L, J_F in Eq. (5.1). The thermodynamic limit is $E(s)$ with continuous $s = S/N$ in the interval $[0, 1]$. The ladder is not frustrated along either axis. $E(s)$ is continuous, monotonic and concave up for $(0, J_F)$ or $(J_L, 0)$, with $E''(s) > 0$ for all s. Concave up $E(s)$ is typical for no or weak frustration.

The situation is completely different at the singlet/F degeneracy with J_L, J_F in Eq. (5.3) where, except at the end points, $E(s)$ is unstable to disproportionation into $(1 - s)E(0) + sE(1)$. At general J_L, J_F, the ladder has domains with unstable $E''(s) < 0$ for some s as well as domains with $E''(s) > 0$ for all s. We call the dimer phase the domain with $E''(s) < 0$ for at least one s. It separates domains along the J_L and J_F axes, respectively, with $E''(s) > 0$ for all s.

The quantum phase diagram is presented in Sec. 5.2 along with that of classical spins. The $E''(S, 2N)$ analysis in Sec. 5.3 is based on exact diagonalization (ED) of Eq. (5.1) with periodic boundary conditions up to $2N = 24$ spins and density matrix renormalization group (DMRG) calculations on longer ladders up to $2N = 48$. We consider spin correlations and chains with higher symmetry in Sec. 5.4. The Haldane-DAF phase at $J_F \to \infty$ is rigorously related to the spin-1 Heisenberg AF chain, and the AF phase at $J_L \to \infty$ to the $J_1 - J_2$ model. Sec. 5.5 is a brief summary.

5.2 Quantum phase diagram

The singlet phases of Eq. (5.1) in the J_L, J_F plane are necessarily close to the origin, where J_L and J_F are comparably small, or close to the J_L or J_F axis, where the other exchanges are small. Most of the quadrant is F. To discuss ranges of J_L and J_F, we show the phase diagram for $J_L \geq J_F/2$ in Fig. 5.2 (a) and for $J_F/2 \geq J_L$ in Fig. 5.2 (b). The red line is the singlet/F boundary, Eq. (5.3), that is also the nonmagnetic/F boundary of classical spins. The calculated

points on the boundary are ED for $2N = 24$ spins. The dashed black line is the exact dimer line at $J_L = J_F/2 \leq 1$ with $\varepsilon_0 = -3/4$. Arrows on the right axes mark $J_L = J_F/2 = 1/2$, the singlet/F boundary at $J_L \to \infty$ or $J_F \to \infty$.

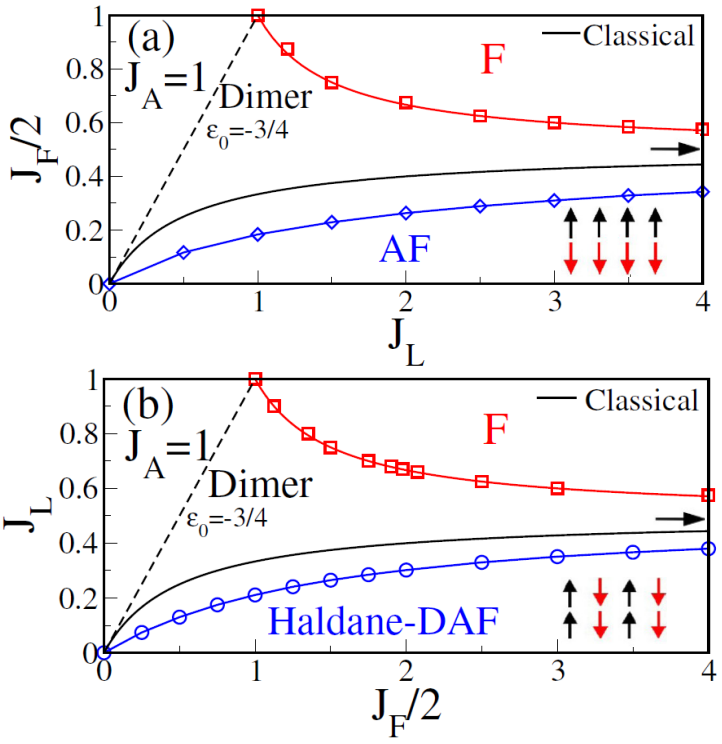

Figure 5.2: Quantum phase diagram of the ladder for (a) $J_L \geq J_F/2$ and (b) $J_F/2 \geq J_L$. The red line is the singlet/F boundary, Eq. (5.3), also for classical spins. Solid black lines are the AF/Spiral and DAF/Spiral boundaries of classical spins [2]. The exact energy is $\varepsilon_0 = -3/4$ is along the dashed black line. Arrows at the right axis mark $J_F/2 = J_L = 1/2$. The blue lines are the AF/dimer boundary in (a) and the Haldane-DAF/dimer boundary in (b), with $E''(s) > 0$ for all states from the line to either axis. The dimer phase between the blue and red lines has $E''(s) < 0$ for one or more states.

It is instructive to mention the exact nonmagnetic phases of classical spins, the Spiral, AF and DAF phases that are fully presented in Ref. [2] . The Spiral phase is bounded by the red and black line in each panel of Fig. 5.2. The black lines are identical since the classical boundaries are symmetric about the line $J_L = J_F/2$ along which F exchanges cancel exactly. As sketched in Fig. 5.2 (a), classical spins in the AF phase are antiparallel in legs and correspond to the Néel

state with spins $\ldots\alpha\beta\alpha\beta\ldots$ in Fig. 5.1, although spin fluctuations preclude long range order in $1D$ quantum systems. The double-period antiferromagnetic (DAF) phase of classical spins in Fig. 5.2 (b) has parallel spins in rungs $2r$, $2r-1$ and antiparallel rungs that correspond to $\ldots\alpha\alpha\beta\beta\ldots$ along the ladder. Parallel spins in rungs and antiparallel rungs along along the legs suggest a spin-1 chain with AF exchange whose singlet-triplet gap was predicted by Haldane to be finite [112]. The phases of classical spins have long range order.

The AF phase of quantum spins in Fig. 5.2 (a) is between the J_L axis and the blue line while the Haldane-DAF phase in Fig. 5.2 (b) is between the J_F axis and the blue line. The curvature is positive, $E''(s) > 0$, in both for all $s = S/N$ from $1/N$ to $1-1/N$. The dimer phase is between the blue and red lines in both panels. The blue line with $E''(1) = 0$ is the boundary to the dimer phase based on $E(s, 2N)$ calculations in finite systems. The curvature first changes sign at $s = 1$ in the thermodynamic limit or at $S = N-1$ in systems of $2N$ spins.

We emphasize the different origins of the nonmagnetic phases of classical spins and the singlet phases of quantum spins. The ground state of Eq. (5.1) is minimized at J_L, J_F with respect to the orientation of classical spins [2]. The curvature of $E(S, 2N)$ distinguishes between quantum singlet phases. Although similar in some respect, the singlet quantum phases and nonmagnetic classical phases of the F-AF ladder are fundamentally different. The singlet phases are gapped. We speculate that spin fluctuations rationalize the smaller area of singlet quantum phases in Fig. 5.2 compared to the AF and DAF phases of classical spins. For completeness, we note that Hida *et al.* [2] have discussed topological phases of ladders with open boundary conditions and $J_F > 1/2$, $J_L > 1$ in Eq. (5.1). Topological phases are beyond the scope of the present study.

5.3 Curvature

We use two numerical methods, ED and DMRG, to solve Eq. (5.1) at $J_A = 1$ and variable J_L, J_F in sectors with $0 \leq S^z \leq N$. The state is a singlet if $E(S, 2N)$ appears only in the $S^z = 0$ sector. ED to $2N = 24$ spins returns the lowest energies $E(S^z, 2N)$ and generates a preliminary phase diagram. DMRG is then used for larger systems.

DMRG is a well-established numerical technique [121,149,179] for the ground state and low-lying excited states of correlated $1D$ systems. We use a modified DMRG algorithm [194] that adds four new sites (instead of two) to the superblock at each step. This avoids interaction terms between old blocks in models with second neighbor exchange, here J_L. All calculations are performed with periodic boundary conditions. We obtain truncation errors of 10^{-10} on keeping 512 eigenvectors of the density matrix and 4 or 5 finite sweeps. Systems up to 48 spins were used for finite-size scaling of phase boundaries.

$E(S, 2N)$ is the lowest energy per dimer in sector $S \leq N$ of a $2N$-spin ladder with J_L, J_F in Eq. (5.1). With $s = S/N$ and system size $2N$, the numerical approximation to the curvature is

$$E''(s, 2N) = N^2[E(s + N^{-1}) + E(s - N^{-1}) - 2E(s)] \tag{5.4}$$

The end points are $s = 1/N$ and $s = 1 - 1/N$.

Curvature calculations for $2N = 24$ are shown in Fig. 5.3 (a) at constant $J_F = 0.50$, variable J_L, and in Fig. 5.4 (a) at constant $J_L = 0.25$, variable J_F. In either case, $E''(s, 24)$ decreases with s and changes sign with decreasing J_L at $J_F = 0.50$ or with decreasing J_F at $J_L = 0.25$. The first appearance of $E''(s, 24) < 0$ is at $s = 1 - 1/6$, approximately when $J_L = 2$ in Fig. 5.3 (a) or when $J_F = 3$ in Fig. 5.4 (a).

The singlet phases in Fig. 5.2 are based on the thermodynamic limit of $E''(s, 2N) = 0$ at $s = 1 - N^{-1}$. The size dependence of $E''(s, 2N)$ at $J_F = 0.50$

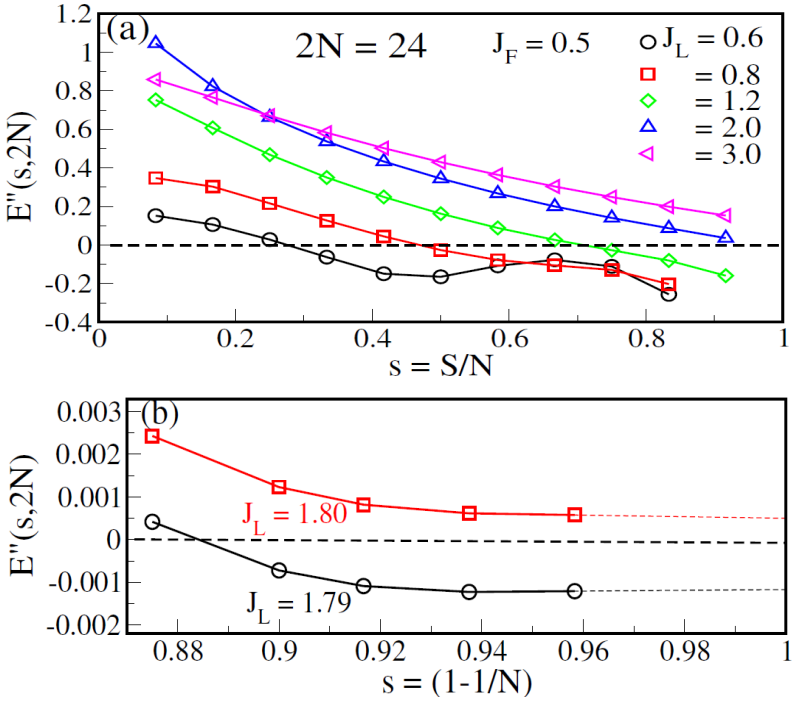

Figure 5.3: (a): Curvature $E''(s, 2N)$ vs. $0 \leq s = S/N \leq 1$ of a 24-spin ladder with $J_F = 0.50$ and variable J_L in Eq. (5.1). $E''(s, 2N)$ decreases with s and becomes negative at $s \leq 1$ for $J_L < 2$. (b): $E''(s, 2N)$ vs. $s = 1 - N^{-1}$ at $2N = 16$, 20, 24, 32, 48 and $J_L = 1.79$ or 1.80. The limit $(1.797, 0.50)$ generates a point on the dimer/AF boundary in Fig. 5.2 (a).

and two values of J_L is shown in Fig. 5.3 (b) for $2N = 16, 20, 24, 32$ and 48. Linear extrapolation returns $E''(1) = 0$ at $J_L = 1.793$, $J_F = 0.50$. This point is on the dimer/AF boundary in Fig. 5.2 (a). The same analysis of $E''(s, 2N)$ at $J_L = 0.25$ and two values of J_F is shown in Fig. 5.4 (b). The limit $E''(1) = 0$ is at $J_L = 0.25$, $J_F = 2.692$, a point on the dimer/Haldane-DAF boundary in Fig. 5.2 (b).

The evaluation of $E''(s, 2N)$ at $s = 1 - N^{-1}$ is very demanding numerically at large N. The calculated $E(s, 2N)$ must be accurate to 6 or 7 decimal places. Eq. (5.4) has differences between large numbers that return $E''(1 - N^{-1})$ of order 10^{-3} when multiplied by N^2.

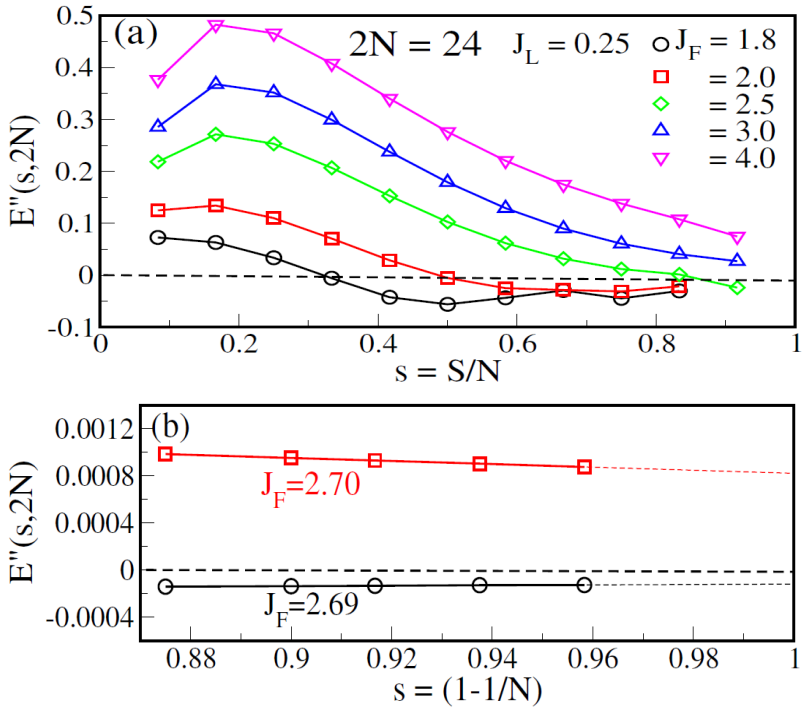

Figure 5.4: Curvature $E''(s,2N)$ vs. $0 \le s = S/N \le 1$ of a 24-spin ladder with $J_L = 0.25$ and variable J_F in Eq. (5.1). $E''(s,2N)$ decreases with s and becomes negative at $s \le 1$ for $J_F < 3$. (b): $E''(s,2N)$ vs. $s = 1 - N^{-1}$ at $2N = 16$, 20, 24, 32, 48 and $J_L = 2.69$ or 2.70. The limit $(0.25, 2.692)$ gives a point on the Dimer/Haldane-DAF boundary in Fig. 5.2 (b).

5.4 Singlet phases

The dimer phase has at least one state with $E''(s) < 0$. The other two phases have $E''(s) > 0$ for all states. The Haldane-DAF phase extends to arbitrarily large J_F provided that $2J_L < 1$, and the AF phase to large J_L provided that $J_F < 1$. We characterize the phases using $\varepsilon_T(J_L, J_F)$ and spin correlations functions

$$C(m,n) = \langle \vec{S}_m \cdot \vec{S}_n \rangle. \tag{5.5}$$

The expectation value is with respect to the singlet ground state of Eq. (5.1) at J_L, J_F. By symmetry, the ladder with periodic boundary conditions has three bond orders: $C(2,3)$ for rungs $2r$, $2r+1$ in Fig. 5.1, $C(1,2)$ for rungs $2r-1$, $2r$

and $C(1,3)$ for r, $r+2$ in either leg.

All $C(m,n)$ are zero at $J_L = J_F/2 \leq 1$ except $C(2,3) = -3/4$. In Fig. 5.2 (a) with $J_L > J_F/2$, the $C(m,n)$ are ≥ 0 (≤ 0) when $n-m$ is an even (odd) integer. When $J_F > 2J_L$, the bond orders are $C(1,2) > 0$ and $C(2,3)$, $C(1,3) < 0$. The sign of $C(m,n)$ for more distant spins follows the DAF pattern in Fig. 5.2 (b). The $C(m,n)$ are finite ranged in general for gapped phases. The gap $\varepsilon_T(J_L, J_F)$ is 1 at the origin and decreases more slowly with J_F than with J_L.

Spins in rungs $2r-1$, $2r$ are triplet paired when $J_F >> 1$. The ground state is 3^N-fold degenerate at $J_A = J_L = 0$. The spin-1 Heisenberg chain has AF exchange J between adjacent rungs $S_{2r-1} + S_{2r}$ and Haldane gap [3] $\Delta(J)/J = 0.411$. Connections between ladders and the $S = 1$ chain have already been noted [2, 4, 188].

We follow the quantitative evolution of the Haldane-DAF phase of the ladder to $S = 1$ chains as $J_F \to \infty$ by rewriting Eq. (5.1) as

$$H_{F-AF}(J_L, J_F) = -J_F \sum_{r=1}^{N} \vec{S}_{2r-1} \cdot \vec{S}_{2r} + (1 - 2J_L)/4 \times \sum_{r=1}^{N} (\vec{S}_{2r-1} + \vec{S}_{2r}) \cdot (\vec{S}_{2r+1} + \vec{S}_{2r+2}) + V'. \tag{5.6}$$

The first term corresponds to noninteracting triplets. The second is the $S = 1$ chain with AF exchange $(1 - 2J_L)/4 > 0$ between neighbors. The operator V' contains all other exchanges. The coefficients are: $(3 + 2J_L)/4$ for exchange between spins $2r$, $2r+1$; $-(1 + 2J_L)/4$ for exchange between spins r, $r+2$; and $-(1 - 2J_L)/4$ for exchange between spins $2r-1$, $2r+3$. Virtual states at finite J_F lead to effective Hamiltonians with excitations of order $1/J_F$. Eq. (5.6) adiabatically connects ladders with finite J_F and $2J_L < 1$ to $S = 1$ AF chains with $V' = 0$ in the limit $J_F \to \infty$.

There are two limits: $J_F \to \infty$ at any system size and $N \to \infty$. We followed the J_F dependence of $\varepsilon_T(J_L, J_F)$ and of correlations between adjacent rungs at

Table 5.1: Spin correlations $\langle (S_1 + S_2).(S_3 + S_4) \rangle$ and gaps $\varepsilon_T(J_L, J_F)$ of the ladder, Eq. (5.1) with 16 spins, variable J_F and $J_L = 0$ or 0.25.

	$\langle (S_1 + S_2) \cdot (S_3 + S_4) \rangle$		$\varepsilon_T(J_L, J_F)$	
J_F	$J_L = 0$	$J_L = 0.25$	$J_L = 0$	$J_L = 0.25$
10	−1.404	−1.393	0.187	0.121
40	−1.416	−1.416	0.157	0.083
100	−1.417	−1.417	0.152	0.078
200	−1.417	−1.417	0.150	0.076
∞	−1.417	−1.417	0.148	0.074
$S = 1$	−1.417		0.148	0.074

$2N = 16$. The ED results in Table 5.1 are for $J_L = 0$ and 0.25. The gaps and correlations converge smoothly, with $J_F = 200$ at the limit for $2N = 16$. They match the correlations of the finite $S = 1$ chain, −1.4171, and gap $\Delta = 0.593555$. Spin correlations depend weakly on J_L at finite J_F, but not in the limit. The $J_L = 0$ and 0.25 gaps in Eq. (5.6) are $\Delta/4$ and $\Delta/8$, respectively, in quantitative agreement with the finite $S = 1$ chain. Identical $J_F \to \infty$ limits hold at different system sizes and hence in the thermodynamic limit.

The $J_F \to \infty$ limit equalizes the bond orders $C(2,3) = (1,3) = C(2,4) = C(1,4)$ among the constituent spins of adjacent $S = 1$ rungs. The limit enforces higher symmetry: a reflection or C_2 rotation that interchanges the legs in Fig. 5.1. Correlations $C(m,n)$ among more distant $S = 1$ rungs also become equal. The gap $\varepsilon_T(J_L, J_F)$ decreases with increasing J_F and $J_L < 1/2$ to $(1 - 2J_L)\Delta(1)/4 > 0$, proportional to $\Delta(1) = 0.411$.

The quantitative relation between the $S = 1$ AF chain and the F-AF ladder only holds in the limit $J_F \to \infty$ since the ladder has lower symmetry. For the same reason, the $J_1 - J_2$ model with exchange J_1 to first neighbors and J_2 to second neighbors is related to the ladder with alternating first-neighbors exchanges only in the limit $J_L \to \infty$. The corresponding $J_1 - J_2$ model has $J_2 = -J_L$ and $J_1 = (1 - J_F)/2 > 0$. Now $J_L \to \infty$ enforces higher translational symmetry, one spin per unit cell instead of two.

As shown in Table 5.2 for $2N = 16$ spins, the bond orders $C(1,2)$ and $(2,3)$ are equalized as $J_L \to \infty$. The average of $C(1,2)$ and $C(2,3)$ at $J_L = 200$ is $C_{av} = 0.3140$ at $J_F = 0$ and 0.3132 at $J_F = 0.5$. The 16-spin $J_1 - J_2$ model with $J_2 = -200$ returns 0.3140 at $J_1 = 0.5$ and 0.3132 at $J_1 = 0.25$, in quantitative agreement with C_{av}. The spin gaps at $J_1 = 0.5$ and 0.25 are 0.1254 and 0.0626 instead of 0.1255 and 0.0630 in Table 5.2. In the present context, the limit has been reached for 16 spins by $J_L = -J_2 = 200$.

Table 5.2: Bond orders and gap $\varepsilon_T(J_L, J_F)$ of the ladder, Eq. (5.1), with 16 spins, variable J_L and $J_F = 0$ or 0.5. $C_{av} = [C(1,2)+C(2,3)]/2$ and $C_{dif} = C(1,2)-C(2,3)$.

J_L	J_F	$-C_{av}$	C_{dif}	ε_T
10	0	0.3419	0.0297	0.1360
	0.5	0.3263	0.0434	0.0731
50	0	0.3180	0.0057	0.1271
	0.5	0.3153	0.0085	0.0645
200	0	0.3140	0.0007	0.1255
	0.5	0.3140	0.0021	0.0630

Quite generally, $S = 1/2$ chains with short-range isotropic exchange and one spin per unit cell are either gapless with a nondegenerate ground state or gapped with a doubly degenerate ground state [137,195]. The phase diagram of the J_1-J_2 model has been discussed previously [1,196,197]. The nondegenerate ground state at $J_1 > 0$ and $J_2 < 0$ indicates a gapless chain. Alternating exchanges $J_A = 1$ and $-J_F$ lead to gapped chains with two spins per unit cell. It follows that the AF phase of the ladder is gapped for finite J_L but gapless as $J_L \to \infty$.

The AF and Haldane-DAF phases of the ladder are directly related to models with higher discrete symmetry, the $S = 1$ AF chain as $J_F \to \infty$ and the $J_1 - J_2$ model as $J_L \to \infty$. As seen in Tables 5.1 and 5.2, the limits are already emerging at $J_F = J_L = 10$, especially for spin correlations, and the lower symmetry of the ladder increases $\varepsilon_T(J_L, J_F)$. The dimer phase is bounded by the other phases in Fig. 5.2 except in the limits $J_L \to \infty$, $J_F = 1$ or $J_F \to \infty$, $2J_L = 1$ when there is no net AF interaction, respectively, between legs or rungs $2r - 1$, $2r$.

5.5 Summary and conclusion

The curvature $E''(s)$ of the states with lowest energy $E(s)$ per dimer and spin $0 \leq s = S/N \leq 1$ indicates that the F-AF ladder with J_L, J_F in Eq. (5.1) has three singlet quantum phases shown in Fig. 5.2. The Dimer phase has $E''(s) < 0$ for one or more states. All states have $E''(s) > 0$ in the Haldane-DAF and AF phases. Increasing J_F at constant $J_L < 1/2$ leads to a $S = 1$ chain with $J = (1-2J_L)\Delta(1)/4 > 0$ in the limit $J_F \to \infty$. Increasing J_L at constant $J_F < 1$ leads to a $J_1 - J_2$ model with $J_1 = (1 - J_F)/2 > 0$ and $J_2 = -J_L$ in the limit $J_L \to \infty$.

The states $E(s)$ also governs the $0K$ magnetization $M(h)$ per dimer [198] in magnetic field h. $M(h)$ increases continuously to $M(h) = 1$ in the AF and Haldane-DAF phases up to the saturation field h_S at which the absolute ground state is the lowest Zeeman component of the F phase. $M(h)$ is a unit step function at the dimer/F boundary where an infinitesimal h breaks the degeneracy. The magnetization transition is first order, discontinuous at h_S. The phase boundaries based on continuous/discontinuous $M(h_S)$ coincide [198] with the blue lines in Fig. 5.2 based on curvatures.

ED and DMRG are well suited for curvature calculations that require the thermodynamic limits of $E''(1)$ in Eq. (5.4). Numerical accuracy remains challenging in systems under study with small $\varepsilon_T(J_L, J_F)$, for example at or close to the dimer/F boundary, and spin correlations of intermediate range. The frustrated F-AF ladder with three exchanges J_L, J_F, J_A is related to several spin chains with two exchanges and higher symmetry.

Chapter 6

Spin-1/2 string correlations and singlet-triplet gaps of frustrated ladders with ferromagnetic legs and alternate ferromagnetic and antiferromagnetic rungs

6.1 Introduction

The spin-1/2 Heisenberg antiferromagnet (HAF) with isotropic AF exchange $J_1 > 0$ between first neighbors has been central to theoretical studies of correlated many-spin systems, including the famous exact $1D$ solution based on the Bethe ansatz and the magnetism of inorganic [199] and organic [200] materials that contain $1D$ spin-1/2 chains. The addition of AF exchange $J_2 > 0$ between second neighbors introduces frustration and leads to interesting ground state properties such a bond order waves [201], spiral phases [36, 139, 202] and spin liquids [37] due to quantum fluctuations. The $J_1 - J_2$ model has been successfully applied

to the magnetism of crystals with $1D$ chains of $S = 1/2$ of transition metal ions such as $Cu(II)$ [185, 203].

Dimerized chains have lower symmetry and different J_1 with neighbors to the right and left. The AFAF model [4] has alternate $J_A = 1$ to one neighbor and variable $-J_F$ to the other. The model has attracted much attention since its approximate realization in some materials, eg. $Na_2Cu_2TeO_6$ [189,190], $CuNb_2O_6$ [191] and $(CH_3)_2NH_2CuCl_3$ [192]. The AFAF model is the frustrated F-AF ladder in Fig. 6.1 with spin $S_r = 1/2$ at site r and $J_L = 0$. The recent study [204] of weakly-doped $Sr_{14}Cu_{24}O_{41}$ using resonant inelastic X-ray scattering illustrates the scope spin-1/2 ladders. Other two leg ladders singlet ground states may exhibit superconductivity on tuning the exchange interactions. [145, 205, 206].

The $J_F \to \infty$ limit of the AFAF model is the spin-1 HAF that has been intensively studied theoretically and numerically since Haldane predicted it to be gapped [112]. The ground state of the AFAF model with exchange $-J_L$ between second neighbors has interesting topological properties [2, 188] as do AFAF models [188] with spins $S > 1/2$, that are the focus of current research. The topological properties of AFAF models with $J_2 < 0$ pose open problems.

We study in this chapter the F-AF ladder in Fig. 6.1 with three isotropic exchanges: F exchange $-J_L$ between neighbors r, $r+2$ in legs, F exchange $-J_F$ at rungs $2r-1$, $2r$ and AF exchange J_A at rungs $2r$, $2r+1$. We consider parameters J_L, J_F and $J_A = 1$ leading to a singlet ($S = 0$) ground state $G(J_L, J_F)$. The ladder reduces to important models in special cases. It is the spin-1/2 HAF at $J_L = 0$ and $-J_F = J_A$ with one spin per unit cell and the AFAF model at $J_L = 0$ and $-J_F \neq J_A$ with two spins per unit cell. The ladder is frustrated except when $J_L = 0$ or $J_F = 0$. The limit $J_F \to \infty$ is the spin-1 HAF with $J = (1 - 2J_L)/4 > 0$ between adjacent F rungs. The limit $J_L \to \infty$ is a $J_1 - J_2$ model with $J_1 = (1 - J_F)/2 > 0$ and $J_2 = -J_L$. The symmetry is higher [198] at infinite J_F or J_L .

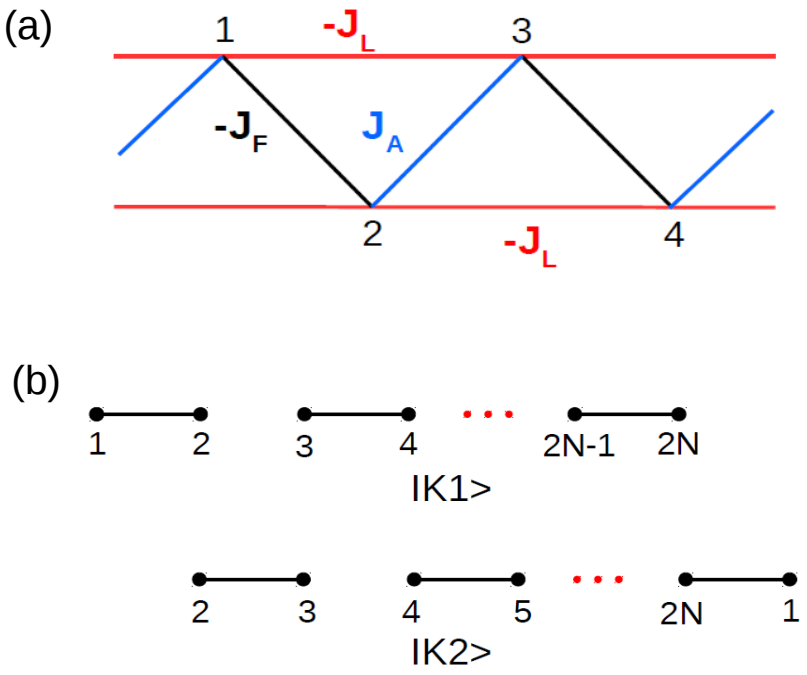

Figure 6.1: (a) The F-AF spin-1/2 ladder with F exchange $-J_L < 0$ between spins r and $r+2$ in either leg, F exchange $-J_F$ in rungs $2r-1$, $2r$ and AF exchange J_A in rungs $2r$, $2r+1$. (b) Kekulé diagrams $|K1\rangle$ and $|K2\rangle$ with singlet-paired spins $(2r\text{–}1, 2r)$ and $(2r, 2r+1)$, $r = 1$ to N.

The spin Hamiltonian with $J_A = 1$ as the unit of energy is

$$H_{F-AF}(J_L, J_F) = \sum_{r=1}^{N} (\boldsymbol{S}_{2r} \cdot \boldsymbol{S}_{2r+1} - J_F \boldsymbol{S}_{2r-1} \cdot \boldsymbol{S}_{2r}) - J_L \sum_{r=1}^{2N} \boldsymbol{S}_r \cdot \boldsymbol{S}_{r+2}. \tag{6.1}$$

The total spin $S \leq N$ and its z component S^z are conserved. We consider systems of $2N$ spins with periodic boundary conditions and seek the thermodynamic limit $N \to \infty$. The ground state $G(J_L, J_F)$ in that limit has two noteworthy features. First, it is either a singlet or ferromagnetic [193] for any J_L, J_F and $J_A = 1$. Second, the exact $G(J_L, J_F)$ is a product of singlet-paired spins along a line where F exchanges cancel exactly. Both are central in the following. A product

of singlet-paired spins is the exact ground state at special points of other $1D$ and $2D$ spin-1/2 systems [27, 32, 64, 77, 134, 188, 202, 207, 208].

We develop three themes. The first is string correlation functions in spin-1/2 chains. Den Nijs and Rommelse [114] and Tasaki [209] pointed out a hidden $Z_2 \times Z_2$ symmetry that can be measured by string correlation functions. Oshikawa [210] generalized the symmetry to Haldane chains with arbitrary integer $S > 1$. The critical theory of quantum spin chains by Affleck and Haldane [211] includes models with half-integer S and Z_2 symmetry. All the models considered [210,211] have equal isotropic exchange between either integer or half-integer S. The F-AF ladder has instead alternate $-J_F$ and $J_A = 1$ between first neighbors. It has two spins per unit cell in general, two string correlation functions and Z_2 symmetry only in limits with one spin per unit cell.

The string correlation function $O(p - p')$ between consecutive spins from p to p' in the spin-1 HAF is finite in the limit $|p - p'| \to \infty$. Hida [4] adapted the spin-1 expression to string correlation functions of the AFAF model ($J_L = 0$ in Eq. 6.1) with open boundary conditions. The string correlation functions $O(r - r')$ necessarily have an even number of consecutive spins-1/2 in Eq. 6.2 of ref. [4].

We use this expression in general. The string correlation function for an even number N of consecutive spins-1/2 is

$$g_1(N) = \langle G|exp(i\pi \sum_{j=1}^{N} S_j^z)|G\rangle. \tag{6.2}$$

The expectation value is with respect to the ground state in the thermodynamic limit or in finite systems with periodic boundary conditions. The general expression for spin-1/2 strings is well defined without reference to the spin-1 HAF. The initial spin is arbitrary in systems with one spin per unit cell. Since the F-AF ladder has two, the string correlation function $g_2(N)$ runs from $j = 2$ to $N + 1$ in Eq. 6.2. In either case string correlation functions of $2p \leq 2N$ spins can be

evaluated for $2N$-spin ladders. The choice $2p = N$ is convenient for taking the thermodynamic limit.

The exact ground state along the line $J_L = J_F/2 \leq 1$ is the Kekulé valence bond (VB) diagram $|K2\rangle$ in Fig. 6.1 with singlet-paired spins $2r$, $2r+1$ shown as lines, and as shown in Sec. 6.4, $g_2(N) = 1$, $g_1(N) = 0$ at any system size. To evaluate string correlation functions, we obtain the ground state $G(J_L, J_F, 2N)$ in increasingly large systems of $2N$ spins using exact diagonalization (ED) and density matrix renormalization group (DMRG) calculations. We interpret the results in terms of VB diagrams.

VB diagrams are an explicit general way to construct [212, 213] correlated many-spin states in real space with conserved $S \leq N$ for $2N$ spins-1/2. The spins are placed at the vertices of the regular $2N$ polygon. A line (m, n) between vertices m and n represents normalized singlet-paired spins whose phase is fixed by $m < n$

$$(m, n) = (\alpha_m \beta_n - \beta_m \alpha_n)/\sqrt{2}. \tag{6.3}$$

A legal (linearly independent) singlet diagram $|q\rangle$ has N lines (m, n), an N-fold product of singlet-paired spins, that connects all $2N$ vertices once without any crossing lines. Diagrams with crossing lines are not linearly independent since they can be resolved into legal diagrams. The normalized singlet ground state is formally a linear combination of singlet diagrams,

$$|G(J_L, J_F, 2N)\rangle = \sum_q C(q, J_L, J_F)|q\rangle. \tag{6.4}$$

The sum is over $R_0(2N)$ singlet diagrams that depends only on system size. The coefficients $C(q, J_L, J_F)$ depend on models, parameters and boundary conditions as well as system size. We find below the diagrams $|q\rangle$ that are eigenfunctions of the string operator in Eq. 6.2. The VB analysis accounts for the remarkable result of increasing string correlation functions $g_2(N)$ with system size. Conver-

gence to string order $g_2(\infty)$ is from below.

The second theme is to recognize three regimes of the F-AF ladder in the positive quadrant of the J_L, J_F plane. Near the origin, in Eq. 6.1 is a system of N dimers with exchange $J_A = 1$ between spins $2r$, $2r+1$, a singlet ground state, and frustrated F interactions between adjacent dimers. The singlet-triplet gap $\varepsilon_T(J_L, J_F)$ is large, spin correlations are short ranged, and small systems suffice for the thermodynamic limit. Increasing $J_F > 1$ while maintaining a singlet ground state leads to N rungs $2r-1$, $2r$ with triplet ($S = 1$) ground states and net AF exchange $1 - 2J_L > 1$ between adjacent rungs. Increasing $J_L > 1$ while maintaining a singlet ground state leads to F legs with net AF exchange $1 - J_F > 0$ between spins in different legs. Results for general J_L, J_F are understood qualitatively this way.

The third theme is dimerization. The nondegenerate singlet ground state of Eq. 6.1 is a bond order wave (BOW). The bond orders along the line $J_L = J_F/2 \leq 1$ are $\langle S_2 \cdot S_3 \rangle = -3/4$ for singlet-paired spins and $\langle S_1 \cdot S_2 \rangle = 0$ due to cancelling F exchanges. Interchanging $-J_F$ and $J_A = 1$ reverses the BOW without changing the energy spectrum. Increasing J_F reduces the BOW to [198] $\langle S_1 \cdot S_2 \rangle = 1/4$ and $\langle S_2 \cdot S_3 \rangle = -0.350$ in the limit $J_F \to \infty$. Increasing J_L to infinity leads to $\langle S_1 \cdot S_2 \rangle = \langle S_2 \cdot S_3 \rangle = -1/4$ and suppresses dimerization.

We discuss F-AF ladders with parameters J_L, J_F in Eq. 6.1 leading to singlet ground states. The chapter organized as follows. Sec. 6.2 summarizes the numerical methods used to obtain thermodynamic limits. Sec. 6.3 presents the singlet-triplet gap $\varepsilon_T(J_L, J_F)$ in the three regimes. String correlation functions $g_1(N)$ and $g_2(N)$ are defined in Sec. 6.4 for spin-1/2 systems with two spins per unit cell. The $g_2(N)$ minimum at N^* is a collective estimate of the range of ground-state spin correlations, while $g_1(N)$ decreases exponentially with system size for $N \geq N^*$. In Sec. 6.5 we consider string correlation functions of the $J_1 - J_2$ model with one spin per unit cell and spontaneous dimerization for some parameters. Sec. 6.6 is a brief summary.

6.2 Methods

We use two numerical methods, ED and DMRG, to solve Eq. 6.1 at $J_A = 1$ and variable J_L, J_F in sectors with $S^z = 0$ or 1 for $2N$ spins-1/2 or for the HAF with n spins-1. ED up to 24 spins-1/2 is sufficient for the thermodynamic limit of systems with short-range correlations or large $\varepsilon_T(J_L, J_F)$. DMRG with periodic boundary conditions is used for larger systems. The ground state is a singlet when the lowest energy in the $S^z = 0$ sector does not appear in other sectors. We also perform VB calculations to obtain the coefficients $C(q)$ in Eq. 6.4 in systems of $2N \leq 16$ spins.

DMRG is a well-established numerical technique for the ground state and low-lying excited states of correlated $1D$ systems [121, 149, 179]. We use a modified DMRG algorithm that adds four new sites (instead of two) to the superblock at each step [194]. This avoids interaction terms between old blocks in models with second neighbor exchange, here $-J_L$. All calculations are performed with periodic boundary conditions. We obtain truncation errors of 10^{-10} or less on keeping 512 eigenvectors of the density matrix and 4 or 5 finite sweeps. Systems up to $2N = 192$ spins-1/2 or $n = 64$ spins-1 were used for finite-size scaling.

There are additional external and internal checks on the accuracy of DMRG calculations. External checks are spin-1 calculations using other numerical methods [209, 214] or DMRG with open boundary conditions [3]. Excellent agreement for spin correlation functions to 6 or 7 decimal places is due at least partly to the large Haldane gap [3] of the spin-1 HAF. Internal checks rely on the singlet/F boundary [193] at

$$J_F = 2J_L/(2J_L - 1), \qquad 2J_L, J_F \geq 1. \tag{6.5}$$

The F energy per dimer is independent of system size,

$$\varepsilon_F(J_L, J_F) = -(2J_L + J_F - 1)/4. \tag{6.6}$$

The singlet ground state per dimer, $\varepsilon_0(J_L, J_F, 2N)$, is size dependent in general but must become size independent at the boundary. ED returns two states with $S^z = 0$ and one with $S^z = 1$ at $\varepsilon_0 = \varepsilon_F$. There are additional $S^z = 0$ and 1 states just above ε_F. The DMRG accuracy at $2N = 32$ drops to 4 or 5 decimal places for the dense spectrum at the boundary.

6.3 Singlet-triplet gap

Near the origin of the J_L, J_F plane, the singlet ground state energy per dimer is conveniently written in terms of $J_\pm = J_L \pm J_F/2$,

$$\varepsilon_0(J_L, J_F) = -\frac{3}{4} - \frac{3J_-^2}{4(2 + J_+)} + 0(J_-^3). \tag{6.7}$$

Spins $2r$, $2r + 1$ are dimers with exchange $J_A = 1$ and J_L, J_F cancel exactly when $J_- = 0$. The range of J_- at constant J_+ is from $-J_+$ at $(0, J_F)$ to J_+ at $(2J_L, 0)$. The ground state is a singlet for $J_+ \leq 2$, degenerate with $\varepsilon_F = -3/4$ at $J_L = 1$, $J_F = 2$. The virtual states at $(2 + J_+)$ in second-order perturbation theory are singlet linear combinations of adjacent triplet dimers. ED results for $\varepsilon_0(J_L, J_F, 2N) + 3/4$ are listed in Table 6.1 for $2N = 16$ and 24 at constant J_+ and $J_- = \pm J_+$. The size dependence is weak. Differences at $J_- = \pm J_+$ are of order J_-^3.

The upper panel of Fig. 6.2, shows $\varepsilon_T(J_L, J_F)$ at constant J_+ for $2N = 16$ and 24 as a function of $-J_+ \leq J_- \leq J_+$. The gap decreases from $\varepsilon_T(0, 0) = 1$ with increasing J_+ and is asymmetric in J_-. The size dependence is weak except at $J_+ = 2$, $J_- > 0$. The cusp at $J_- \approx 0$ and $J_+ = 0.4$ is due to lifting the N-fold degeneracy of localized triplets at $2r$, $2r+1$. The lowest triplet is nondegenerate with wavevector $k = 0$ or π that switches from π to 0 with increasing J_-.

The lower panel of Fig. 6.2 zooms in on $\varepsilon_T(J_L, J_F, 2N)$ at $J_+ = 2.0$ and $-0.4 \leq J_- \leq 0.4$, which includes the singlet/F boundary at $J_- = 0$. The crossing points at positive and negative J_- are due to finite size. The singlet and F

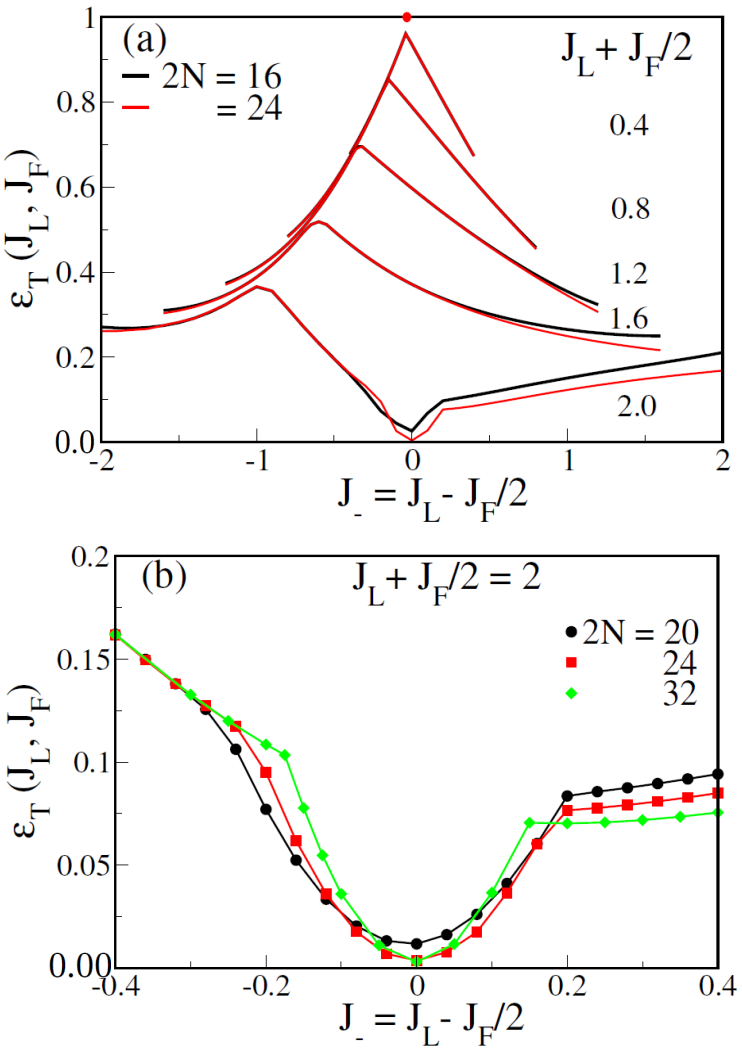

Figure 6.2: (a) Singlet-triplet gap $\varepsilon_T(J_L, J_F)$ vs. $J_- = J_L - J_F/2$ at constant $J_+ = J_L + J_F/2$ and system sizes $2N = 16$ and 24. The range is $-J_+ \leq J_- \leq J_+$, and $\varepsilon_T(0,0) = 1$. (b) $\varepsilon_T(J_L, J_F)$ at constant $J_+ = 2$ vs. $-0.4 \leq J_- \leq 0.4$ at $2N = 20$, 24 and 32. The crossing points are $\varepsilon_T = N(\varepsilon_F - \varepsilon_0)$.

ground states are extensive while ε_T is intensive. In finite systems, the extensive difference $N(\varepsilon_F - \varepsilon_0)$ at the singlet/F boundary is a parabola, $-N$ times the J_-^2 term of Eq. 6.7. The calculated $\varepsilon_T(J_L, J_F, 2N)$ at $J_+ = 2$, $J_- = 0$ are $\varepsilon_T(20) = 0.0118$, $\varepsilon_T(24) = 0.0037$ and $\varepsilon_T(32) \approx 0.0031 \pm 0.001$. As mentioned in Sec. 6.2, the dense spectrum at the boundary limits the numerical accuracy. The gaps of finite ladders in the lower panel are well approximated by parabolas with

Table 6.1: Ground-state energy ε_0 per dimer at constant J_+ and $J_- = \pm J_+$. ED at system sizes 16 and 24; the J_-^2 term of Eq. 6.7.

$J_+ = J_L + J_F/2$	$J_- = J_L - J_F/2$	$\varepsilon_0(16) + 3/4$	$\varepsilon_0(24) + 3/4$	J_-^2 term, Eq. 6.7
0.4	0.4	−0.0486	−0.0486	−0.05
	−0.4	−0.0498	−0.0498	
0.8	0.8	−0.1604	−0.1599	−0.1714
	−0.8	−0.1679	−0.1678	
1.2	1.2	−0.3069	−0.3046	−0.3375
	−1.2	−0.3220	−0.3217	
1.6	1.6	−0.4742	−0.4695	−0.5333
	−1.6	−0.4945	−0.4939	

finite $\varepsilon_T \approx 0.003$ at $J_- = 0$, crossing points at $\varepsilon_T = N(\varepsilon_F - \varepsilon_0)$ and asymmetry due to J_-^3.

The size dependence of $\varepsilon_T(J_L, J_F)$ is much weaker at $J_F > 2$ than at $J_L > 1$. In either case the singlet/F boundary, Eq. 6.5, limits the magnitude of the other exchange. Fig. 6.3 shows $\varepsilon_T(J_L, J_F)$ at system sizes $2N = 16$ and 24 as a function of J_L at the indicated J_F. The maximum gap decreases and broadens with increasing J_F where triplets with different wave vectors are closely spaced. The $k = 0$ triplet is lowest when the gap is decreasing and (almost) vanishes at the singlet/F boundary. The $k = \pi$ triplets at $J_L = 0$ have the strongest size dependence.

The spins $2r-1$, $2r$ form triplets when J_F is large; the ground state degeneracy is 3^N at $J_A = J_L = 0$. To study the large J_F regime of the ladder, we rewrite Eq. 6.1 as

$$H_{F-AF}(J_L, J_F) = -J_F \sum_{r=1}^{N} \vec{S}_{2r-1} \cdot \vec{S}_{2r} + (1 - 2J_L)/4 \times \sum_{r=1}^{N} (\vec{S}_{2r-1} + \vec{S}_{2r}) \cdot (\vec{S}_{2r+1} + \vec{S}_{2r+2}) + V'. \tag{6.8}$$

The first term corresponds to noninteracting dimers with triplet ground states.

The second term is the spin-1 HAF with exchange $J = (1 - 2J_L)/4 > 0$ between neighboring rungs $2r, 2r - 1$. The operator V' contains all other exchanges. The coefficients are: $(3+2J_L)/4$ for exchange between spins $2r$, $2r+1$; $-(1+2J_L)/4$ for exchange between spins r and $r+2$; and $-(1-2J_L)/4$ for exchange between spins $2r-1$ and $2r+3$. Virtual excitations at finite J_F lead to effective Hamiltonians with excitations of order $1/J_F$. Eq. 6.8 adiabatically connects ladders with finite J_F and $2J_L < 1$ to the spin-1 HAF with $V' = 0$ in the limit $J_F \to \infty$.

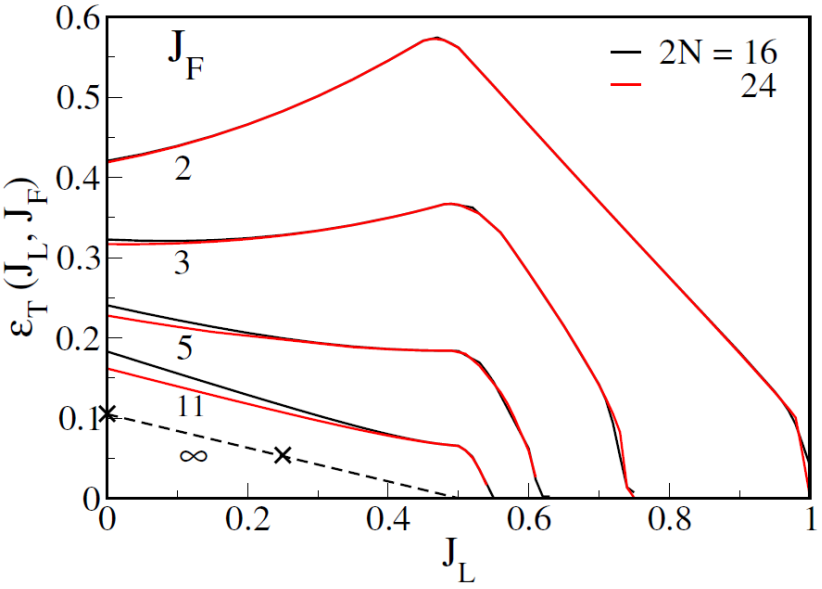

Figure 6.3: Singlet-triplet gap $\varepsilon_T(J_L, J_F)$ vs. J_L at constant J_F and system sizes $2N = 16$ and 24. The gaps are < 0.005 at the singlet/F boundary, $2J_L = J_F/(J_F - 1)$. The dashed line is $(1 - 2J_L)\Delta(1)/4$ where $\Delta(1) = 0.4105$ is the Haldane gap; [3] the crosses at $J_L = 0$ and 0.25 are for $J_F = 200$ and $2N = 64$.

DMRG with open boundary conditions returns [3] $\Delta(1) = 0.4105$ for the Haldane gap. We find $\Delta(1) = 0.4106$ for 48 spins-1 and periodic boundary conditions. The dashed line in Fig. 6.3 is $(1 - 2J_L)\Delta(1)/4$. The gaps indicated by crosses at $J_L = 0$ and $1/2$ are 0.1055 and 0.0538, respectively, at $J_F = 200$ and system size $2N = 64$.

The size dependence of $\varepsilon_T(J_L, J_F)$ is shown in Fig. 6.4 at constant $J_L = 1.5$, variable J_F in the upper panel and at constant $J_F = 1.5$, variable J_L in the lower

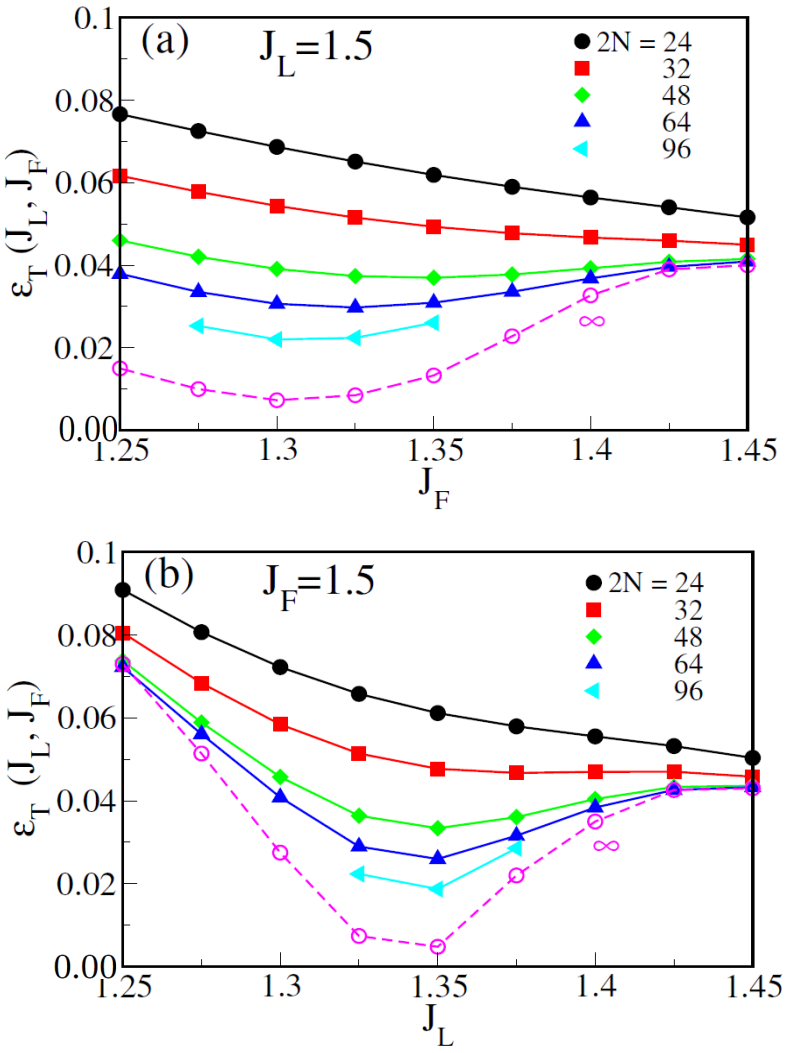

Figure 6.4: Size dependence of singlet-triplet gaps $\varepsilon_T(J_L, J_F)$ at (a) constant $J_L = 1.5$, variable J_F and (b) constant $J_F = 1.5$, variable J_L. The dashed line is the $1/N$ extrapolation from $2N = 24$ to $2N = 64$ or 96.

panel. The singlet/F boundary is $(1.5, 1.5)$ where the estimated gap is < 0.005. Both panels show $\varepsilon_T(J_L, J_F, 2N)$ minima in finite ladders and increasing gaps with weak size dependence at $(1.5, 1.45)$ or $(1.45, 1.5)$. The dashed lines are $1/N$ extrapolations. The remarkably small gap in Fig. 6.4 (a) has been noted [2] previously using DMRG with open boundary conditions. Small $\varepsilon_T(J_L, J_F)$ with a minimum are found at $J_A = 1$ and comparable J_L, J_F with $J_L + J_F \approx 2.8$. We do not have an explanation for a minimum gap.

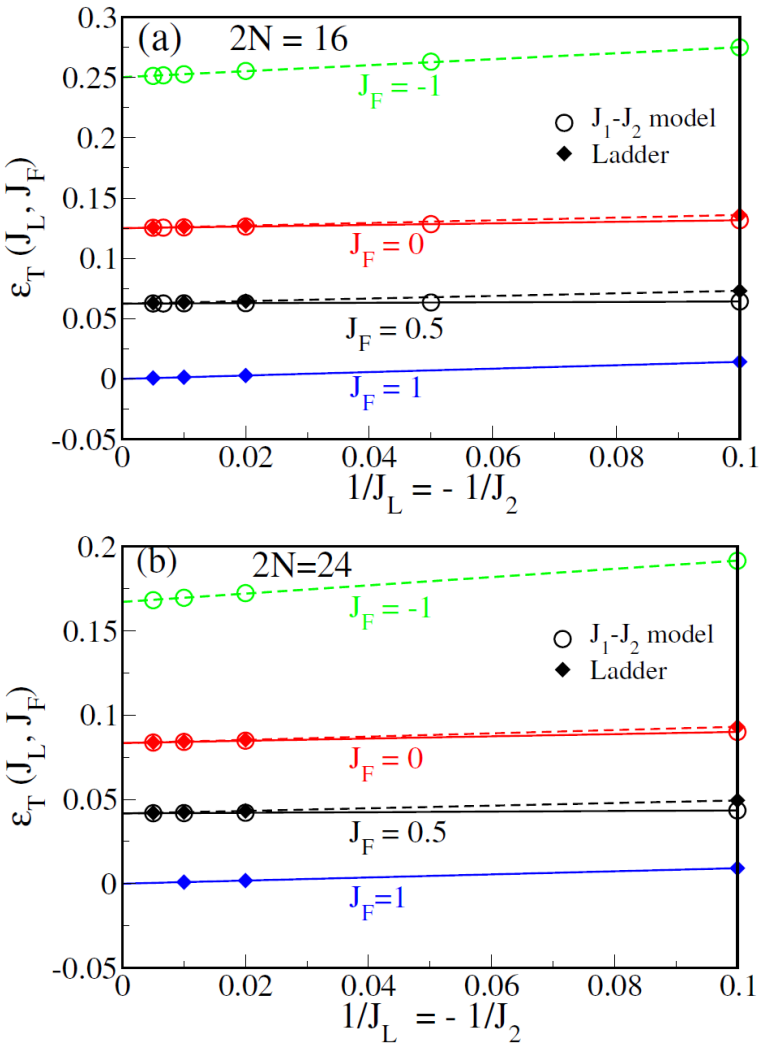

Figure 6.5: Singlet-triplet gaps $\varepsilon_T(J_L, J_F)$ vs. $1/J_L = -1/J_2$ at constant $J_F = -1, 0, 0.5$ and 1 at system sizes $2N = 16$ in (a) and 24 in (b). Open symbols refer to $J_1 - J_2$ models with $J_1 = (1 - J_F)/2$ and $J_2 = -J_F$. The ladder at $J_F = -1$ is a $J_1 - J_2$ model. The $1/J_L = 0$ gaps are $(1 - J_F)/2N$ for both. The $J_F = 1$ gap is finite in ladders, zero in $J_1 - J_2$ models.

Fig. 6.5 shows the J_L dependence of $\varepsilon_T(J_L, J_F)$ for the indicated J_F at $2N = 16$ and 24 in the upper and lower panels, respectively. The ladder with $-J_F = 1$ in Eq. 6.1 is a $J_1 - J_2$ model with $J_1 = 1$ and $J_2 = -J_L$. Ladders with other J_F have two spins per unit cell and correspond to alternating $J_1 - J_2$ models with $J_1 = (1 - J_F)/2$ and alternation $\pm(1 + J_F)/2$. Since the $J_1 - J_2$ model has noninteracting legs at $J_1 = 0$, the gap at $J_F = 1$ is entirely due to alternation.

The gaps at $J_F = 0$ and $1/2$ in Fig. 6.5 are equal at $1/J_L = 0$. As expected, alternating exchanges increase the gap when J_L is finite.

Eq. 6.1 conserves total S but not the spins $S_A = S_B \leq N/2$ of each leg. Equal J' between all spins in different legs leads to separately conserved S, S_A and S_B. Angular momentum addition returns $\varepsilon_T = J'$ when $J' > 0$. The mean-field approximation for $-J_F$ and $J_A = 1$ is $J' = (1 - J_F)/N$. The same result holds for the $J_1 - J_2$ model with $2N$ exchanges $J_1 = (1 - J_F)/2$. In the limit $J_L \to \infty$, the gap at system size $2N$ is

$$\varepsilon_T(J_F, 2N) = (1 - J_F)/N, \qquad J_F \leq 1, J_L \to \infty. \tag{6.9}$$

Eq. 6.9 agrees quantitatively with the numerical results at $1/J_L = 0$ in Fig. 6.5 for ladders and $J_1 - J_2$ models. Alternation increases ε_T.

The mean-field approximation has apparently not been recognized in systems with F exchange $-J_L$ in legs. The ladder with $J_F = 0$ and $J_A > 0$ in Fig. 6.1 has been studied numerically [47] and field theoretically [46]. The F state is unconditionally unstable when $J_A > 0$, as expected on general grounds; it can be stabilized [46,47] by an Ising contribution to the isotropic exchange $-J_L$. Eq. 6.9 is consistent with general expectations and provides quantitative gaps for finite ladders with $-J_F \leq 1$ in Eq. 6.1. The mean-field $\varepsilon_T(J_F, 2N)$ is elementary at $1/J_L = 0$ and rigorously decreases as $1/N$. It is a good approximation to at least $1/J_L = 0.1$.

We conclude this Section by highlighting the difference between no net AF exchange and no exchange. The ladder at $J_F \to \infty$ is a spin-1 HAF with $J = (1 - 2J_L)/4$. The singlet/F boundary is at $J = 0$ where the energy per dimer is $\varepsilon_0 = \varepsilon_F = -J_F/4$. Since the boundary in Eq. 6.5 is at $2J_L > 1$ when J_F is finite, the ground state is a singlet at $1 - 2J_L = 0$ and no net exchange, with per dimer energy

$$\varepsilon_0(1/2, J_F)/J_F = -1/4 - c/J_F^2. \tag{6.10}$$

The first-order energy of Eq. 6.8 is zero at $2J_L = 1$. There is a second-order correction because $J_A = 1$ and $-J_L = 1/2$ are between different spins, $2r$, $2r+1$ for J_A and r, $r+2$ for J_L. Eq. 6.10 holds for $J_F > 10$ with $c = 0.516$ at both $2N = 16$ and 24.

The $J_L \to \infty$ limit of the ladder is a $J_1 - J_2$ model. The singlet/F boundary is at $J_1 = 0$ with $\varepsilon_0 = -J_L/2$ when $J_F = 1$. The boundary of the ladder, $2J_L = J_F/(J_F - 1)$, is at $J_F > 1$ when J_L is finite. The ground state is a singlet at $J_F = 1$ and no net exchange between legs. But $\varepsilon_0(J_L, 1)$ has second-order corrections in $1/J_L$ since J_A and J_F are between different spins. We find $\varepsilon_0(J_L, 1)/J_L = -1/2 - d/J_L^2$ for $J_L > 10$ with $d = 0.271$ and 0.282 at $2N = 16$ and 24.

6.4 String correlation functions

We obtain an explicit relation between spin-1 and spin-1/2 string correlation functions. Girvin and Arovas define [113] string correlation functions of consecutives $s = 1$ spins as

$$\tilde{g}(n) = -\langle s_1^z (expi\pi \sum_{j=2}^{n} s_j^z) s_{n+1}^z \rangle. \tag{6.11}$$

The expectation value is with respect to the singlet ground state in the thermodynamic limit or in finite chains with periodic boundary conditions. The $(n-1)$ spins-1 in the exponent can be written as $2(n-1)$ spins-1/2 with $s_j = S_{2j-1} + S_{2j}$. The other spins are $s_1 = S_1 + S_2$ and $s_{n+1} = S_{2n+1} + S_{2n+2}$. To have strings of consecutive spins-1/2, Hida [4] chose spins S_2 and S_{2n+1} and used the spin-1/2 identity,

$$-4S_m^z S_n^z = expi\pi(S_m^z + S_n^z) \tag{6.12}$$

to shift those spins into the exponent. This leads to $g_2(N)$ with N consecutive spins from 2 to $N+1$ in Eq. 6.2. As anticipated [4] on including the factor of 4,

the string order $g_2(\infty)$ in the limit $J_F \to \infty$ is equal to $\tilde{g}(\infty)$.

The spin-1/2 string correlation function defined in Eq. 6.2 is not limited to either $J_F \to \infty$ or $N \to \infty$. Systems with two spin spins per unit cell have two strings of N spins. The string $g_1(N)$ in Eq. 6.2 has $N/2$ exchanges $-J_F$ and $N/2-1$ exchanges $J_A = 1$ while $g_2(N)$ has $N/2$ exchanges J_A and $N/2-1$ exchanges $-J_F$. The size dependencies of $g_1(N)$ and $g_2(N)$ are very different.

The string operator $\hat{g}_1(N)$ has an even number N of consecutive spins from 1 to N. Singlet VB diagrams $|q\rangle$ in systems of $2N$ spins have N lines (m,n) that correspond to singlet-paired spins in Eq. 6.3. Repeated use of Eq. 6.12 leads to

$$exp(i\pi \sum_{j=1}^{N} S_j^z)|q\rangle = |q\rangle, \quad 1 \le m,n \le N$$
$$= |q\rangle_T, \quad otherwise. \tag{6.13}$$

Diagrams $|q\rangle$ with $1 \le m,n \le N$ are eigenfunctions of with unit eigenvalue. The factor of 4 in Eq. 6.12 is required for normalization, $\langle q|q\rangle = 1$. The eigenfunctions are all possible singlets based on spins in the string.

Diagrams $|q\rangle$ that are not eigenfunctions contain one or more pairs of bridging lines (m,n) with only one spin in the string. Then $\hat{g}_1(N)|q\rangle$ generates a diagram $|q\rangle_T$ with triplet-paired spins $(m,n)_T = (\alpha_m\beta_n + \beta_m\alpha_n)/\sqrt{2}$ at all bridging lines. Spin orthogonality ensures $\langle q|q\rangle_T = 0$ but finite $\langle q'|q\rangle_T$ is possible with other singlets $|q'\rangle$. The Appendix summarizes two general properties of singlet VB diagrams, overlaps and dimensions. Overlaps $S_{q'q} = \langle q'|q\rangle$ are needed to evaluate expectation values. $R_0(2N)$ in Table 6.2 is the number of singlet diagrams at system size $2N$. A string of N spins has $R_0(N)$ eigenfunctions, each $R_0(N)$-fold degenerate, without any bridging lines. The relative number of diagrams with bridging lines increases with system size as indicated by the decreasing ratio $R_0(N)^2/R_0(2N)$ in Table 6.2.

We compute the string correlation functions $g_2(N)$ and $g_1(N)$ of the F-AF ladder with $2N$ spins Eq. 6.1. The upper panel of Fig. 6.6 shows the size

Table 6.2: $R_0(2N)$ is the number of singlet VB diagrams for $2N$ spins. $R_0(N)$ is the number of eigenstates of an N-spin string. Eq. A4 is Stirling's approximation.

$2N$	$R_0(2N)$	$R_0(N)$	$R_0(N)^2/R_0(2N)$	Eq. A4
12	132	5	0.189	0.199
16	1430	14	0.137	0.143
20	16796	42	0.105	0.109
24	208012	132	0.0838	0.0861

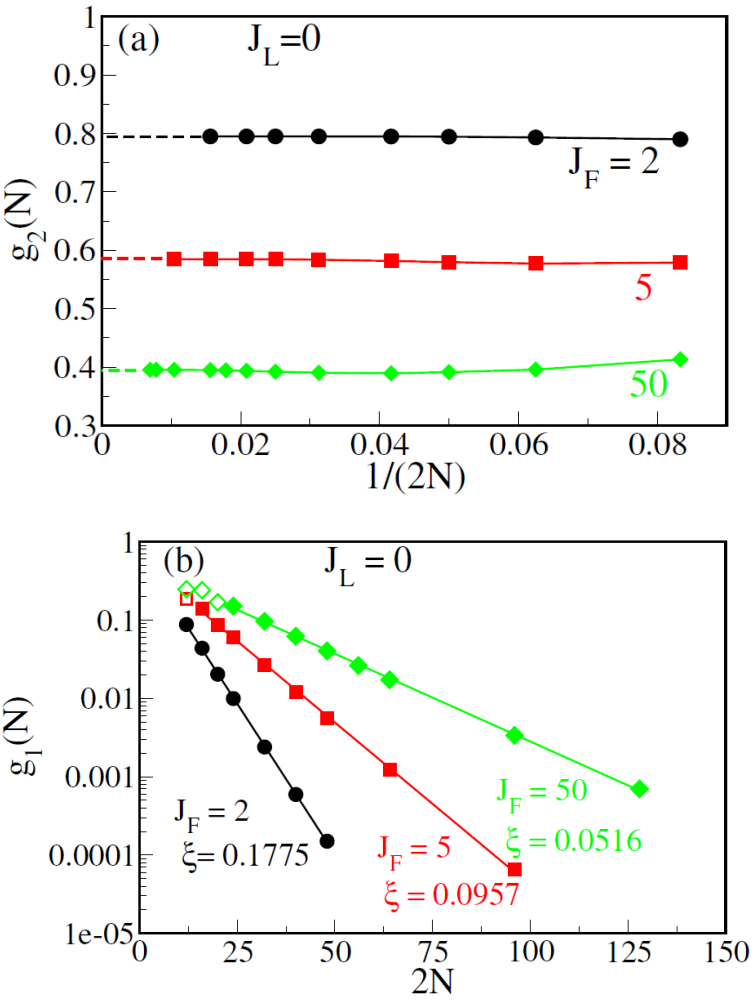

Figure 6.6: (a) String correlation functions $g_2(N)$ at system size $2N$, $J_L = 0$ and $J_F = 2, 5$ and 50; linear extrapolation to string order $g_2(\infty)$. (b) $g_1(N)$ for the same J_L, J_F with solid symbols for $N \geq N^*$, the minimum of $g_2(N)$, open symbols for $N < N^*$. The lines are Eq. 6.15 with the indicated ξ.

dependence of $g_2(N)$ as $1/(2N)$ from $2N = 12$ to 144 at $J_L = 0$ and $J_F = 2$, 5 and 50. The lower panel shows $g_1(N)$ on a logarithmic scale. At any system size, $g_2(J_F)$ is larger than $g_1(J_F)$ and decreases with J_F while $g_1(J_F)$ increases with J_F. Although not evident on the scale of Fig. 6.6, $g_2(N)$ at $J_F = 2$ increases from 0.789978 at $2N = 12$ and extrapolates to $g_2(\infty) = 0.794918$. At $J_F = 5$ and 50, $g_2(N)$ has a shallow minimum at $N^* = 8$ and 12, respectively. Convergence to $g_2(\infty)$ is again from below.

The following statements summarize results for other parameters J_L, J_F. String correlation functions satisfy the inequality,

$$1 \geq g_2(N) > g_1(N) \geq 0. \tag{6.14}$$

The function $g_2(N)$ has a shallow minimum at system size $2N^*$. The size dependence of $g_1(N)$ is exponential for $N \geq N^*$

$$g_1(N) = g_1(N^*)exp[-2\xi(N - N^*)], \quad N \geq N^*. \tag{6.15}$$

The $g_2(N)$ minima in Fig. 6.6 are $N^* = 4$, 8 and 12, respectively, for $J_F = 2$, 5 and 50. The lines for $N \geq N^*$ in the lower panel are Eq. 6.15 with the indicated ξ.

We interpret $g_2(N)$ and $g_1(N)$ in terms of the VB ground state, Eq. 6.4, with coefficient $C(q)$ for diagram $|q\rangle$. The exact ground state is $|K2\rangle$ when $J_L = J_F/2 \leq 1$, with $C(K2) = 1$ and $C(q) = 0$ for all other $|q\rangle$. The expectation values are $g_2(N) = 1$ and $g_1(N) = 0$ independent of system size. The shortest string is $N = 4$ since consecutive spins return the spin correlation function $-4\langle S_1^z S_2^z\rangle$.

The ground state is a linear combination of singlet diagrams $|q\rangle$ when $|J_L - J_F/2| > 0$. The representative singlet VB diagrams $|q\rangle$ in Fig. 6.7 have N lines (m, n); lines not shown explicitly are between neighbors $(m, m+1)$. The diagram $|a2\rangle$ differs from $|K2\rangle$ by two lines, $(2, 5)$ and $(3, 4)$. The N symmetry-related diagrams with a line $(2r, 2r + 3)$ have equal $C(q)$. The N diagrams $|a1\rangle$ in Fig.

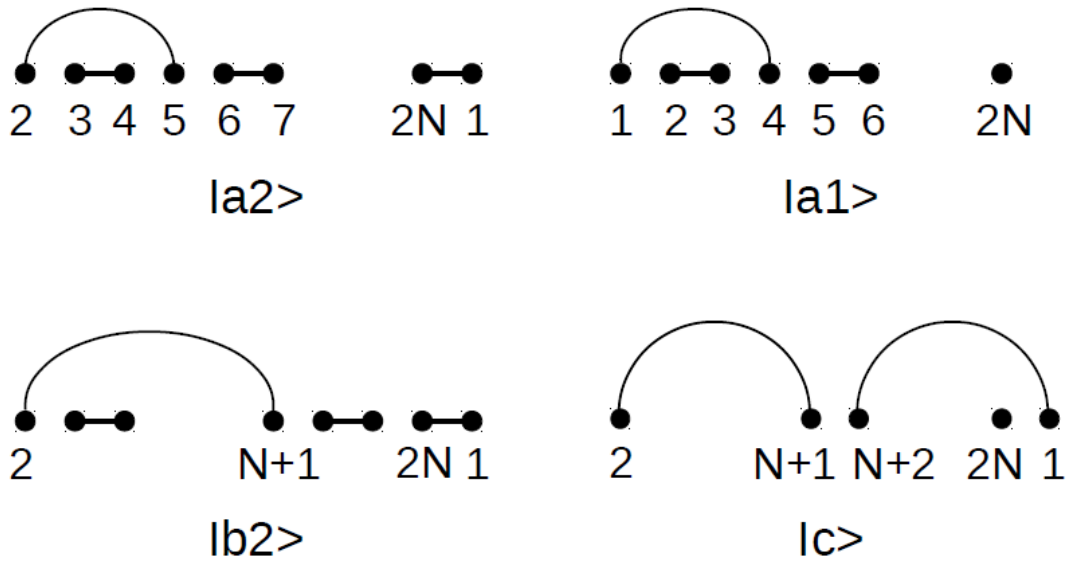

Figure 6.7: Representative singlet VB diagrams $|q\rangle$ with N lines (m, n) in ladders with $2N$ spins and C_N translational symmetry: $|a2\rangle$ has one line $(2, 5)$ of length 3 and $(N-1)$ lines of unit length; $|a1\rangle$ has one line $(1, 4)$ of length 3; $|b2\rangle$ has one line $(2, N+1)$ of length $N-1$, the maximum length; $|c\rangle$ has two lines of length $N-1$, $(2, N+1)$ and $(N+2, 1)$.

6.7 with a line $(2r-3, 2r)$ have equal $C(a1) < C(a2)$ since only line $(2, 3)$ is shared with $|K2\rangle$. Diagram $|b2\rangle$ has a line $(2r, 2r+N-1)$ of length $N-1$, the longest at system size $2N$. Diagram $|c\rangle$ has two lines of length $N-1$ and $(N-2)$ lines of unit length.

Table 6.3 shows the size dependence of selected coefficients $C(q)$ at $J_L = 0$, $J_F = 5$. The strong decrease of $C(K1)$ with system size is due to the overlap $\langle K1|K2\rangle = (-2)^{-(N+1)}$. The decrease of $C(a1)$ is also due to overlap. As shown in the Appendix, diagrams $|q\rangle$ that differ from $|K2\rangle$ by a finite number of lines are asymptoticly orthogonal to diagrams $|q'\rangle$ that differ from $|K1\rangle$ by a finite number of lines. The size dependence of $C(b2)$ illustrates the range of spin correlations, which is short at $J_L = 0$, $J_F = 5$, consistent with large $\varepsilon_T(0, 5)$ in Fig. 6.3. Diagram $|c\rangle$ has two lines of maximum length, and short-range spin correlations explain its size dependence.

Turning to string correlation functions, we note that $(N-2)$ of the diagrams $|a2\rangle$ are eigenfunctions of $\hat{g}_2(N)$ while two diagrams have bridging lines, either

Table 6.3: Ground-state coefficient $C(q)$ of diagrams $|q\rangle$ in Eq. 1 with $J_L = 0$, $J_F = 5$ and $2N$ spins. $|K1\rangle$ and $|K2\rangle$ are shown in Fig. 6.1, and $|a2\rangle$, $|a1\rangle$, $|b2\rangle$ and $|c\rangle$ in Fig. 6.7.

$C(q)\backslash 2N$	8	12	16
$C(K2)$	0.7583	0.6454	0.5607
$C(K1)$	0.1188	0.0217	0.0034
$C(a2)$	0.2981	0.2545	0.2213
$C(a1)$	0.0763	0.00556	0.00027
$C(b2)$	0.2981	0.0833	0.00045
$C(c)$	0.1172	0.0109	0.00144

$(2N, 3)(1, 2)$ or $(N, N+3)(N+1, N+2)$. The relative number of bridging lines in $|a2\rangle$ decreases with system size. On the other hand, only two diagrams $|b2\rangle$ are eigenfunctions of $\hat{g}_2(N)$; the other $(N-2)$ have bridging lines. As seen in Table 6.2, the relative number of diagrams with bridging lines increases with system size, and so do their coefficients $C(q)$ for parameters J_L, J_F that increase the range of spin correlations.

Since the ladder is gapped, spin correlations are finite ranged and $C(q)$ must be small for diagrams with lines (m, n) that exceed the range. We suppose N^* to be an estimate of the range. Then $g_2(N)$ and $g_1(N)$ decrease with system size up to $2N^*$ because the bridging lines increase more rapidly than eigenstates in Table 6.2. By hypothesis, $C(q)$ is negligible for diagrams with line longer than N^*. Then $g_2(N)$ increases when $N > N^*$ because diagrams with lines shorter than N^* are only bridging at the ends of increasingly long strings. The range N^* limits finite $C(q)$ to diagrams that differ from $|K2\rangle$ by a specified number of lines. The exponential decrease of $g_1(N)$ for $N > N^*$ in Eq. 6.15 is consistent with the asymptotic orthogonality of diagrams such as $|a2\rangle$ and $|a1\rangle$ that differ from $|K2\rangle$ and $|K1\rangle$, respectively, by two lines. It follows that $g_1(\infty) = 0$ and that $C(q) = 0$ in the thermodynamic limit for the $R_0(2N)/2$ diagrams $|q\rangle$ whose squared overlap is larger with $|K1\rangle$ than with $|K2\rangle$.

The panels of Fig. 6.8 show the size dependence of $g_2(N)$ and $g_1(N)$ in

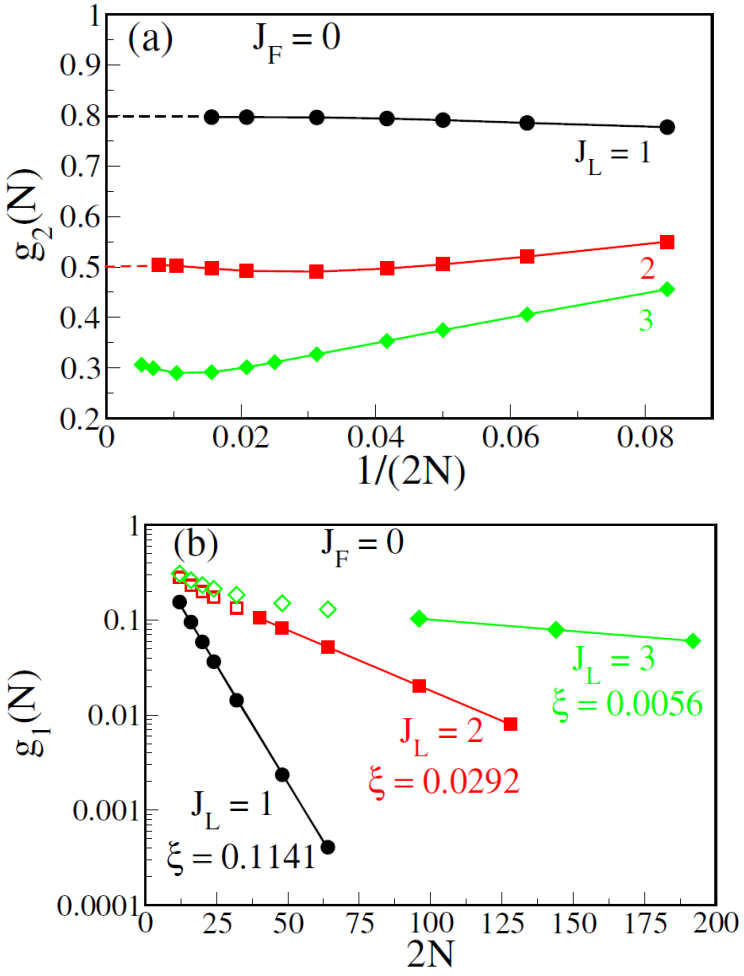

Figure 6.8: (a) String correlation functions $g_2(N)$ at system size $2N$ and $J_F = 0, J_L = 1, 2$ and 3. Linear extrapolation to string order $g_2(\infty)$. (b) $g_1(N)$ for the same J_L, J_F; solid symbols for $N \geq N^*$, open symbols for $N < N^*$. The lines are Eq. 6.15 with the indicated ξ.

ladders with $2N$ spins, $J_F = 0$ and $J_L = 1$, 2 and 3. The $g_2(N)$ minima are $N^* = 4$, 16 and 48 for $J_L = 1$, 2 and 3. Larger systems are required for accurate extrapolation of $g_2(N)$ at $J_L = 3$. The solid lines $g_1(N)$ in the lower panel are Eq. 15 with the indicated ξ.

Table 6.4 lists the string order $g_2(\infty)$, the minimum N^* of $g_2(N)$ and the spin gap ε_T for representative parameters J_L, J_F. We recall that $g_2(\infty) = 1 = C(K2)$ when $J_L = J_F/2 \leq 1$ while ε_T decreases from 1 at the origin to ≈ 0.003 at

Table 6.4: String order $g_2(\infty)$, minimum N^* of $g_2(N)$ and gap ε_T in the thermodynamic limit for J_L, J_F in Eq. 6.1.

J_L	J_F	$g_2(\infty)$	N^*	ε_T
0.25	1	0.98144	–	0.777
1	1.5	0.98143	4	0.242
1	1	0.941	4	0.340
0.5	0	0.926	4	0.610
1	0	0.797	4	0.370
0	2	0.795	4	0.416
0.5	5	0.675	6	0.183
0.25	5	0.634	6	0.196
0	5	0.585	8	0.225
2	0	0.503	16	0.110
2	0.5	0.490	24	0.053
2	1	< 0.09	> 100	0.016
0	50	0.396	12	0.11
3	0	~ 0.31	48	0.038

the singlet/F boundary. A $g_2(N)$ minimum at N^* requires J_L, J_F that lead to significant $C(q)$ for diagrams $|q\rangle$ with lines (m, n) longer than 4, the shortest string. The first two entries at $|J_L - J_F/2| = 0.25$ have almost equal $g_2(\infty)$ but quite different gaps; $g_2(N)$ has a minimum at $2N = 8$ for the smaller ε_T but not for the larger one, and the coefficients $C(K2)$, $C(a2)$ are by far the largest in either case. Systems with $N^* = 4$ or 8 in the Table return $g_2(\infty) > 0.75$ or > 0.5, respectively. The exponential decrease of $g_1(N)$ for $N \geq N^*$ in Figs. 6.6 (b) and 6.8 (b) starts around $g_1(N^*) \approx 0.1$. The interpretation is that $C(q)$ is small for diagrams with lines (m, n) longer than N^*. String order $g_2(\infty) < 0.25$ indicates longer-ranged spin correlations with $N^* > 50$ and gaps $\varepsilon_T < 0.1$.

The $g_2(N^*)$ minimum is exceptionally shallow at $J_L = 0.5$ and $J_F = 5$. Short-range correlations are to be expected at zero net exchange $1 - 2J_L$ between F rungs. We find constant $g_2(N)$ for $N \geq N^*$ to three decimal places, very small $g_1(N^*) < 0.02$ and the only deviation from exponential behavior seen so far. Spin correlations at $J_F = 5$ in Table 6.4 are shorter-ranged at $J_L = 0.5$ than at

$J_L = 0$.

There is no net exchange between legs when $J_F = 1$. The $J_L = 2$ gaps in Table 6.4 decrease from $J_F = 0$ to $J_F = 1$. In contract to zero net exchange between rungs, however, N^* at $J_L = 2$ increases from 16 at $J_F = 0$ to 24 at $J_F = 0.5$ and exceeds 100 at $J_F = 1$. Longer ladders than $2N \approx 200$ will be required for $g_2(\infty) < 0.25$. For example, $g_2(N)$ is still decreasing at $2N = 192$ at $J_L = 1.5$, $J_F = 1.3$ or at $J_F = 1.5$, $J_L = 1.35$, the parameters with $\varepsilon_T < 0.01$ in Fig. 6.4.

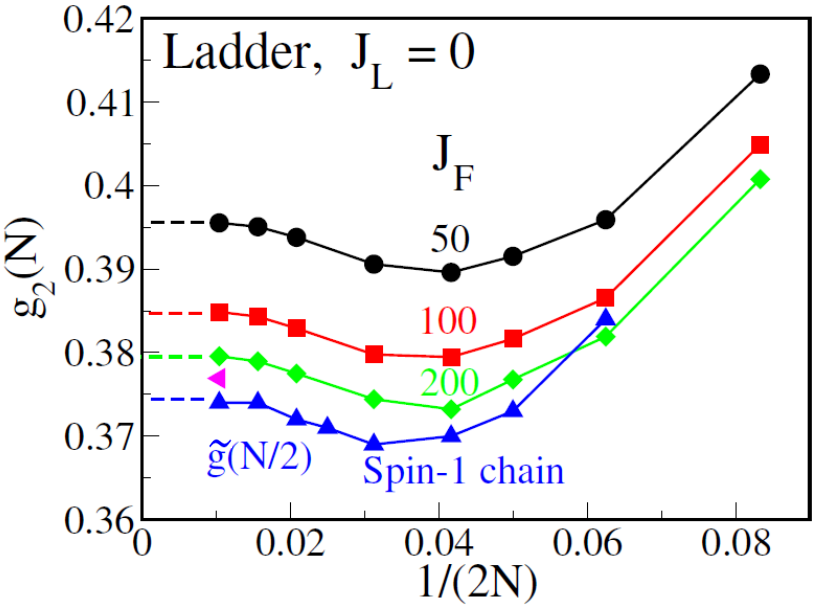

Figure 6.9: Size dependence of $g_2(N)$ at $J_L = 0$ and the indicated J_F from $2N = 12$ to 96. The string correlation function $\tilde{g}(N/2)$ is for the HAF with N spins-1. The magenta point at $2N = 96$ is for $J_F = 400$.

We now turn to the $J_F \to \infty$ limit of the ladder, the spin-1 HAF with $J = 1/4$ at $J_L = 0$. Fig. 6.9 compares the size dependence of $g_2(N)$ at system size $2N$, $J_L = 0$, and J_F with $\tilde{g}(N/2)$, Eq. 6.11, the string correlation function for N spins-1. Note the expanded scale. The string orders $\tilde{g}(\infty)$ and $g_2(\infty)$ are equal in the limit $J_F \to \infty$ by construction [4], as discussed above, but $g_2(N)$ is not equal to $\tilde{g}(N/2)$ at either finite J_F or finite N. The $\tilde{g}(N/2)$ minimum occurs

at $N = 16$ spins-1. The string order is [3] $\tilde{g}(\infty) = 0.374325$ while we obtain $\tilde{g}(\infty) = 0.37427$ at 48 spins-1. We find $g_2(48) = 0.37692$ for 96 spins-1/2 and $J_F = 400$, and string order 0.37427 on linear extrapolation to $1/J_F = 0$.

The $\tilde{g}(N/2)$ minimum is a new result. Previous studies considered $\tilde{g}(p)$ at constant system size n and hence constant spin correlations with periodic [113] or open [3] boundary conditions; $\tilde{g}(p, n)$ decreases with p up to $n/2$ in small cyclic systems or to $\tilde{g}(\infty)$ as shown in Fig. 6.5 of ref. [3]. The corresponding spin-1/2 function $g_2(2p, 2N)$ has variable p at constant system size $2N$, and it also decreases to $2p = N$ or to $g_2(\infty)$ in the thermodynamic limit. We have instead studied the size dependence of $g_2(N, 2N)$ and found an unanticipated minimum at N^*. Convergence to string order $g_2(\infty)$ is from below. The VB analysis rationalizes the size dependencies of both $g_2(N, 2N)$ and $\tilde{g}(n/2, n)$.

Finite string order $g_2(\infty)$ and gap ε_T are expected on general grounds in dimerized ladders with $-J_F \neq J_A$ and two spins per unit cell. The ground state is a BOW. The limit $J_F \to \infty$ generates inversions centers at the centers of rungs, and the ladder becomes a spin-1 HAF with $J = (1 - 2J_L)/4 > 0$ and Z_2 symmetry.

6.5 Spontaneous dimerization

The F-AF ladder, Eq. 6.1, has two string correlation functions with an even number N of consecutive spins-1/2. The nondegenerate ground state is a BOW due to alternate first-neighbor exchanges $-J_F$ and $J_A = 1$. We set $-J_F = 1$ in this Section and discuss the $J_1 - J_2$ model with $J_1 = 1$ and $J_2 = -J_L$. The model has one spin per unit cell, C_{2N} translational symmetry, and inversion symmetry σ at sites. The ground state for $2N$ spins, N even is odd under inversion, $\sigma = -1$. The coefficients of $|K1\rangle$ and $|K2\rangle$ or of $|a2\rangle$ and $|a1\rangle$ in Table 6.3 are then equal with opposite sign. We have $C(q') \pm C(q)$ for symmetry-adapted linear combinations of singlets $|q\rangle$ and $|q'\rangle = \sigma|q\rangle$. The lowest singlet excited state has

$\sigma = 1$ symmetry and $C(q') = C(q)$.

The string correlation function $g_-(N)$ is the ground-state expectation value. Hida [4] applied field theory to the spin-1/2 HAF ($J_2 = 0$) and concluded that $g_-(N)$ is proportional to $N^{-1/4}$, consistent with ED up to $2N = 24$. Fig. 6.10 shows the size dependence of $g_-(N)$ at $J_2 = 0$ from $2N = 12$ to 192, The exponent $\gamma(0) = 0.270$ is the best fit, in good agreement with field theory. Since the model with $J_2 < 0$ is not frustrated, the size dependence of $g_-(N)$ at $J_2 = -2$ and -4 in Fig. 6.10 is also fit as $AN^{-\gamma}$.

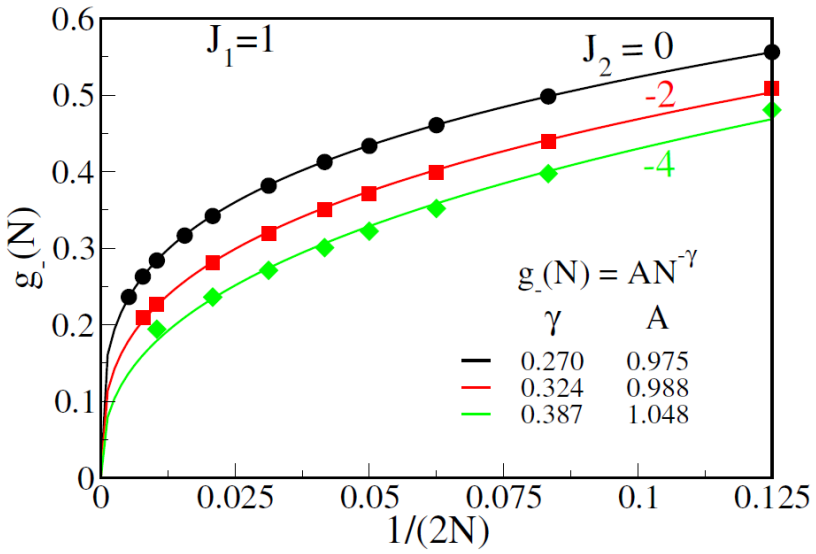

Figure 6.10: Size dependence of the string correlation function $g_-(N)$ of $J_1 - J_2$ models with $2N$ spins, $J_1 = 1$ and $J_2 = 0, -2$ and -4. The $J_2 = 0$ expression [4] is used at $J_2 = -2$ and -4.

The $J_1 - J_2$ model is frustrated when $J_2 > 0$. The ground state is doubly degenerate in the dimer phase [1] $J_c = 0.2411 \leq J_2 \leq 1/2$. In finite systems, the singlets $\sigma = -1$ and $+1$ are the ground and first excited states, respectively. They are degenerate at $J_2 = 1/2$, the Majumdar-Ghosh point [32], where the exact $\sigma = \pm 1$ ground states are the plus and minus linear combinations of $|K1\rangle$ and $|K2\rangle$. The system is spontaneously dimerized.

The broken-symmetry state $|K2\rangle$ at $J_2 = 1/2$ returns $g_2(N) = 1$, $g_1(N) = 0$ as discussed for the ladder while $|K1\rangle$ has $g_1(N) = 1$, $g_2(N) = 0$. Due to overlaps, the string correlations functions $g_\pm(N)$ are size dependent. A straightforward calculation leads to

$$g_-(N) = 1/2 + 1/(2^N + 2). \tag{6.16}$$

The $g_+(N)$ expression has minus signs in Eq. 6.16. Convergence to the thermodynamic limit is exponential.

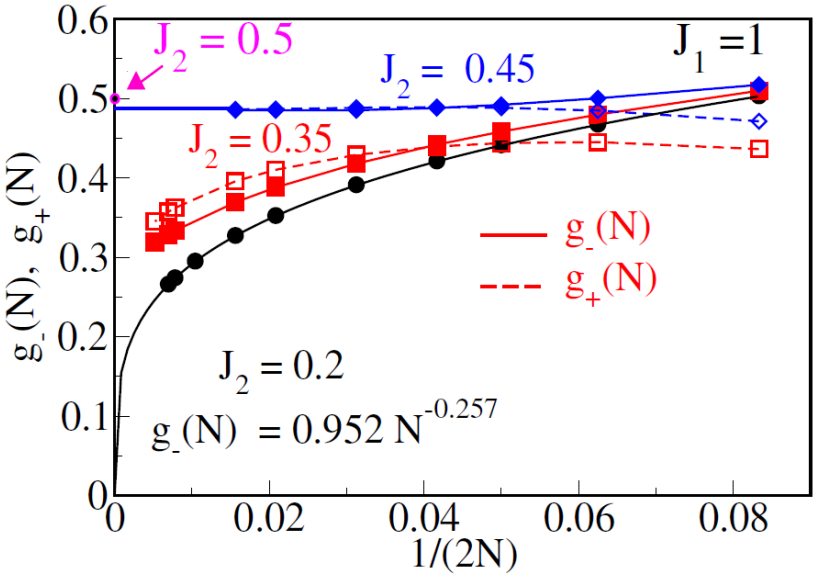

Figure 6.11: String correlation function $g_-(N)$ at $J_2 = 0.2$ in the gapless phase, fit as in Fig. 6.10. Solid and dashed lines are $g_-(N)$ and $g_+(N)$ at $J_2 = 0.35$ and 0.45 in the gapped dimer phase. The point at $J_2 = 0.5$ is exact. The lines at $J_2 = 0.35$ are to guide the eye.

Fig. 6.11 shows the size dependence of $g_-(N)$ at $J_2 = 0.20 < J_c$ in the gapless phase and both string correlation functions at $J_2 = 0.45$ and 0.35 in the dimer phase. The $g_-(N)$ points at $J_2 = 0.20$ are fit to $AN^{-\gamma}$ as in Fig. 6.10 with $\gamma = 0.257$. The point at 0.50 is exact for $J_2 = 0.5$. The $g_-(0.45, N)$ and $g_+(0.45, N)$ curves cross twice before converging to string order $g_-(\infty) = g_+(\infty) = 0.485$. Rapid size convergence and slightly reduced string order are expected close to

$J_2 = 1/2$. We did not anticipate curve crossing; the ground state is odd under inversion at all system sizes.

The $J_2 = 0.35$ string correlation functions in Fig. 6.11 cross at system size $2N \approx 32$. The functions $g_+(N)$ and $g_-(N)$ are expected to have equal string order $g(\infty) > 0$. The difference $g_+(N) - g_-(N)$ increases to 0.029 at $2N = 144$ and decreases to 0.026 at $2N = 192$. Larger systems are required to evaluate the string order. The small gap $\varepsilon_T(1, 0.35) = 0.006$ also points to long but finite-ranged spin correlations.

6.6 Summary and conclusions

We have presented spin-1/2 string correlation functions and string order in general. The F-AF ladder, Eq. 6.1, at specific parameters J_L, J_F and $J_A = 1$ reduces to important spin-1/2 models with singlet ground states. It has two N-spin string correlation functions, $g_1(N)$ and $g_2(N)$, at system size $2N$, N even. Since the ladder is gapped, with $\varepsilon_T(J_L, J_F) > 0$ except in the limit $J_L \to \infty$, the string order is $g_2(\infty) > 0$, $g_1(\infty) = 0$. As shown in Fig. 6.9, the string order $g_2(\infty)$ in the limit $J_F \to \infty$ is equal to $\tilde{g}(\infty)$ of the spin-1 HAF, and the limits are approached from below.

The ground state near the origin of the $J_L - J_F$ plane consists of rungs with AF exchange J_A that are weakly coupled by frustrated F exchanges $-J_L$ and $-J_F$ in Fig. 6.1. Short-range spin correlations are indicated by the gaps $\varepsilon_T(J_L, J_F)$ in Fig. 6.2, by string order $g_2(\infty) > 3/4$ and by convergence to the thermodynamic limit at system size $2N = 24$. The regime $J_F > 3$, $J_L \leq 1/2$ has reduced $\varepsilon_T(J_L, J_F)$, finite $g_2(\infty)$ and spin correlations of intermediate range as indicated by the minimum N^* of $g_2(N)$. The regime $J_L > 2$, $J_F \leq 1$ has small $\varepsilon_T(J_L, J_F)$ that vanishes as $1/J_L$ in Fig. 6.4. The range of spin correlations is $N^* \approx 50$ at $J_L = 3$ and increases rapidly with J_L. The gapless $J_1 - J_2$ model with $J_2 = -J_L$ is the limit $J_L \to \infty$. The model is frustrated when $J_2 > 0$ and

illustrates spontaneous dimerization in the dimer phase with finite ε_T and string order.

String correlation functions of the F-AF ladder directly probe ground-state spin correlations and their range. They afford more nuanced information than the binary choice of finite range in gapped systems and infinite range in gapless systems. The estimated range of spin correlations at J_L, J_F and $J_A = 1$ in Eq. 6.1 is N^*, the minimum of $g_2(N)$. The VB interpretation accounts for convergence to string order $g_2(\infty)$ from below and the exponential decrease of $g_1(N)$ for $N \geq N^*$. Ranges up to $N^* \sim 100$ are accessible in DMRG calculations up to system size $2N = 200$.

The spin-1 HAF has one spin-1 per unit cell and can be written in terms of two spins-1/2 as $s_j = S_{2j-1} + S_{2j}$ with F exchange $-J_F$ in rungs and AF exchange $J/4$ between adjacent rungs. There are now two spins per unit cell and $J_F \to \infty$ excludes singlet-paired rungs. In the VB treatment of finite spin-1 HAFs, Eq. 6.1 was expressed [215] in terms of spin-1/2 operators in a way that gave vanishing matrix elements for diagrams $|q\rangle$ with singlet-paired rungs $2j-1$, $2j$. F alignment in rungs clearly requires AF exchange and two spins per unit cell in order to have a singlet ground state.

6.7 Appendix

We summarize the overlap of singlet VB diagrams and the size dependence of the singlet sector. In systems of $2N$ spins, singlet diagrams $|q\rangle$ have N lines (m, n) that correspond to normalized singlet-paired spins in Eq. 6.3 and connect the vertices of the $2N$ polygon without any crossing lines. The overlaps are

$$S_{q'q} = \langle q'|q\rangle = (-2)^{-N+I(q',q).} \tag{A1}$$

$I(q', q)$ is the number of disconnected lines called islands by Pauling when the diagrams are superimposed. The superposition of any diagram with itself gen-

erates N islands of doubled lines (m,n) and unit overlap. The other extreme, illustrated by $\langle K1|K2\rangle = (-2)^{-N+1}$, is a single island for diagrams without any (m,n) in common. $I(q',q)$ is the number of shared lines (m,n) plus the number of islands with lines connecting vertices at unshared (m,n). The Kekulé diagrams have no shared (m,n); their overlap of any $|q\rangle$ satisfies the relation,

$$I(q,K1) + I(q,K2) = N+1 \tag{A2}$$

Overlap magnitudes are necessarily larger with one of the Kekulé diagrams when N is even, and overlap magnitude uniquely relates half of the diagrams to $|K1\rangle$, the other half to $|K2\rangle$. The Kekulé diagrams are orthogonal in the thermodynamic limit, as are diagrams that differ from either by a finite number of lines (m,n).

All eigenfunctions $|q\rangle$ of the string operator $\hat{g}_1(N)$ in Eq. 6.13 have $1 \le m,n \le N$. All other $|q\rangle$ have one or more pairs of bridging lines (m,n) with only one end in the string 1 to N. Then $\hat{g}_1(N)|q\rangle$ generates triplet-paired spins $(m,n)_T = (\alpha_m\beta_n + \beta_m\alpha_n)/\sqrt{2}$ at all bridging lines. For example, $\hat{g}_1(N)|K2\rangle$ generates diagram $|K'\rangle$ with unchanged (m,n) except for two bridging lines that become $(2N,1)_T$ and $(N,N+1)_T$. The overlap of diagrams with triplets is zero unless the triplets are in the same island, in which case $S_{qq'}$ is Eq. (A1). We have $\langle K'|K2\rangle = 0$ due to spin orthogonality and $\langle K'|K1\rangle = (-2)^{-N+1}$ since both triplets are in the same island.

The dimensions of the VB basis have long been known. The number of singlet diagrams in systems of $2N$ spins is

$$R_0(2N) = \frac{(2N)!}{N!(N+1)!}. \tag{A3}$$

The string operator for N spins has $R_0(N)$ eigenfunctions $|q\rangle$ with $N/2$ lines in the string. The degeneracy of each is $R_0(N)$ since $|q\rangle$ also has $N/2$ lines with (m,n) not in the string. The ratio of eigenstates to the total number of singlets

is, using Stirling's approximation,

$$\frac{R_0(N)^2}{R_0(2N)} \approx \frac{8e(N+1)^{N+3/2}}{\sqrt{\pi}(N+2)^{N+3}}. \tag{A4}$$

Chapter 7

Magnon condensation in F-AF ladder

7.1 Introduction

We have already discussed the frustration induced phases in presence and absence of magnetic field. The F-AF ladder model has some similarities with the $J_1 - J_2$ model with ferromagnetic J_1 and antiferromagnetic J_2. This type of $J_1 - J_2$ model shows many interesting phases like spin-nematic [90], multipolar [91, 92], vector chiral [92, 197] etc. in presence of magnetic field.

The multipolar phase is generally characterized by a jump in the magnetization curve ($M-h$) greater than 1 and finite magnon binding energy, indicating the condensation of multi-magnons. As an example, condensation of two magnons to form a boson stabilizes the quadrupolar (QP) or spin-nematic phase which is discussed in detail in Chubukov *et al.* [93]. This type of feature is very similar to the formation of Cooper pairs in superconductors [216], the only difference being that instead of electrons, magnons form this bound or pair state. Similarly, octupolar and hexadecapolar phases arise from the number of paired magnons 3 and 4 respectively (2 corresponds to the quadrupolar phase).

The spin-nematic phase can not be detected directly but they can be explored indirectly by using inelastic neutron scattering (INS) method and other measurements like magnetic susceptibility measurement [217]. $LiCuVO_4$ is such a candidate material where spin-nematic or quadrupolar phase has been detected by INS and NMR data analysis [218]. At higher magnetic field, multi-magnon bound state is stable due to attractive interactions between the magnons.

In order to find out an alternative way to detect this phase, Parvej and Kumar [90] analyzed the dynamical structure factor $S(q,\omega)$ and found that the momentum (q_m) of the most intense peak of $S(q,\omega)$ for a given M varies linearly with M, which is directly confirmed by the INS experiments. For other multipolar phases (> 2), the characterization has been made based on the pitch angle calculated from spin density and correlation function but for higher order case, this procedure is not accurate due to the degeneracy in gs energy.

Hikihara *et al.* [91] gave a detailed explanation of different types of multi-magnon bound states. Spin-nematic phase is analogous to Tomonaga-Luttinger liquid (TLL) of hard-core boson. It is described as the bound-state of two magnons with total momentum $k = \pi$. In this case transverse spin correlations, $\langle s_0^+ s_1^- \rangle$ is of short range order. Nematic correlations, $\langle s_0^+ s_1^+ s_l^- s_{l+1}^- \rangle$ as well as longitudinal spin correlations $\langle s_0^z s_1^z \rangle - \langle s_0^z \rangle \langle s_l^z \rangle$ exhibit power law decay. In this phase, nematic correlations decay slowly compared to the longitudinal spin correlations. Triatic phase is nothing but three magnon bound state with total momentum $k = \pi$. Correlation function $\langle s_0^+ s_1^+ s_2^+ s_l^- s_{l+1}^- s_{l+2}^- \rangle$ shows quasi-long range order. On the other hand both transverse correlations, $\langle s_0^+ s_l^- \rangle$ and nematic correlations, $\langle s_0^+ s_1^+ s_l^- s_{l+1}^- \rangle$ decay exponentially showing short range order. For multi-magnon case with m number of bound states, the correlation $\langle s_1^+ s_2^+ .... s_m^+ .... s_1^- s_2^- s_m^- \rangle$ show quasi-long range order in the system.

Multipolar order has been detected in spin-1/2 models on the square lattice, the triangular lattice, and the two-leg ladder lattice. In 2020, multi-magnon bound state has been predicted in Heisenberg spin-1/2 model on two dimensional

kagome lattice in Schnack *et al.* [219]. Recently, on 2023 Sambunath *et al.* [220] has shown the existence of interesting quadrupolar or n-type spin nematic phases in 3/4 and 5/5 skewed ladders at very low magnetic field.

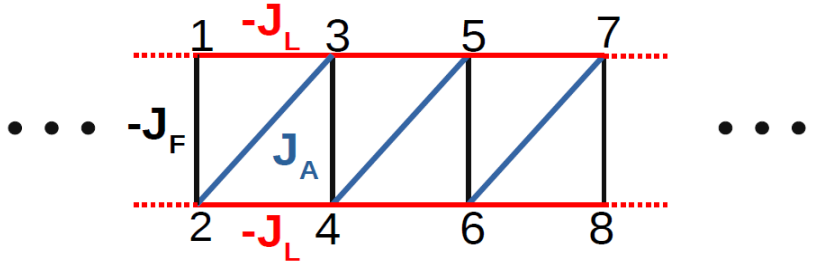

Figure 7.1: The F-AF spin-1/2 ladder with F exchange $-J_L < 0$ between spins r and $r+2$ in either leg, F exchange $-J_F$ in rungs $2r-1$, $2r$ and AF exchange J_A in rungs $2r$, $2r+1$.

In this work, we have taken a two-legged ladder model consisting of two ferromagnetic legs with interaction strength $-J_L$ and alternating ferro- and anti-ferromagnetic rungs with interaction strength $-J_F$ and J_A respectively, as shown in Fig. 7.1. The ladder is frustrated except when $J_L = 0$ or $J_F = 0$. This ladder model reduces to important models in special cases. These are the spin-1/2 HAF at $J_L = 0$ and $-J_F = J_A$ with one spin per unit cell and the AFAF model at $J_L = 0$ and $-J_F = J_A$ with two spins per unit cell. On the other hand, this model behaves like a spin-1 HAF chain at $J_F \to \infty$ and at $J_L \to \infty$ the system can be mapped to the $J_1 - J_2$ model.

Here we have studied the nature of the $M-h$ curve, which reveals interesting phenomena in the system at different interaction strengths. Depending on the nature of the $M - h$ curve, we have also constructed the phase diagram in the $J_L - J_F$ plane in the presence of an external field. We also calculated binding energy for differnt interaction strength. Finite value of binding energy signifies the formation of magnon-bound states. The detailed study has been discussed in different sections below.

7.2 Model Hamiltonian and numerical methods

The ladder has $2N$ spins-1/2 with isotropic ferromagnetic (F) exchange $-J_L$ between neighbors in legs, F exchange $-J_F$ at rungs $2r-1$, $2r$ and AF exchange J_A at rungs $2r$, $2r+1$. We set $J_A = 1$ as the unit of energy and impose periodic boundary conditions,

$$H_{F-AF}(J_L, J_F) = \sum_{r=1}^{N} (\boldsymbol{S}_{2r} \cdot \boldsymbol{S}_{2r+1} - J_F \boldsymbol{S}_{2r-1} \cdot \boldsymbol{S}_{2r}) + \sum_{r=1}^{2N} (-J_L \boldsymbol{S}_r \cdot \boldsymbol{S}_{r+2} - h S_r^z). \tag{7.1}$$

The ladder is equivalent to a $1D$ chain with two spins per unit cell, exchange $-J_L$ between second neighbors and alternating exchanges $-J_F$ and J_A between first neighbors. The total spin $S \leq N$ and its z component S^z are conserved. The last term is the interaction with a magnetic field h. To solve this interesting model, we use the ED and the DMRG methods.

7.3 Magnetization

In systems with isotropic exchange, the field dependence of the lowest Zeeman component of any state $E(S, 2N)$ with spin S and $S^z = S$ is

$$E(S^z, h, 2N) = E(S, 2N) - hS^z, \quad 0 \leq S^z = S \leq N. \tag{7.2}$$

We take J_L, J_F leading to a singlet ground state at $h = 0$ and obtain the lowest energies $E(S^z, h, 2N)$. Increasing h generates multiple level crossings until $S = S^z = N$ becomes the absolute ground state.

Since the field dependence of $E(N, h, 2N)$ is extensive, the stabilization per dimer of the F state is $\epsilon_F - h$. The field-induced crossing with the singlet ground

state is at $h = \epsilon_F - \epsilon_0$. On the other hand, $h = \epsilon_T$ is the field-induced crossing of the triplet and singlet ground states. At equal h we obtain

$$\epsilon_T(J_L, J_F) = \epsilon_F(J_L, J_F) - \epsilon_0(J_L, J_F). \tag{7.3}$$

If $\epsilon_F - \epsilon_0 < \epsilon_T$, $M(h)$ is a step function at h_s. Conversely, if ϵ_T is smaller, $M(h) = 1/N$ at $h = \epsilon_T$ and it is not a step function.

$M(h)$ is continuous at h_s if the S^z crossing between $N-1$ and $N-2$ occurs at lower h than the crossing between N and $N-1$ at h_s. If instead $h_s < h$, there is a 2/N discontinuity at $M(h_s)$ and $S^z = N-1$ is never the ground state. The condition $h = h_s$ leads to

$$E(N, 2N) + E(N-2, 2N) = 2E(N-1, 2N). \tag{7.4}$$

$M(h_s)$ is discontinuous if $2E(N-1, 2N)$ is larger than the left-hand side. [90,197, 221,222] Due to attractive interactions or binding energy, the double excitation $E(N-2, 2N)$ is lower than two single excitations when $2E(N-1, 2N)$ is larger.

The magnetization curves in Fig. 7.2 are for $J_F = 0$, $2N = 24$ spins in Eq. 7.1 and variable $J_L \geq 0$. The N steps of $M(h)$ correspond to reversing 12 spins. Increasing the system size increases the number of steps but not the saturation field $h_s = 1$, a step function at $J_L = 0$. Exchange $J_L > 0$ between dimers generates a triplet band with $\epsilon_T(J_L, 0) < 1$ and continuous $M(h)$ in the thermodynamic limit. Increasing J_L lowers the $M(h) > 0$ threshold. Continuous $M(h)$ with $h_s = 1$ are also found at $J_L = 0$ and variable $J_F > 0$.

Fig. 7.3 illustrates discontinuous $M(h)$, specifically for $J_F = 1/2$, $2N = 24$ spins and variable $J_L \geq J_F/2$. $M(h)$ is a step function at $h_s = 3/4$ when $J_L = 1/4$ and $\epsilon_0(1/4, 1/2) = -3/4$. Increasing J_L lowers saturation field to $h_s = 1 - J_F = 1/2$. $M(h)$ is a step function until $\epsilon_T = \epsilon_F - \epsilon_0$ in Eq. 7.3, at $J_L = 0.640$ for $2N = 24$, already in the thermodynamic limit.

The same procedure holds for variable $J_F/2 \geq J_L$ at constant J_L. $M(h)$

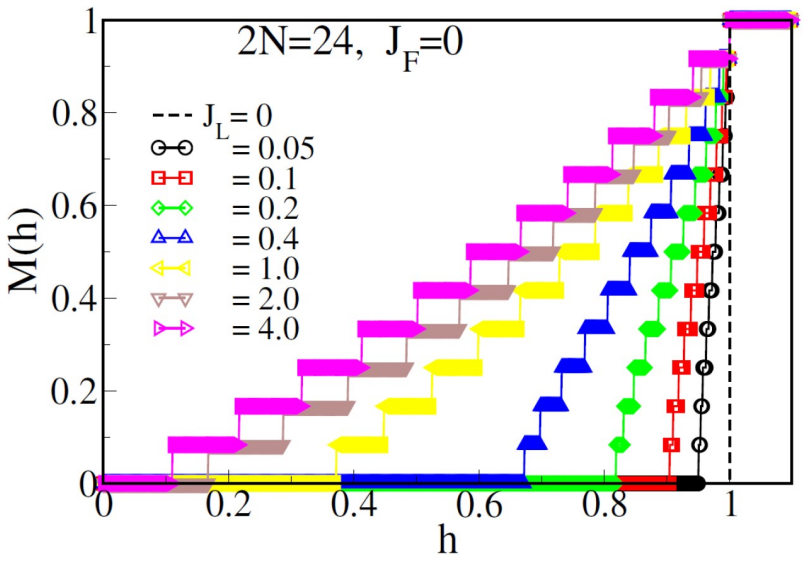

Figure 7.2: Magnetization $M(h)$ of Eq. 7.1 with $2N = 24$ spins, $J_F = 0$ and variable $J_L \geq 0$. $M(h)$ is a step function at $h_s = 1$ when $J_L = 0$ and continuous when $J_L > 0$.

is initially a step function at $h_s = 1 - J_L$ when $J_L > 1/2$ and remains a step function with increasing J_F up to the dimer/F boundary.

7.4 Preliminary check: binding energy calculation

For two magnon bound state we calculate binding energy defined as-

$$\Delta = 1/2[E(S^z) + E(S^z + 2) - 2E(S^z + 1)] \tag{7.5}$$

Negative value of binding energy signifies formation of 2-magnon bound states which means the energy required to form magnon bound state is less than creation of single magnons. For step jumps more than 2 states can be also considered as the formation of multi-magnon bound state. Here we calculated the energy required to form a single magnon from the M-h curve and on the other hand when we calculate the energy difference of the step jumps, we clearly see that

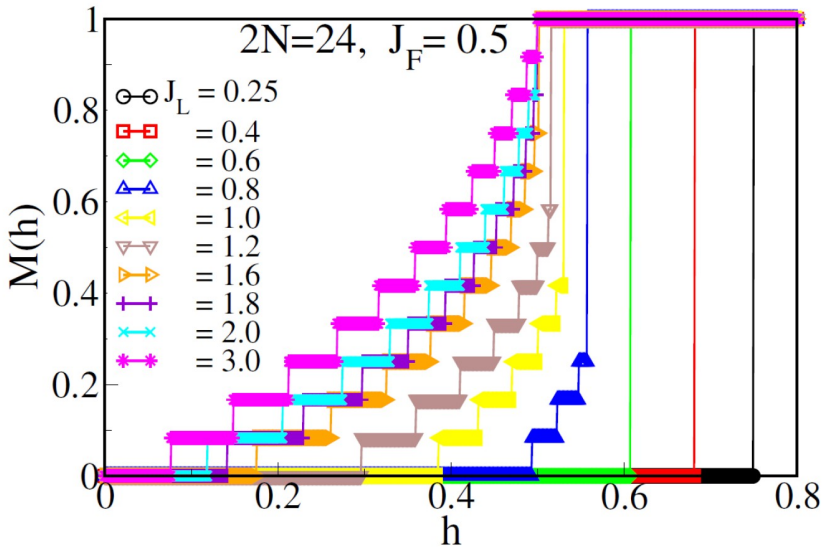

Figure 7.3: Magnetization $M(h)$ of Eq. 7.1 with $2N = 24$ spins, $J_F = 1/2$ and variable $J_L \geq J_F/2$. $M(h)$ is a step function from $h_s = 0.75$ at $J_L = 0.25$ to $h_s = 0.59$ at $J_L = 0.640$. $M(h)$ is discontinuous at $h_s = 0.5$ up to $J_L = 1.81$.

the energy required to direct jump i.e to form bound pairs is lower than energy needed to form single magnon as shown in Fig. 7.2 and Fig. 7.3. The per magnon binding energy of an n-magnon bound state, can be defined as following,

$$\Delta = 1/n[(E(S^z - n) - E(S^z)) - n(E(S^z - 1) - E(S^z))] \tag{7.6}$$

where $E(S^z)$ is the gs energy with the z-component of the total spin S. For stabilization of a n-magnon condensed state, the corresponding binding energy Δ should be negative and finite.

7.5 Phase diagram

Phase diagram of this ladder model is shown in $J_L - J_F$ plane when magnetic field is applied in the system. The magnetization curve shows interesting behavior which has been discussed in detail in earlier section. $J_L = J_F/2$ is the perfect dimer line. Below perfect dimer line (region: I), the magnetization curve is show-

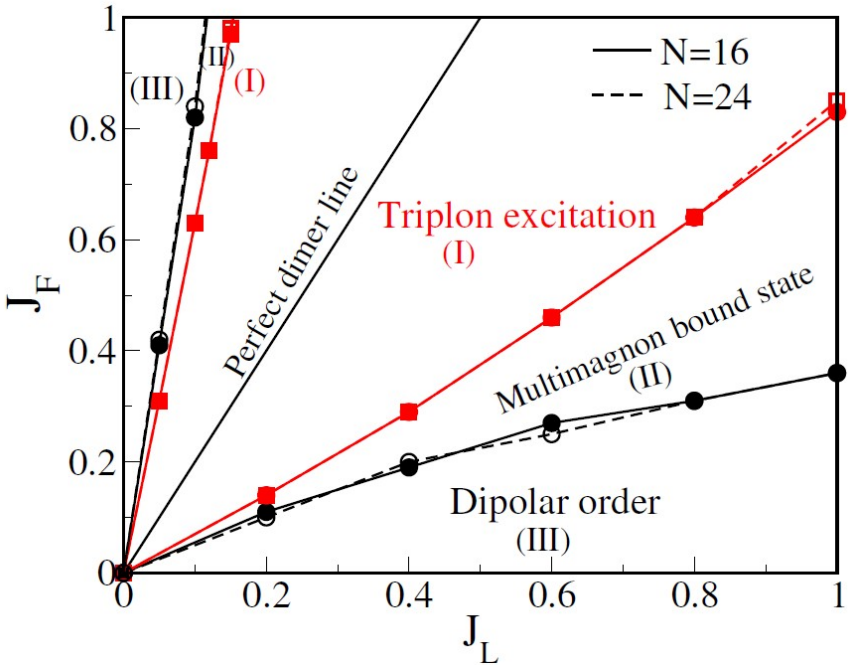

Figure 7.4: Phase diagram in presence of magnetic field in $J_L - J_F$ plane. Three different regimes have been shown in the phase diagram: (I) jump in magnetization curve is unity, (II) jump is present but it is not unity and (III) No step jump. System size dependence in the phase boundary is very weak.

ing a step jump of unity. Below that regime (region: II), there is a intermediate region which is showing step jump less than unity and below that region (region: III), there is no step jump.

7.6 Finite size scaling

Fig. 7.5 shows the finite size scaling at $J_L = 0.8$ and $J_F = 0.42$ for two different system sizes 48 and 64. Here, it should be mentioned that for larger system size calculations, we used DMRG in open boundary condition. We observe that the transition point is independent on system size in Fig. 7.5. There is a very large plateau which is coming mainly due to the edge spins in open boundary condition and completely disappears in periodic boundary condition.

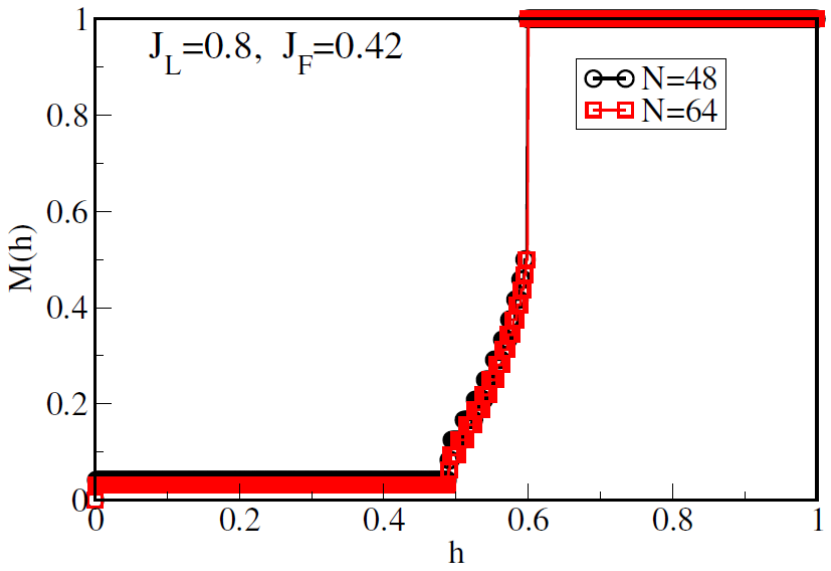

Figure 7.5: The transition point is weakly dependent on system size. Plateau arises due to the edge spins in open boundary condition and disappears in periodic boundary condition.

7.7 Summary and conclusion

The ladder model with ferromagnetic legs and alternating ferro- and antiferromagnetic rungs shows interesting features in magnetization curve in present of external field. The magnetization curve is showing step jumps which depends on interaction strength. For $J_L = J_F/2$ the system behaves like isolated dimers and at finite field the dimers are broken and triplons are generated. The magnetization curves show step jumps. On the other hand, the attractive interactions between the magnons show formation of multi-magnon bound states.

Chapter 8

Conclusion

In this thesis, our main focus is to investigate various quantum phases in presence of competiting interactions in low dimensional systems specially two leg ladder models and Shastry-Sutherland lattice model. These systems are very much fasicinating to study because of their realization in real materials as well as existence of different types of exotic phases at different interaction limits.

We have carried out a comparative study on a two-legged ladder model with both normal and zigzag ladder configurations. The two legs are of ferromagnetic and antiferromagnetic types and the rungs are either ferromagnetic or antiferromagnetic. We have observed that the magnetization always varies from $N/4$ to $N/2$ in case of zigzag ladder, but for normal ladder it varies from 0 to $N/4$ and $N/4$ to $N/2$ depending on the ratio of interaction strength on each leg. Here N is the system size. We have constructed the full phase diagrams for these two models. For the normal ladder the phase diagram consists of five different phases: ferromagnetic, antiferromagnetic, non-collinear ferrimagnetic, $m - 1/4$ and dimer phase. On the other hand, with the introduction of diagonal bond interaction, i.e. in the case of the zigzag ladder, the system has a completely different phase diagram, consisting of ferromagnetic, non-collinear ferrimagnetic and spin-fluid phases. The color gradient in the phase diagram indicates the

change in magnetization as a function of interaction strength. The non-collinear ferrimagnetic phase is very interesting to study. It shows a quasi-long range order and this type of magnetization is of a non-conventional type as the values of the magnetization are not quantized to a particular value, but depend on the interaction strength.

In the next chapter, we have discussed the quantum phase diagram of ferromagnetically coupled Shastry-Sutherland lattice model. The phase diagram is consisting of dimer-stripe $(0, \pi)$, dimer-stripe $(\pi, 0)$, dimer, x-spiral, y-spiral and FM phases. The spiral phase was predicted by a previous study using mean-field calculations, but the ED could not confirm it. Our DMRG calculations confirm the spiral phase though it occupies only a very small region in the phase diagram. We also calculated the phase boundaries using larger system size which is more accurate than the previous study. Phase boundaries of these quantum phases are determined using the correlation functions and gs energies. We also notice that the correlation length during the whole phase diagram is very small.

We have studied a two leg ladder model with ferromagnetic legs and alternating ferro- and antiferromagnetic rungs. Earlier study shows that the phase diagram is consiting of only dimer, Haldane and FM phase. In this project, we reconstructed the whole phase diagram. The spin-spin correlations identify two more phases in the system: antiferromagnetic (AF) and double-period antiferromagnetic (DAF). The phase boundaries are calculated from curvature calculations. We have also shown in a quantitave way that this model is behaving like a $J_1 - J_2$ model for large leg interaction limit. On the other hand, it is adiabatically connected to spin-1 chain for very large value of rung interaction.

Next for this same model we studied its topological properties in the ground state by calculating the string order parameter. String order parameter is a hidden order parameter of a system which is used to identify its topological properties where edge mode is absent or singlet-triplet gap does not follow exponential decay with system size. Spin-1/2 string correlation functions $g_1(N)$ and

$g_2(N)$ are defined for an even number N of consecutive spins in systems with two spins per unit cell; the ladder has string order $g_2(\infty) > 0$ and $g_1(\infty) = 0$. In this project we propose that the minimum N^* of $g_2(N)$ is related to the range of ground-state spin correlations. Here, $g_1(N)$ decreases exponentially for $N \geq N^*$. The VB interpretation accounts for convergence to string order parameter.

The last project which is still going on related to magnon condensation with this similar model. Here, in presence of magnetic field, we have observed different kinds of jumps in magnetization curve which is connected to formation of different numbers of magnon bound pairs so called multi-magnon bound state. We also map this model to a hard-core boson system. Here, our main goal is to plot the quantum phase diagram of this system in presence of magnetic field and to identify the diferent bound states region in the phase diagram.

In conclusion, main focus of our study is to investigate various quantum phases in presence of competiting interactions in $1D$ and $2D$ systems. We also constructed the quantum phase diagrams of these model Hamiltonians. The phases are identified based on magnetization and the nature of the spin-spin correlation function. Additionally, we were interested in observing how the ground state properties change in the presence of a magnetic field. Furthermore, we studied the topological aspect and corresponding string correlation function behavior.

References

[1] Z. G. Soos, A. Parvej and M. Kumar, "*Numerical study of incommensurate and decoupled phases of spin-1/2 chains with isotropic exchange J_1, J_2 between first and second neighbors*", J. Condens. Matter Phys. **28** (mar, 2016) 175603. xiii, 14, 15, 16, 47, 48, 72, 100, 127

[2] K. Hida, K. Takano and H. Suzuki, "*Topological phases of the spin-$\frac{1}{2}$ ferromagnetic–antiferromagnetic alternating Heisenberg chain with frustrated next-nearest-neighbour interaction*", J. Phys. Soc. Jpn **82** (2013) 064703. xvii, 90, 91, 93, 94, 98, 104, 114

[3] S. R. White and D. A. Huse, "*Numerical renormalization-group study of low-lying eigenstates of the antiferromagnetic S=1 Heisenberg chain*", Phys. Rev. B **48** (Aug, 1993) 3844–3852. xviii, 98, 109, 113, 126

[4] K. Hida, "*Crossover between the Haldane-gap phase and the dimer phase in the spin-$\frac{1}{2}$ alternating Heisenberg chain*", Phys. Rev. B **45** (Feb, 1992) 2207–2212. xix, 98, 104, 106, 117, 125, 127

[5] A. Szabo and N. Ostlund, *"Modern Quantum Chemistry: Introduction to Advanced Electronic Structure Theory"*. Dover Publications, Inc., Mineola, first edition ed., 1996. 3

[6] M. C. Gutzwiller, "*Effect of correlation on the ferromagnetism of transition metals*", Phys. Rev. Lett. **10** (Mar, 1963) 159–162. 5

[7] J. Hubbard, "*Electron correlations in narrow energy bands*", Proc. Roy. Soc. (London), Ser. A **276** (11, 1963) . 5

[8] J. Kanamori, "*Electron Correlation and Ferromagnetism of Transition Metals*", Prog. Theor. Phys. **30** (09, 1963) 275–289. 5

[9] E. Dagotto, "*Correlated electrons in high-temperature superconductors*", Rev. Mod. Phys. **66** (Jul, 1994) 763–840. 5

[10] G. D. Mahan, *"Many-Particle Physics"*. Springer New York, NY, 3 ed., 2000. 5

[11] R. J. Baxter, "*One-dimensional anisotropic Heisenberg chain*", Ann. Phys. **70** (1972) 323–337. 7

[12] C. N. Yang and C. P. Yang, "*One-dimensional chain of anisotropic spin-spin interactions. i. proof of Bethe's hypothesis for ground state in a finite system*", Phys. Rev. **150** (Oct, 1966) 321–327. 7

[13] C. N. Yang and C. P. Yang, "*One-dimensional chain of anisotropic spin-spin interactions. ii. properties of the ground-state energy per lattice site for an infinite system*", Phys. Rev. **150** (Oct, 1966) 327–339. 7

[14] C. N. Yang and C. P. Yang, "*One-dimensional chain of anisotropic spin-spin interactions. iii. applications*", Phys. Rev. **151** (Nov, 1966) 258–264. 7

[15] H. A. Bethe, "*Zur Theorie der Metalle. I. Eigenwerte und Eigenfunktionen der linearen Atomkette*", Zeit. für Physik **71** (1931) 205–226. 7

[16] L. Hulthe;n, *Über das Austauschproblem eines Kristalles*. PhD thesis, , Stockholm College, 1938. 7

[17] J. des Cloizeaux and J. J. Pearson, "*Spin-wave spectrum of the antiferromagnetic linear chain*", Phys. Rev. **128** (Dec, 1962) 2131–2135. 7

[18] S. Sachdev, *"Quantum Phase Transitions"*. Cambridge University Press, 2011, 10.1017/CBO9780511973765. 7

[19] A. W. Sandvik, "*Computational studies of quantum spin systems*", AIP Conf. Proc. **1297** (2010) 135. 8, 9, 47

[20] T. Kuramoto, "*Magnetic and critical properties of alternating spin Heisenberg chain in a magnetic field*", J. Phys. Soc. Jpn. **67** (1998) 1762–1766. 9

[21] E. Lieb and D. Mattis, "*Ordering energy levels of interacting spin systems*", J. Math. Phys. **3** (1962) 749–751. 9, 49

[22] N. B. Ivanov and J. Richter, "*Phase diagram of a frustrated mixed-spin ladder with diagonal exchange bonds*", Phys. Rev. B **69** (Jun, 2004) 214420. 10

[23] K. Hida, "*Ferrimagnetic states in $S = 1/2$ frustrated Heisenberg chains with period 3 exchange modulation*", J. Condens. Matter Phys. **19** (mar, 2007) 145225. 10

[24] K. Hida and K. Takano, "*Frustration-induced quantum phases in mixed spin chain with frustrated side chains*", Phys. Rev. B **78** (Aug, 2008) 064407. 10

[25] R. R. Montenegro-Filho and M. D. Coutinho-Filho, "*Frustration-induced quantum phase transitions in a quasi-one-dimensional ferrimagnet: Hard-core boson map and the tonks-girardeau limit*", Phys. Rev. B **78** (Jul, 2008) 014418. 10

[26] S. C. Furuya and T. Giamarchi, "*Spontaneously magnetized Tomonaga-Luttinger liquid in frustrated quantum antiferromagnets*", Phys. Rev. B **89** (May, 2014) . 10

[27] S. Furukawa, T. Dodds and Y. B. Kim, "*Ferromagnetically coupled dimers on the distorted Shastry-Sutherland lattice: Application to $(CuCl)LaNb_2O_7$*", Phys. Rev. B **84** (2011) 054432. 10, 11, 19, 73, 84, 86, 90, 106

[28] D. Maiti, D. Dey and M. Kumar, "*Frustrated spin-1/2 ladder with ferro- and antiferromagnetic legs*", J. Magn. Magn. Mater. **446** (2018) 170–176. 11, 16, 17, 48, 49, 50, 59, 64, 65, 68, 84

[29] A. Lavarélo, G. Roux and N. Laflorencie, "*Melting of a frustration-induced dimer crystal and incommensurability in the J_1-J_2 two-leg ladder*", Phys. Rev. B **84** (Oct, 2011) 144407. 11

[30] P. Müller, J. Richter and D. Ihle, "*Thermodynamics of frustrated ferromagnetic spin-$\frac{1}{2}$ Heisenberg chains: Role of interchain coupling*", Phys. Rev. B **95** (Apr, 2017) 134407. 11

[31] Q. Luo, S. Hu, J. Zhao, A. Metavitsiadis, S. Eggert and X. Wang, "*Ground-state phase diagram of the frustrated spin-$\frac{1}{2}$ two-leg honeycomb ladder*", Phys. Rev. B **97** (Jun, 2018) 214433. 11, 12

[32] C. K. Majumdar and D. K. Ghosh, "*On next-nearest-neighbor interaction in linear chain. ii*", J. Math. Phys. **10** (1969) 1399–1402. 14, 47, 48, 72, 90, 106, 127

[33] T. Hamada, J.-i. Kane, S.-i. Nakagawa and Y. Natsume, "*Exact solution of ground state for uniformly distributed rvb in one-dimensional spin-1/2 Heisenberg systems with frustration*", J. Phys. Soc. Jpn. **57** (1988) 1891–1894. 14

[34] K. Okamoto and K. Nomura, "*Fluid-dimer critical point in S= 1/2 antiferromagnetic Heisenberg chain with next nearest neighbor interactions*", Phys. Lett. A **169** (1992) 433–437. 14, 47, 48

[35] S. R. White, R. M. Noack and D. J. Scalapino, "*Resonating valence bond theory of coupled Heisenberg chains*", Phys. Rev. Lett. **73** (Aug, 1994) 886–889. 15, 48, 49, 71, 72

[36] M. Kumar, A. Parvej and Z. G. Soos, "*Level crossing, spin structure factor and quantum phases of the frustrated spin-1/2 chain with first and second neighbor exchange*", J. Condens. Matter Phys. **27** (jul, 2015) 316001. 15, 47, 48, 71, 103

[37] L. Savary and L. Balents, "*Quantum spin liquids: a review*", Rep. Prog. Phys. **80** (nov, 2016) 016502. 15, 71, 103

[38] A. W. Sandvik, E. Dagotto and D. J. Scalapino, "*Spin dynamics of $SrCu_2O_3$ and the Heisenberg ladder*", Phy. Rev. B **53** (1996) R2934–R2937. 16, 48, 71

[39] D. C. Johnston, J. W. Johnson, D. P. Goshorn and A. J. Jacobson, "*Magnetic susceptibility of $(VO)_2P_2O_7$: A one-dimensional spin-1/2 heisenberg antiferromagnet with a ladder spin configuration and a singlet ground state*", Phys. Rev. B **35** (Jan, 1987) 219–222. 16, 48, 71

[40] N. Maeshima, M. Hagiwara, Y. Narumi, K. Kindo, T. C. Kobayashi and K. Okunishi, "*Magnetic properties of $S = 1/2$ zigzag spin chain compound $(N_2H_5)CuCl_3$*", J. Condens. Matter Phys. **15** (may, 2003) 3607–3618. 16, 20, 47, 48

[41] S. E. Dutton, M. Kumar, M. Mourigal, Z. G. Soos, J.-J. Wen, C. L. Broholm, N. H. Andersen, Q. Huang, M. Zbiri, R. Toft-Petersen and R. J. Cava, "*Quantum spin liquid in frustrated one-dimensional $LiCuSbO_4$*", Phys. Rev. Lett. **108** (May, 2012) 187206. 16, 21, 47, 48, 71

[42] M. Mourigal, M. Enderle, B. Fåk, R. K. Kremer, J. M. Law, A. Schneidewind, A. Hiess and A. Prokofiev, "*Evidence of a bond-nematic phase in $LiCuVO_4$*", Phys. Rev. Lett. **109** (jul, 2012) . 16, 47, 48, 71

[43] S.-L. Drechsler, O. Volkova, A. N. Vasiliev, N. Tristan, J. Richter, M. Schmitt, H. Rosner, J. Málek, R. Klingeler, A. A. Zvyagin and B. Büchner, "*Frustrated cuprate route from antiferromagnetic to ferromagnetic spin-$\frac{1}{2}$ Heisenberg chains: Li_2ZrCuO_4 as a missing link near the quantum critical point*", Phys. Rev. Lett. **98** (Feb, 2007) 077202. 16, 21, 47, 48

[44] K. Hida, "*Haldane Gap in the Spin-1/2 Double Chain Heisenberg Antiferromagnet Numerical Diagonalization and Projector Monte Carlo Study*", J. Phys. Soc. Jpn. **60** (1991) 1347. 17

[45] S. P. Strong and A. J. Millis, "*Competition between singlet formation and magnetic ordering in one-dimensional spin systems*", Phys. Rev. B **50** (Oct, 1994) 9911–9923. 17

[46] A. K. Kolezhuk and H. J. Mikeska, "*Phase transitions in the heisenberg spin ladder with ferromagnetic legs*", Phys. Rev. B **53** (Apr, 1996) R8848–R8850. 17, 116

[47] M. Roji and S. Miyashita, "*Competition between classical ordered state and quantum state in ferromagnetic chains coupled by antiferromagnetic bonds*", J. Phys. Soc. Jpn. **65** (1996) 883–886. 17, 116

[48] K. Sekiguchi and K. Hida, "*Partial ferrimagnetism in $S = 1/2$ Heisenberg ladders with a ferromagnetic leg, an antiferromagnetic leg, and antiferromagnetic rungs*", J. Phys. Soc. Jpn. **86** (2017) 084706. 17, 49

[49] T. Hakobyan, J. H. Hetherington and M. Roger, "*Phase diagram of the frustrated two-leg ladder model*", Phys. Rev. B **63** (Mar, 2001) 144433. 17

[50] G. Barcza, O. Legeza, R. M. Noack and J. Sólyom, "*Dimerized phase in the cross-coupled antiferromagnetic spin ladder*", Phys. Rev. B **86** (Aug, 2012) 075133. 17

[51] T. Ogino, R. Kaneko, S. Morita and S. Furukawa, "*Ground-state phase diagram of a spin-$\frac{1}{2}$ frustrated xxz ladder*", Phys. Rev. B **106** (Oct, 2022) 155106. 17

[52] N. Ahmadi, J. Abouie, R. Haghshenas and D. Baeriswyl, "*Frustrated mixed-spin ladders: Evidence for a bond-order wave phase between rung-singlet and haldane phases*", Phys. Rev. B **106** (Nov, 2022) 174419. 17

[53] G. Giri, D. Dey, M. Kumar, S. Ramasesha and Z. G. Soos, "*Quantum phases of frustrated two-leg spin-$\frac{1}{2}$ ladders with skewed rungs*", Phys. Rev. B **95** (Jun, 2017) 224408. 17

[54] S. Das, D. Dey, M. Kumar and S. Ramasesha, "*Quantum phases of a frustrated spin-1 system: The 5/7 skewed ladder*", Phys. Rev. B **104** (Sep, 2021) 125138. 17

[55] S. Das, D. Dey, S. Ramasesha and M. Kumar, "*Quantum phase transition in skewed ladders: an entanglement entropy and fidelity study*", The European Physical Journal B **95** (2022) 147. 17

[56] N. D. Mermin and H. Wagner, "*Absence of ferromagnetism or antiferromagnetism in one- or two-dimensional isotropic Heisenberg models*", Phys. Rev. Lett. **17** (Nov, 1966) 1133–1136. 17, 72

[57] A. Auerbach, *"Spin Wave Theory"*, pp. 113–127. Springer New York, New York, NY, 1994. 17, 31

[58] K. G. Wilson, "*The renormalization group: Critical phenomena and the kondo problem*", Rev. Mod. Phys. **47** (Oct, 1975) 773–840. 17, 37

[59] K. G. Wilson, "*The renormalization group and critical phenomena*", Rev. Mod. Phys. **55** (Jul, 1983) 583–600. 17, 37

[60] D. P. Arovas and A. Auerbach, "*Functional integral theories of low-dimensional quantum Heisenberg models*", Phys. Rev. B **38** (Jul, 1988) 316–332. 17

[61] C. M. Bender and T. T. Wu, "*Anharmonic oscillator. ii. a study of perturbation theory in large order*", Phys. Rev. D **7** (Mar, 1973) 1620–1636. 17

[62] C. Lanczos, "*An iteration method for the solution of the eigenvalue problem of linear differential and integral operators*", J. Res. Natl. Bur. Stand. **45** (Oct., 1950) . 18, 35

[63] E. R. Davidson, "*The iterative calculation of a few of the lowest eigenvalues and corresponding eigenvectors of large real-symmetric matrices*", J. Comput. Phys. **17** (1975) 87–94. 18, 35

[64] B. S. Shastry and B. Sutherland, "*Exact ground state of a quantum mechanical antiferromagnet*", Physica B+ C **108** (1981) 1069–1070. 18, 72, 106

[65] A. Koga and N. Kawakami, "*Quantum phase transitions in the Shastry-Sutherland model for* $SrCu_2(BO_3)_2$", Phys. Rev. Lett. **84** (06, 2000) 4461–4. 18

[66] N. Xi, H. Chen, Z. Y. Xie and R. Yu, "*Plaquette valence bond solid to antiferromagnet transition and deconfined quantum critical point of the Shastry-Sutherland model*", Phys. Rev. B **107** (Jun, 2023) L220408. 18, 38

[67] Y. I. Dublenych, "*Ground states of the Ising model on the Shastry-Sutherland lattice and the origin of the fractional magnetization plateaus in rare-earth-metal tetraborides*", Phys. Rev. Lett. **109** (Oct, 2012) 167202. 18, 19

[68] L. Ye, T. Suzuki and J. G. Checkelsky, "*Electronic transport on the Shastry-Sutherland lattice in Ising-type rare-earth tetraborides*", Phys. Rev. B **95** (May, 2017) 174405. 18

[69] P. W. Leung and Y. F. Cheng, "*Absence of hole pairing in a simple* $t - J$ *model on the Shastry-Sutherland lattice*", Phys. Rev. B **69** (May, 2004) 180403. 18

[70] B.-J. Yang, Y. B. Kim, J. Yu and K. Park, "*Doped valence-bond solid and superconductivity on the Shastry-Sutherland lattice*", Phys. Rev. B **77** (Mar, 2008) 104507. 18

[71] H. Kageyama, K. Yoshimura, R. Stern, N. V. Mushnikov, K. Onizuka, M. Kato, K. Kosuge, C. P. Slichter, T. Goto and Y. Ueda, "*Exact dimer ground state and quantized magnetization plateaus in the two-dimensional spin system $SrCu_2(BO)_2$*", Phys. Rev. Lett. **82** (Apr, 1999) 3168–3171. 19, 72

[72] M. Kim and M. Aronson, "*Spin liquids and antiferromagnetic order in the Shastry-Sutherland-lattice compound Yb_2Pt_2Pb*", Phys. Rev. Lett. **110** (2013) 017201. 19

[73] P. Corboz and F. Mila, "*Tensor network study of the Shastry-Sutherland model in zero magnetic field*", Phys. Rev. B **87** (2013) 115144. 19, 72

[74] J. Yang, A. W. Sandvik and L. Wang, "*Quantum criticality and spin liquid phase in the Shastry-Sutherland model*", Phys. Rev. B **105** (Feb, 2022) L060409. 19, 72

[75] D. C. Ronquillo and M. R. Peterson, "*Identifying topological order in the Shastry-Sutherland model via entanglement entropy*", Phys. Rev. B **90** (Nov, 2014) 201108. 19, 73

[76] H. Kageyama, T. Kitano, N. Oba, M. Nishi, S. Nagai, K. Hirota, L. Viciu, W. JB, J. Yasuda, Y. Baba et al., "*Spin-singlet ground state in two-dimensional s= 1/ 2 frustrated square lattice:$(CuCl)LaNb_2O_7$*", J. Phys. Soc. Jpn. **74** (2005) 1702–1705. 19, 73

[77] C. Tassel, J. Kang, C. Lee, O. Hernandez, Y. Qiu, W. Paulus, E. Collet, B. Lake, T. Guidi, M.-H. Whangbo et al., "*Ferromagnetically coupled Shastry-Sutherland quantum spin singlets in $(CuCl)LaNb_2O_7$*", Phys. Rev. Lett. **105** (2010) 167205. 19, 73, 86, 87, 106

[78] M. Matsuda and K. Katsumata, "*Magnetic properties of a quasi-one-dimensional magnet with competing interactions: $SrCuO_2$*", J. Magn. Magn. Mater. **140-144** (1995) 1671–1672. 20

[79] Y. Hosokoshi, K. Katoh, K. Inoue and T. Goto, "*Construction of a quantum-spin system of $S = 1/2$ antiferromagnetic chain with the next-nearest-neighbor interactions*", J. Phys. Soc. Jpn. **68** (1999) 2910–2913. 20

[80] K. Okunishi, Y. Hieida and Y. Akutsu, "*Middle-field cusp singularities in the magnetization process of one-dimensional quantum antiferromagnets*", Phys. Rev. B **60** (Sep, 1999) R6953–R6956. 20

[81] K. Okunishi and T. Tonegawa, "*Magnetic phase diagram of the $S = 1/2$ antiferromagnetic zigzag spin chain in the strongly frustrated region: Cusp and plateau*", J. Phys. Soc. Jpn. **72** (2003) 479–482. 20

[82] K. Okunishi and T. Tonegawa, "*Fractional S^z excitation and its bound state around the 1/3 plateau of the $S = 1/2$ Ising-like zigzag XXZ chain*", Phys. Rev. B **68** (Dec, 2003) 224422. 20

[83] A. A. Nersesyan, A. O. Gogolin and F. H. L. Eßler, "*Incommensurate spin correlations in spin- 1/2 frustrated two-leg Heisenberg ladders*", Phys. Rev. Lett. **81** (Jul, 1998) 910–913. 21

[84] T. Hikihara, M. Kaburagi and H. Kawamura, "*Ground-state phase diagrams of frustrated spin-S XXZ chains: Chiral ordered phases*", Phys. Rev. B **63** (Apr, 2001) 174430. 21

[85] M. Kaburagi, H. Kawamura and T. Hikihara, "*Spin and chiral orderings of frustrated quantum spin chains*", J. Phys. Soc. Jpn. **68** (1999) 3185–3188. 21

[86] S. Park, Y. J. Choi, C. L. Zhang and S.-W. Cheong, "*Ferroelectricity in an $S = 1/2$ chain cuprate*", Phys. Rev. Lett. **98** (Jan, 2007) 057601. 21

[87] M. Hase, H. Kuroe, K. Ozawa, O. Suzuki, H. Kitazawa, G. Kido and T. Sekine, "*Magnetic properties of $Rb_2Cu_2Mo_3O_{12}$ including a one-dimensional spin-1/2 Heisenberg system with ferromagnetic first-nearest-neighbor and antiferromagnetic second-nearest-neighbor exchange interactions*", Phys. Rev. B **70** (Sep, 2004) 104426. 21, 71

[88] O. S. Volkova, I. S. Maslova, R. Klingeler, M. Abdel-Hafiez, Y. C. Arango, A. U. B. Wolter, V. Kataev, B. Büchner and A. N. Vasiliev, "*Orthogonal spin arrangement as possible ground state of three-dimensional Shastry-Sutherland network in $Ba_3Cu_3In_4O_{12}$*", Phys. Rev. B **85** (Mar, 2012) 104420. 21, 48

[89] S. E. Dutton, M. Kumar, Z. G. Soos, C. L. Broholm and R. J. Cava, "*Dominant ferromagnetism in the spin-1/2 half-twist ladder 334 compounds, $Ba_3Cu_3In_4O_{12}$ and $Ba_3Cu_3Sc_4O_{12}$*", J. Condens. Matter Phys. **24** (mar, 2012) 166001. 21

[90] A. Parvej and M. Kumar, "*Multipolar phase in frustrated spin-1/2 and spin-1 chains*", Phys. Rev. B **96** (Aug, 2017) 054413. 21, 22, 84, 133, 134, 137

[91] T. Hikihara, L. Kecke, T. Momoi and A. Furusaki, "*Vector chiral and multipolar orders in the spin-$\frac{1}{2}$ frustrated ferromagnetic chain in magnetic field*", Phys. Rev. B **78** (Oct, 2008) 144404. 21, 22, 72, 133, 134

[92] J. Sudan, A. Lüscher and A. M. Läuchli, "*Emergent multipolar spin correlations in a fluctuating spiral: The frustrated ferromagnetic spin-$\frac{1}{2}$ Heisenberg chain in a magnetic field*", Phys. Rev. B **80** (Oct, 2009) 140402. 21, 22, 133

[93] A. V. Chubukov, "*Chiral, nematic, and dimer states in quantum spin chains*", Phys. Rev. B **44** (Sep, 1991) 4693–4696. 21, 133

[94] B. Thielemann, C. Rüegg, H. M. Rønnow, A. M. Läuchli, J.-S. Caux, B. Normand, D. Biner, K. W. Krämer, H.-U. Güdel, J. Stahn, K. Habicht, K. Kiefer, M. Boehm, D. F. McMorrow and J. Mesot, "*Direct observation of magnon fractionalization in the quantum spin ladder*", Phys. Rev. Lett. **102** (Mar, 2009) 107204. 22

[95] H. Katsura, N. Nagaosa and A. V. Balatsky, "*Spin current and magnetoelectric effect in noncollinear magnets*", Phys. Rev. Lett. **95** (Jul, 2005) 057205. 23

[96] T. Momoi and K. Totsuka, "*Magnetization plateaus of the Shastry-Sutherland model for $SrCu_2(BO_3)_2$: spin-density wave, supersolid, and bound states*", Phys. Rev. B **62** (Dec, 2000) 15067–15078. 23, 72

[97] K. Siemensmeyer, E. Wulf, H.-J. Mikeska, K. Flachbart, S. Gabáni, S. Mat'aš, P. Priputen, A. Efdokimova and N. Shitsevalova, "*Fractional magnetization plateaus and magnetic order in the Shastry-Sutherland magnet TmB_4*", Phys. Rev. Lett. **101** (Oct, 2008) 177201. 23

[98] M. Orendáč, S. Gabani, P. Farkasovsky, E. Gažo, J. Kacmarcik, M. Marcin, G. Pristáš, K. Siemensmeyer, N. Shitsevalova and K. Flachbart, "*Ground state and stability of the fractional plateau phase in metallic Shastry–Sutherland system TmB_4*", Sci. Rep. **11** (03, 2021) . 23

[99] A. V. Syromyatnikov and A. Y. Aktersky, "*Elementary excitations in the ordered phase of spin-$\frac{1}{2}$ J_1–J_2 model on square lattice*", Phys. Rev. B **99** (Jun, 2019) 224402. 24

[100] N. Shannon, T. Momoi and P. Sindzingre, "*Nematic order in square lattice frustrated ferromagnets*", Phys. Rev. Lett. **96** (Jan, 2006) 027213. 24, 72

[101] Y.-F. Jiang and H.-C. Jiang, "*Nature of quantum spin liquids of the $S = \frac{1}{2}$ Heisenberg antiferromagnet on the triangular lattice: A parallel DMRG study*", Phys. Rev. B **107** (Apr, 2023) L140411. 24, 38

[102] T. Giamarchi, C. Rüegg and O. Tchernyshyov, "*Bose-Einstein condensation in magnetic insulators*", Nat. Phys. **4** (2008) 198–204. 24, 25

[103] T. Matsubara and H. Matsuda, "*A Lattice Model of Liquid Helium, I*", Prog. Theor. Phys. **16** (Dec, 1956) 569–582. 24

[104] T. Nikuni, M. Oshikawa, A. Oosawa and H. Tanaka, "*Bose-Einstein condensation of dilute magnons in $TlCuCl_3$*", Phys. Rev. Lett. **84** (Jun, 2000) 5868–5871. 25, 26

[105] M. Jaime, V. F. Correa, N. Harrison, C. D. Batista, N. Kawashima, Y. Kazuma, G. A. Jorge, R. Stern, I. Heinmaa, S. A. Zvyagin, Y. Sasago and K. Uchinokura, "*Magnetic-field-induced condensation of triplons in han purple pigment $BaCuSi_2O_6$*", Phys. Rev. Lett. **93** (Aug, 2004) 087203. 25

[106] S. Krämer, R. Stern, M. Horvatić, C. Berthier, T. Kimura and I. R. Fisher, "*Nuclear magnetic resonance evidence for a strong modulation of the Bose-Einstein condensate in $BaCuSi_2O_6$*", Phys. Rev. B **76** (Sep, 2007) 100406. 25

[107] M. Matsumoto, "*Microscopic model for the magnetization plateaus in NH_4CuCl_3*", Phys. Rev. B **68** (Nov, 2003) 180403. 25

[108] B. Grenier, Y. Inagaki, L. P. Regnault, A. Wildes, T. Asano, Y. Ajiro, E. Lhotel, C. Paulsen, T. Ziman and J. P. Boucher, "*Ordering and excitations in the field-induced magnetic phase of $Cs_3Cr_2Br_9$*", Phys. Rev. Lett. **92** (Apr, 2004) 177202. 25

[109] T. Masuda, A. Zheludev, H. Manaka, L.-P. Regnault, J.-H. Chung and Y. Qiu, "*Dynamics of composite Haldane spin chains in $IPA - CuCl_3$*", Phys. Rev. Lett. **96** (Feb, 2006) 047210. 25

[110] V. Zapf, M. Jaime and C. D. Batista, "*Bose-einstein condensation in quantum magnets*", Rev. Mod. Phys. **86** (May, 2014) 563–614. 27

[111] F. Pollmann, E. Berg, A. M. Turner and M. Oshikawa, "*Symmetry protection of topological phases in one-dimensional quantum spin systems*", Phys. Rev. B **85** (Feb, 2012) 075125. 27

[112] F. D. M. Haldane, "*Nonlinear field theory of large-spin Heisenberg antiferromagnets: Semiclassically quantized solitons of the one-dimensional easy-axis néel state*", Phys. Rev. Lett. **50** (Apr, 1983) 1153–1156. 27, 31, 90, 94, 104

[113] S. M. Girvin and D. P. Arovas, "*Hidden topological order in integer quantum spin chains*", Phys. Scr. **1989** (jan, 1989) 156. 27, 117, 126

[114] M. den Nijs and K. Rommelse, "*Preroughening transitions in crystal surfaces and valence-bond phases in quantum spin chains*", Phys. Rev. B **40** (Sep, 1989) 4709–4734. 27, 106

[115] K. Hida, "*Crossover between the Haldane-gap phase and the dimer phase in the spin-1/2 alternating Heisenberg chain*", Phys. Rev. B **45** (Feb, 1992) 2207–2212. 27

[116] F. Pollmann, A. M. Turner, E. Berg and M. Oshikawa, "*Entanglement spectrum of a topological phase in one dimension*", Phys. Rev. B **81** (Feb, 2010) 064439. 28

[117] D. Sénéchal, "*An introduction to bosonization*", 1999. 31

[118] S. Rettrup, "*An iterative method for calculating several of the extreme eigensolutions of large real non-symmetric matrices*", J. Comput. Phys. **45** (1982) 100–107. 35

[119] S. R. White and D. A. Huse, "*Numerical renormalization-group study of low-lying eigenstates of the antiferromagnetic $S = 1$ Heisenberg chain*", Phys. Rev. B **48** (Aug, 1993) 3844–3852. 37, 75

[120] J. Biamonte and V. Bergholm, "*Tensor networks in a nutshell*", 2017. arXiv.1708.00006. 37

[121] S. R. White, "*Density matrix formulation for quantum renormalization groups*", Phys. Rev. Lett. **69** (Nov, 1992) 2863–2866. 37, 51, 75, 90, 95, 109

[122] K. Hallberg, X. Q. G. Wang, P. Horsch and A. Moreo, "*Critical behavior of the $S = 3/2$ antiferromagnetic Heisenberg chain*", Phys. Rev. Lett. **76** (Jun, 1996) 4955–4958. 38

[123] U. Schollwöck and T. Jolicoeur, "*Haldane gap and hidden order in the $S = 2$ antiferromagnetic quantum spin chain*", Europhys. Lett. **30** (jun, 1995) 493. 38

[124] X. Qian and M. Qin, "*Absence of spin liquid phase in the $J_1 - J_2$ Heisenberg model on the square lattice*", Phys. Rev. B **109** (Apr, 2024) L161103. 38

[125] R. Verresen, F. Pollmann and R. Moessner, "*Quantum dynamics of the square-lattice Heisenberg model*", Phys. Rev. B **98** (Oct, 2018) 155102. 38

[126] D. Sellmann, X.-F. Zhang and S. Eggert, "*Phase diagram of the antiferromagnetic XXZ model on the triangular lattice*", Phys. Rev. B **91** (Feb, 2015) 081104. 38

[127] M. Kishimoto, K. Morita, Y. Matsubayashi, S. Sota, S. Yunoki and T. Tohyama, "*Ground state phase diagram of the Kitaev-Heisenberg model on a honeycomb-triangular lattice*", Phys. Rev. B **98** (Aug, 2018) 054411. 38

[128] S. Peotta, L. Mazza, E. Vicari, M. Polini, R. Fazio and D. Rossini, "*The XYZ chain with Dzyaloshinsky–Moriya interactions: from spin–orbit-coupled lattice bosons to interacting Kitaev chains*", J. Stat. Mech.: Theory Exp. **2014** (sep, 2014) P09005. 38

[129] J. Y. Lee, Y.-Z. You, S. Sachdev and A. Vishwanath, "*Signatures of a deconfined phase transition on the Shastry-Sutherland lattice: Applications to quantum critical* $SrCu_2(BO_3)_2$", Phys. Rev. X **9** (Nov, 2019) 041037. 38, 72

[130] S. Depenbrock, I. P. McCulloch and U. Schollwöck, "*Nature of the spin-liquid ground state of the* $S = 1/2$ *Heisenberg model on the Kagome lattice*", Phys. Rev. Lett. **109** (Aug, 2012) 067201. 38

[131] Y.-C. He, M. P. Zaletel, M. Oshikawa and F. Pollmann, "*Signatures of Dirac cones in a DMRG study of the Kagome Heisenberg model*", Phys. Rev. X **7** (Jul, 2017) 031020. 38

[132] B. S. Shastry and B. Sutherland, "*Excitation spectrum of a dimerized next-neighbor antiferromagnetic chain*", Phys. Rev. Lett. **47** (1981) 964. 47, 48, 59, 90

[133] F. D. M. Haldane, "*Spontaneous dimerization in the* $S = 1/2$ *Heisenberg antiferromagnetic chain with competing interactions*", Phys. Rev. B **25** (1982) 4925. 47, 48

[134] R. Chitra, S. Pati, H. R. Krishnamurthy, D. Sen and S. Ramasesha, "*Density-matrix renormalization-group studies of the spin-1/2 Heisenberg system with dimerization and frustration*", Phys. Rev. B **52** (Sep, 1995) 6581–6587. 47, 72, 90, 106

[135] S.-i. Tomonaga, "*Remarks on Bloch's Method of Sound Waves applied to Many-Fermion Problems*", Prog. Theor. Phys. **5** (07, 1950) 544–569. 47

[136] J. M. Luttinger, "*An exactly soluble model of a many-fermion system*", J. Math. Phys. **4** (1, 1963) . 47

[137] D. C. Mattis and E. H. Lieb, "*Exact Solution of a Many-Fermion System and Its Associated Boson Field*", J. Math. Phys. **6** (Feb., 1965) 304–312. 47, 100

[138] S. R. White and I. Affleck, "*Dimerization and incommensurate spiral spin correlations in the zigzag spin chain: Analogies to the Kondo lattice*", Phys. Rev. B **54** (Oct, 1996) 9862–9869. 48

[139] M. Kumar, S. Ramasesha and Z. G. Soos, "*Bond-order wave phase, spin solitons, and thermodynamics of a frustrated linear spin-$\frac{1}{2}$ Heisenberg antiferromagnet*", Phys. Rev. B **81** (Feb, 2010) 054413. 48, 52, 75, 103

[140] E. Dagotto and T. M. Rice, "*Surprises on the Way from One- to Two-Dimensional Quantum Magnets: The Ladder Materials*", Science **271** (Feb, 1996) 618–623. 48, 71

[141] B. Koteswararao, A. V. Mahajan, F. Bert, P. Mendels, J. Chakraborty, V. Singh, I. Dasgupta, S. Rayaprol, V. Siruguri, A. Hoser and S. D. Kaushik, "*Magnetic behavior of $Ba_3Cu_3Sc_4O_{12}$*", J. Condens. Matter Phys. **24** (may, 2012) 236001. 48

[142] M. Korotin, I. Elfimov, V. Anisimov, M. Troyer, D. Khomskii and Anisimov, "*Exchange interactions and magnetic properties of the layered vanadates CaV_2O_5, MgV_2O_5, CaV_3O_7, and CaV_4O_9*", Phys. Rev. Lett. **83** (1999) 1387 – 1390. 48

[143] M. Azuma, Z. Hiroi, M. Takano, K. Ishida and Y. Kitaoka, "*Observation of a spin gap in $SrCu_2O_3$ comprising spin-$\frac{1}{2}$ quasi-1d two-leg ladders*", Phys. Rev. Lett. **73** (Dec, 1994) 3463–3466. 48

[144] V. R. Vieira, N. Guihé ry, J. P. Rodriguez and P. D. Sacramento, "*Decoupling of the $S = \frac{1}{2}$ antiferromagnetic zig-zag ladder with anisotropy*", Phys. Rev. B **63** (may, 2001) . 48

[145] E. Dagotto, J. Riera and D. Scalapino, "*Superconductivity in ladders and coupled planes*", Phys. Rev. B **45** (Mar, 1992) 5744–5747. 49, 104

[146] K. Hijii, A. Kitazawa and K. Nomura, "*Phase diagram of $S = \frac{1}{2}$ two-leg XXZ spin-ladder systems*", Phys. Rev. B **72** (Jul, 2005) 014449. 49

[147] H. Suhl and I. K. Schuller, "*Spin-wave theory of exchange-induced anisotropy*", Phys. Rev. B **58** (Jul, 1998) 258–264. 49

[148] T. M. Hong, "*Simple mechanism for a positive exchange bias*", Phys. Rev. B **58** (Jul, 1998) 97–100. 49

[149] U. Schollwöck, "*The density-matrix renormalization group*", Rev. Mod. Phys. **77** (Apr, 2005) 259–315. 51, 75, 95, 109

[150] D. Dey, D. Maiti and M. Kumar, "*An efficient density matrix renormalization group algorithm for chains with periodic boundary condition*", Papers in Physics **8** (nov, 2016) 080006. 52

[151] M. Kumar and Z. G. Soos, "*Decoupled phase of frustrated spin-$\frac{1}{2}$ antiferromagnetic chains with and without long-range order in the ground state*", Phys. Rev. B **88** (Oct, 2013) 134412. 59

[152] E. Lieb, T. Schultz and D. Mattis, "*Two soluble models of an antiferromagnetic chain*", Ann. Phys. **16** (1961) 407–466. 68

[153] M. Oshikawa, M. Yamanaka and I. Affleck, "*Magnetization plateaus in spin chains: "Haldane gap" for half-integer spins*", Phys. Rev. Lett. **78** (Mar, 1997) 1984–1987. 68

[154] Y. Zhou, K. Kanoda and T.-K. Ng, "*Quantum spin liquid states*", Rev. Mod. Phys. **89** (Apr, 2017) 025003. 71

[155] L. Balents, "*Spin liquids in frustrated magnets*", Nature **464** (2010) 199–208. 71, 72

[156] P. A. Lee, "*An end to the drought of quantum spin liquids*", Science **321** (2008) 1306–1307. 71, 72

[157] A. Yagi, K. Matsui, T. Goto, M. Hase and T. Sasaki, "*NMR study on the competing spin chain $Rb_2Cu_2Mo_3O_{12}$*", J. Phys.: Conf. Ser. **828** (mar, 2017) 012016. 71

[158] M. P. Shores, E. A. Nytko, B. M. Bartlett and D. G. Nocera, "*A structurally perfect $S = 1/2$ kagomé antiferromagnet*", J. Am. Chem. Soc. **127** (2005) 13462–13463. 71

[159] J. S. Helton, K. Matan, M. P. Shores, E. A. Nytko, B. M. Bartlett, Y. Yoshida, Y. Takano, A. Suslov, Y. Qiu, J.-H. Chung, D. G. Nocera and Y. S. Lee, "*Spin dynamics of the spin-1/2 kagome lattice antiferromagnet $ZnCu_3(OH)_6(Cl)_2$*", Phys. Rev. Lett. **98** (Mar, 2007) 107204. 71, 72

[160] A. Banerjee et al., "*Proximate Kitaev quantum spin liquid behaviour in a honeycomb magnet*", Nature Materials **15** (2016) 733–740. 71

[161] M. R. Norman, "*Colloquium: Herbertsmithite and the search for the quantum spin liquid*", Rev. Mod. Phys. **88** (Dec, 2016) 041002. 71

[162] J.-B. Fouet, F. Mila, D. Clarke, H. Youk, O. Tchernyshyov, P. Fendley and R. M. Noack, "*Condensation of magnons and spinons in a frustrated ladder*", Phys. Rev. B **73** (Jun, 2006) 214405. 72

[163] A. Leonov and M. Mostovoy, "*Multiply periodic states and isolated skyrmions in an anisotropic frustrated magnet*", Nat. Commun. **6** (2015) 1–8. 72

[164] J. Schulenburg, A. Honecker, J. Schnack, J. Richter and H.-J. Schmidt, "*Macroscopic magnetization jumps due to independent magnons in frustrated quantum spin lattices*", Phys. Rev. Lett. **88** (2002) 167207. 72

[165] B. Kumar and B. Danu, "*Effective models for the magnetization behavior of Shastry-Sutherland model*", 2014. arXiv.1408.3529. 72

[166] S. Chakravarty, B. I. Halperin and D. R. Nelson, "*Two-dimensional quantum Heisenberg antiferromagnet at low temperatures*", Phys. Rev. B **39** (Feb, 1989) 2344–2371. 72

[167] E. Dagotto and A. Moreo, "*Phase diagram of the frustrated spin-*1/2 *Heisenberg antiferromagnet in 2 dimensions*", Phys. Rev. Lett. **63** (Nov, 1989) 2148–2151. 72

[168] J. Sirker, Z. Weihong, O. P. Sushkov and J. Oitmaa, "$J_1 - J_2$ *model: First-order phase transition versus deconfinement of spinons*", Phys. Rev. B **73** (May, 2006) 184420. 72

[169] S. Kundu, A. Shahee, A. Chakraborty, K. M. Ranjith, B. Koo, J. Sichelschmidt, M. T. F. Telling, P. K. Biswas, M. Baenitz, I. Dasgupta, S. Pujari and A. V. Mahajan, "*Gapless quantum spin liquid in the triangular system* $Sr_3CuSb_2O_9$", Phys. Rev. Lett. **125** (Dec, 2020) 267202. 72

[170] E. Manousakis, "*The spin-*1/2 *Heisenberg antiferromagnet on a square lattice and its application to the cuprous oxides*", Rev. Mod. Phys. **63** (Jan, 1991) 1–62. 72

[171] Y. Shirata, H. Tanaka, A. Matsuo and K. Kindo, "*Experimental realization of a spin-*1/2 *triangular-lattice Heisenberg antiferromagnet*", Phys. Rev. Lett. **108** (Jan, 2012) 057205. 72

[172] M. E. Zayed, C. Rüegg, J. L. J., A. M. Läuchli, C. Panagopoulos, S. S. Saxena, M. Ellerby, D. F. McMorrow, T. Strässle, S. Klotz, G. Hamel, R. A. Sadykov, V. Pomjakushin, M. Boehm, M. Jiménez–Ruiz, A. Schneidewind, E. Pomjakushina, M. Stingaciu, K. Conder and H. M. Rønnow, "*4-spin plaquette singlet state in the Shastry–Sutherland compound* $SrCu_2(BO_3)_2$", Nat. Phys. **13** (jul, 2017) 962–966. 72

[173] N. Oba, H. Kageyama, T. Kitano, J. Yasuda, Y. Baba, M. Nishi, K. Hirota, Y. Narumi, M. Hagiwara, K. Kindo, T. Saito, Y. Ajiro and K. Yoshimura, "*Collinear order in frustrated quantum antiferromagnet on square lattice* $CuBrLaNb_2O_7$", Phys. Soc. Jpn. **75** (2006) 113601. 73

[174] A. A. Tsirlin, A. M. Abakumov, C. Ritter and H. Rosner, "$(CuCl)LaTa_2O_7$ *and quantum phase transition in the* $(CuX)LaM_2O_7$

family (X=Cl, Br; M=Nb, Ta)", Phys. Rev. B **86** (Aug, 2012) 064440. 73, 86

[175] H. Kageyama, J. Yasuda, T. Kitano, K. Totsuka, Y. Narumi, M. Hagiwara, K. Kindo, Y. Baba, N. Oba, Y. Ajiro and K. Yoshimura, "*Anomalous magnetization of two-dimensional $S = 1/2$ frustrated square-lattice antiferromagnet $(CuCl)LaNb_2O_7$*", J. Phys. Soc. Jpn. **74** (2005) 3155–3158. 73

[176] A. Kitada, Z. Hiroi, Y. Tsujimoto, T. Kitano, H. Kageyama, Y. Ajiro and K. Yoshimura, "*Bose–Einstein condensation of quasi-two-dimensional frustrated quantum magnet $(CuCl)LaNb_2O_7$*", J. Phys. Soc. Jpn. **76** (2007) 093706. 73

[177] M. Yoshida, N. Ogata, M. Takigawa, J.-i. Yamaura, M. Ichihara, T. Kitano, H. Kageyama, Y. Ajiro and K. Yoshimura, "*Magnetic and structural studies of the quasi-two-dimensional spin-gap system $(CuCl)LaNb_2O_7$*", J. Phys. Soc. Jpn **76** (2007) 104703. 73

[178] Y. Tsujimoto, Y. Baba, N. Oba, H. Kageyama, T. Fukui, Y. Narumi, K. Kindo, T. Saito, M. Takano, Y. Ajiro and K. Yoshimura, "*1/3 magnetization plateau in spin-1/2 square lattice antiferromagnet $(CuBr)Sr_2Nb_3O_{10}$*", J. Phys. Soc. Jpn. **76** (2007) 063711. 73

[179] K. A. Hallberg, "*New trends in density matrix renormalization*", Adv. Phys. **55** (jul, 2006) 477–526. 75, 95, 109

[180] S. Furukawa, M. Sato, S. Onoda and A. Furusaki, "*Ground-state phase diagram of a spin-$\frac{1}{2}$ frustrated ferromagnetic XXZ chain: Haldane dimer phase and gapped/gapless chiral phases*", Phys. Rev. B **86** (Sep, 2012) 094417. 84

[181] Y. Uemura, A. Aczel, Y. Ajiro, J. Carlo, T. Goko, D. Goldfeld, A. Kitada, G. Luke, G. MacDougall, I. Mihailescu et al., "*Muon spin relaxation studies of the frustrated quasi-two-dimensional square-lattice spin system $Cu(Cl, Br)La(Nb, Ta)_2O_7$: Evolution from spin-gap to antiferromagnetic state*", Phys. Rev. B **80** (2009) 174408. 87

[182] A. Kitada, Y. Tsujimoto, H. Kageyama, Y. Ajiro, M. Nishi, Y. Narumi, K. Kindo, M. Ichihara, Y. Ueda, Y. Uemura et al., "*Quantum phase transition in $(CuCl)La(Nb_{1-x}Ta_x)_2O_7$*", Phys. Rev. B **80** (2009) 174409. 87

[183] Y. Tsujimoto, A. Kitada, H. Kageyama, M. Nishi, Y. Narumi, K. Kindo, Y. Kiuchi, Y. Ueda, Y. J. Uemura, Y. Ajiro et al., "*Synthesis, structural and magnetic properties of the solid solution*

$(CuCl_{1-x}Br_x)LaNb_2O_7(0 \leq x \leq 1)$", J. Phys. Soc. Jpn. **79** (2009) 014709. 87

[184] K. Uchinokura, "*Spin-Peierls transition in $CuGeO_3$ and impurity-induced ordered phases in low-dimensional spin-gap systems*", J. Condens. Matter Phys. **14** (feb, 2002) R195. 89

[185] M. Hase, I. Terasaki, K. Uchinokura, M. Tokunaga, N. Miura and H. Obara, "*Magnetic phase diagram of the spin-Peierls cuprate $CuGeO_3$*", Phys. Rev. B **48** (Oct, 1993) 9616–9619. 89, 104

[186] S. Calder, L. D. Sanjeewa, V. O. Garlea, J. Xing, R. J. Terry and J. W. Kolis, "*Magnetic interactions in the one-dimensional spin-chain metal-organic compounds $M(N_2H_5)_2(SO_4)_2$ ($M = Cu, Co, Mn$)*", Phys. Rev. Mater. **6** (Dec, 2022) 124407. 89

[187] I. S. Jacobs, J. W. Bray, H. R. Hart, L. V. Interrante, J. S. Kasper, G. D. Watkins, D. E. Prober and J. C. Bonner, "*Spin-peierls transitions in magnetic donor-acceptor compounds of tetrathiafulvalene (TTF) with bisdithiolene metal complexes*", Phys. Rev. B **14** (Oct, 1976) 3036–3051. 89, 90

[188] S. Sahoo, D. Dey, S. K. Saha and M. Kumar, "*Haldane and dimer phases in a frustrated spin chain: an exact groundstate and associated topological phase transition*", J. Condens. Matter Phys. **32** (may, 2020) 335601. 90, 98, 104, 106

[189] L.-F. Lin, R. Soni, Y. Zhang, S. Gao, A. Moreo, G. Alvarez, A. D. Christianson, M. B. Stone and E. Dagotto, "*Electronic structure, magnetic properties, and pairing tendencies of the copper-based honeycomb lattice* $Na_2Cu_2TeO_6$", Phys. Rev. B **105** (Jun, 2022) 245113. 90, 104

[190] S. Gao, L.-F. Lin, A. F. May, B. K. Rai, Q. Zhang, E. Dagotto, A. D. Christianson and M. B. Stone, "*Weakly coupled alternating $S = \frac{1}{2}$ chains in the distorted honeycomb lattice compound* $Na_2Cu_2TeO_6$", Phys. Rev. B **102** (Dec, 2020) 220402. 90, 104

[191] K. Kodama, H. Harashina, H. Sasaki, M. Kato, M. Sato, K. Kakurai and M. Nishi, "*Neutron scattering study on the quasi-one-dimensional spin-gap system $CuNb_2O_6$*", J. Phys. Soc.Jpn **68** (1999) 237–241. 90, 104

[192] M. B. Stone, W. Tian, M. D. Lumsden, G. E. Granroth, D. Mandrus, J.-H. Chung, N. Harrison and S. E. Nagler, "*Quantum spin correlations in an organometallic alternating-sign chain*", Phys. Rev. Lett. **99** (Aug, 2007) 087204. 90, 104

[193] D. Dmitriev, V. Krivnov and A. Ovchinnikov, "*Exactly solvable spin ladder model with degenerate ferromagnetic and singlet states*", Eur Phys J B : Condensed Matter and Complex Systems **14** (March, 2000) 91–97. 90, 91, 105, 109

[194] S. K. Saha, D. Dey, M. Kumar and Z. G. Soos, "*Hybrid exact diagonalization and density matrix renormalization group approach to the thermodynamics of one-dimensional quantum models*", Phys. Rev. B **99** (May, 2019) 195144. 95, 109

[195] D. Allen and D. Sénéchal, "*Non-abelian bosonization of the frustrated antiferromagnetic spin-1/2 chain*", Phys. Rev. B **55** (Jan, 1997) 299–308. 100

[196] K. Okamoto and K. Nomura, "*Fluid-dimer critical point in $S = 1/2$ antiferromagnetic Heisenberg chain with next nearest neighbor interactions*", Phys. Lett. A **169** (1992) 433–437. 100

[197] A. Parvej and M. Kumar, "*Degeneracies and exotic phases in an isotropic frustrated spin-1/2 chain*", J. Magn. Magn. Mater. **401** (2016) 96–101. 100, 133, 137

[198] M. Chatterjee, M. Kumar and Z. G. Soos, "*Singlet quantum phases and magnetization of the frustrated spin-1/2 ladder with ferromagnetic (F) exchange in legs and alternating F-AF exchange in rungs*", arXiv:2305.12884 (2023) . 101, 104, 108

[199] L. de Jongh and A. Miedema, "*Experiments on simple magnetic model systems*", Adv. Phys. **23** (1974) 1–260. 103

[200] J. S. M. (Ed.), *"Extended Linear Chain Compounds"*. Plenum Press, New York, 1983. 103

[201] M. Kumar and Z. G. Soos, "*Spin-parity and broken symmetry in finite spin-$\frac{1}{2}$ chains with frustrated exchange: Quantum transition from high to low spin*", Phys. Rev. B **85** (Apr, 2012) 144415. 103

[202] S. R. White and I. Affleck, "*Dimerization and incommensurate spiral spin correlations in the zigzag spin chain: Analogies to the Kondo lattice*", Phys. Rev. B **54** (Oct, 1996) 9862–9869. 103, 106

[203] S. K. Saha, M. S. Roy, M. Kumar and Z. G. Soos, "*Modeling the spin-peierls transition of spin-$\frac{1}{2}$ chains with correlated states: J_1-J_2 model,* $CuGeO_3$*, and* $TTF-CuS_4C_4(CF_3)_4$", Phys. Rev. B **101** (Feb, 2020) 054411. 104

[204] Y. Tseng, E. Paris, K. P. Schmidt, W. Zhang, T. C. Asmara, R. Bag, V. N. Strocov, S. Singh, J. Schlappa, H. M. Rønnow et al., "*Momentum-resolved spin-conserving two-triplon bound state and continuum in a cuprate ladder*", Commun. Phys. **6** (2023) 138. 104

[205] N. D. Patel, A. Nocera, G. Alvarez, R. Arita, A. Moreo and E. Dagotto, "*Magnetic properties and pairing tendencies of the iron-based superconducting ladder* $BaFe_2S_3$*: Combined ab initio and density matrix renormalization group study*", Phys. Rev. B **94** (Aug, 2016) 075119. 104

[206] Y. Zhang, L. Lin, J.-J. Zhang, E. Dagotto and S. Dong, "*Pressure-driven phase transition from antiferromagnetic semiconductor to nonmagnetic metal in the two-leg ladders* AFe_2X_3 *(*$A = \mathrm{Ba}, \mathrm{K}$*;* $X = \mathrm{S}, \mathrm{Se}$*)*", Phys. Rev. B **95** (Mar, 2017) 115154. 104

[207] T. Hong, L. Y. Zhu, X. Ke, V. O. Garlea, Y. Qiu, Y. Nambu, H. Yoshizawa, M. Zhu, G. E. Granroth, A. T. Savici, Z. Gai and H. D. Zhou, "*Structural and magnetic properties in the quantum* $S = \frac{1}{2}$ *dimer system* $Ba_3(Cr_{1-x}V_x)_2O_8$ *with site disorder*", Phys. Rev. B **87** (Apr, 2013) 144427. 106

[208] A. A. Tsirlin, R. Nath, C. Geibel and H. Rosner, "*Magnetic properties of* $Ag_2VOP_2O_7$*: An unexpected spin dimer system*", Phys. Rev. B **77** (Mar, 2008) 104436. 106

[209] T. Kennedy and H. Tasaki, "*Hidden symmetry breaking and the Haldane phase in S=1 quantum spin chains*", Commun. Math. Phys. **147** (1992) 431–484. 106, 109

[210] M. Oshikawa, "*Hidden* $Z_2 * Z_2$ *symmetry in quantum spin chains with arbitrary integer spin*", J. Condens. Matter Phys. **4** (1992) 7469–7488. 106

[211] I. Affleck and F. D. M. Haldane, "*Critical theory of quantum spin chains*", Phys. Rev. B **36** (Oct, 1987) 5291–5300. 106

[212] Z. G. Soos and S. Ramasesha, "*Valence-bond theory of linear Hubbard and Pariser-Parr-Pople models*", Phys. Rev. B **29** (May, 1984) 5410–5422. 107

[213] S. Ramasesha and Z. Soos, "*Magnetic and optical properties of exact PPP states of naphthalene*", Chem. Phys. **91** (1984) 35–42. 107

[214] K. Nomura, "*Spin correlation function of the S=1 antiferromagnetic Heisenberg chain by the large-cluster-decomposition Monte Carlo method*", Phys. Rev. B **40** (Aug, 1989) 2421–2425. 109

[215] K. Chang, I. Affleck, G. W. Hayden and Z. G. Soos, "*A study of the bilinear-biquadratic spin-1 antiferromagnetic chain using the valence-bond basis*", J. Condens. Matter Phys. **1** (jan, 1989) 153. 130

[216] P. Fazekas, *"Lecture Notes on Electron Correlation and Magnetism"*. WORLD SCIENTIFIC, 1999, 10.1142/2945. 133

[217] M. Skoulatos, F. Rucker, G. J. Nilsen, A. Bertin, E. Pomjakushina, J. Ollivier, A. Schneidewind, R. Georgii, O. Zaharko, L. Keller, C. Rüegg, C. Pfleiderer, B. Schmidt, N. Shannon, A. Kriele, A. Senyshyn and A. Smerald, "*Putative spin-nematic phase in* $BaCdVO(PO_4)_2$", Phys. Rev. B **100** (Jul, 2019) 014405. 134

[218] M. Enderle, B. Fåk, H.-J. Mikeska, R. K. Kremer, A. Prokofiev and W. Assmus, "*Two-spinon and four-spinon continuum in a frustrated ferromagnetic spin-*1/2 *chain*", Phys. Rev. Lett. **104** (Jun, 2010) 237207. 134

[219] J. Schnack, J. Schulenburg, A. Honecker and J. Richter, "*Magnon crystallization in the kagome lattice antiferromagnet*", Phys. Rev. Lett. **125** (Sep, 2020) 117207. 135

[220] S. Das, D. Dey, M. Kumar and S. Ramasesha, "*Quadrupolar phases and plateau states in skewed ladders*", arXiv:2311.05031 (2023) . 135

[221] H. Onishi, "*Magnetic excitations of spin nematic state in frustrated ferromagnetic chain*", J. Phys. Soc. Jpn. **84** (2015) 083702. 137

[222] M. Sato, T. Hikihara and T. Momoi, "*NMR relaxation rate in the field-induced octupolar liquid phase of spin-*$\frac{1}{2}$ $J_1 - J_2$ *frustrated chains*", J. Phys.: Conf. Ser. **320** (sep, 2011) 012014. 137